University of Twente
Faculty of Electrical Engineering, Mathematics and Computer Science
Chair for Telecommunication Engineering

Design and Simulation of Non-Zero and Zero Dispersion Optical Lattice Wavelength Filters

by

Artha Sejati Ananda

Master Thesis

Executed from August 2003 to June 2004

Supervisor: prof. dr. ir. W.C. van Etten

Advisors: dr. ir. C.G.H. Roeloffzen

Ir. A. Meijerink

Summary

A multiwavelength optical network is an attractive technology to realize the potential of the huge bandwidth and transmission capacity of optical fiber and to build a flexible optical network. Optical filters are needed for multiplexing, demultiplexing, and add/drop functions. The most obvious application of the bandpass filters is to demultiplex very closely spaced wavelength channels.

In this thesis project, the dispersion of the used filters of the add-drop multiplexers (ADM) is the main problem to be overcome. Investigation of the solution for a zero dispersion of the complete ADM device is made. The approach for the analytical filter design synthesis is the digital signal processing technique. In this report, four kinds of filter are designed. Two types of them have linear phase response of the transfer function and hence zero dispersion. The other two filters have non-linear phase response of the transfer function and hence non-zero dispersion. All the filters are designed such as they have a passband flattened amplitude response.

The performance of the proposed filters will be analysed also. Simulations are made for a binary data input to check whether distortion and intersymbol interference occur after filtering.

Contents

1 Introduction

In this chapter, the background that motivates the project of the Master's thesis assignment is described. The organization of the thesis report is also explained afterwards.

1.1 Project Background

Optical communication has become a promising networking technology option to meet the increasing demand on bandwidth of emerging broadband computing and communication applications such as web browsing, e-commerce, video conference, video/audio on-demand processing, online database, etc. Advances in optical technology and the rapid demand of networking bandwidth have stimulated an increasing amount of research in the field of optical networks.

A multiwavelength optical network is an attractive technology to realize the potential of the huge bandwidth and transmission capacity of optical fiber and to build a flexible optical network. Wavelength Division Multiplexing (WDM) is used to divide the band in multiple wavelength sub-bands. A multiplexer (mux) combines the various channels and transfers them simultaneously over a single fiber, while a demultiplexer (demux) does the opposite, splits the aggregate channel into different fibers. Commercial deployment of WDM optical communication systems has boosted the demand for optical filters.

In WDM networks, optical cross-connects or optical add-drop multiplexers do the (de)multiplexing scheme for the individual wavelength channels. An optical cross connect is a device that switches the multiple high-speed optical signals. An optical signal in its path through the network traverses a cascade of WDM filters. Such network component may cause degradation of the optical signal. Degradation can be caused by the magnitude and phase (dispersion) characteristics of the (de)multiplexers.

Recently, work has been performed in a Dutch Technology Foundation STW project called "Flexible Multiwavelength Optical Local Access Network Supporting Multimedia Broadband Services" or "FLAMINGO" [Roe02]. The project consisted of three major tasks:

Task 1: Network issue protocol issues

Task 2: Tunable add-drop wavelength multiplexer

Task 3: Wavelength converter

The add-drop wavelength multiplexers that have been realized have non-zero dispersion filters. The dispersive characteristic of the add-drop multiplexer (ADM) is the main issue in this Master's project.

1.2 The Network Architecture

A typical network architecture for interconnected city rings is shown by Figure 1.1. The design is based on a multiple slotted ring network. The transmission scheme is multiwavelength (WDM). Access to each ring is via an Access Point (AP). Intelligent bridges connect each individual ring. The add-drop multiplexers are part of the AP and bridge.

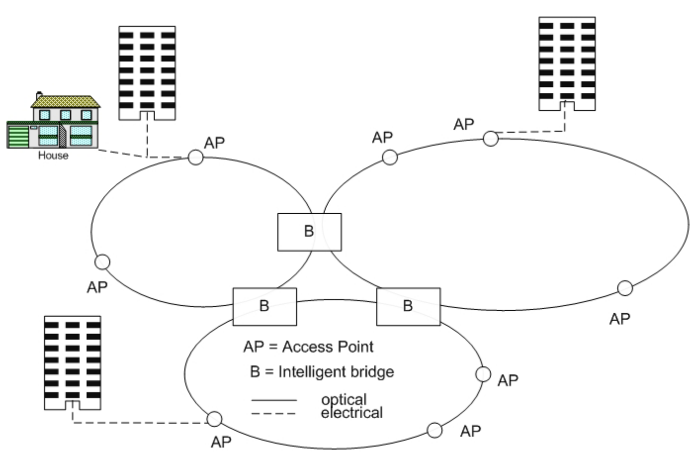

Figure 1.1. A typical network architecture

1.3 Bandpass Filters for Add/Drop Multiplexing

Optical filters are needed for multiplexing, demultiplexing, and add/drop functions. The most obvious application of the bandpass filters is to demultiplex very closely spaced wavelength channels. A bandpass filter is characterized by its transfer function passband width, loss, flatness, dispersion, and stopband isolation. Closer channel spacing requires sharper filter responses to separate channels without introducing cross talk from other channels. The used grid was 200 GHz channel spacing with the center wavelength of 1550 nm.

In multiple wavelength systems, the optically demultiplexed signals are detected and manipulated by an add-drop multiplexer or a switch in order to be routed to a different destination. In this way, each wavelength can be assigned individually and dynamically. This provides flexibility of the networks.

The ADM component developed is based on building blocks as shown in Figure 1.2 [1].

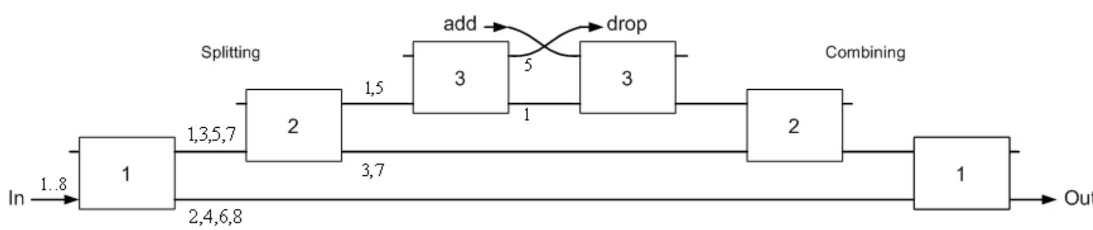

Figure 1.2. Schematic drawing of a 1-from-8 add-drop multiplexer

The 1-from-8 binary tree configuration has splitting and combining parts that comprises of several building blocks. Such blocks are called ‘slicers’ or ‘interleavers’ since the wavelengths will be split up in an alternating way. Referring to Figure 1.2 and 1.3, the first block separates the eight wavelength channels in odd and even numbered wavelengths. The four odd-numbered channels are sent to the next block where the ensemble is split up again in two times two channels. The process continues until only one wavelength remains at the drop port. The remaining wavelengths are led to the combining blocks where the wavelengths are recombined in a reverse manner. A new signal at the same wavelength as the dropped wavelength can be injected at the add port. Each wavelength can be selected to be added/dropped individually. The channel numbers in Figure 1.2 are just examples. Each slicer can be tuned over its free spectral range (FSR). Hence the even and odd numbered channel groups can be interchanged, for example, at the first slicer.

The first and last block of the ADM, indicated with nr. 1, have to split/combine the adjacent channels with wavelength spacing $\Delta\lambda$. Thus they have an FSR or periodicity of twice the channel spacing. Blocks nr. 2 have to split only the odd wavelengths and have a double FSR compared to the first. The last blocks have an FSR that is four times larger than the first ones. This is indicated in Figure 1.3.

The relation between the number of wavelength channels and the number of slicers is given by following equation:

$$\#\text{channels} = 2^{\left(\frac{\#\text{slicers}}{2}\right)} \tag{0.1}$$

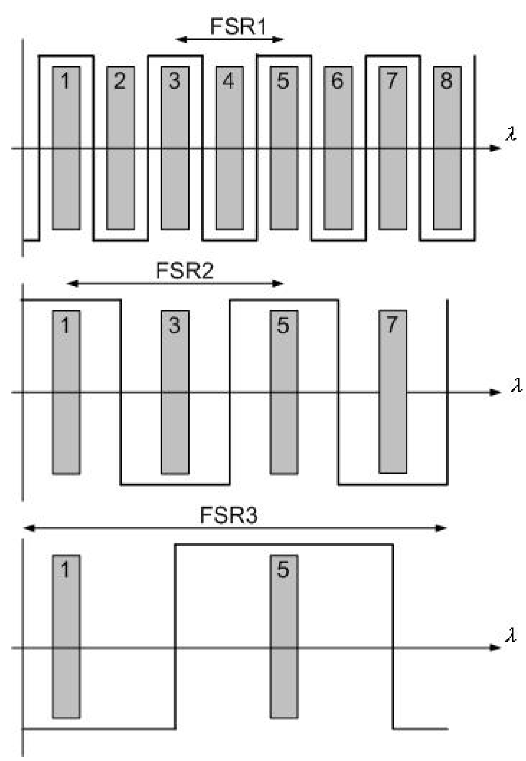

Figure 1.3. Demultiplexer filters responses of 1-from-8 ADM as depicted by Figure 1.2

The used filters were Mach-Zehnder Interferometer (MZI) type. Improvements over a single stage MZI were made, where two and three stages filters that have passband flattening amplitude responses were built. The filters have non-linear phase responses.

1.4 Project Objective

In this thesis project, the dispersion of the used filters of the ADM is the main problem to be overcome. The transfer functions of the filters have a passband flattened amplitude response, but still have a non-linear phase response. Investigation of the solution for a zero dispersion of the complete ADM device shall be made. The approach for the analytical filter design synthesis is the digital signal processing technique. One thing should be emphasized, since the filter is used as an interleaver, it is important to design filters that have the passband width as same as the stopband width.

The performance of the proposed filters will be analysed also. Simulations are made for a binary data input to check whether distortion and intersymbol interference occur.

1.5 Structure of the Report

As Chapter 1 gives introduction and summarizes the background of the thesis project, Chapter 2 gives the theoretical background of the operation principle of the ADM components, which have the Mach–Zender interferometer (MZI) as the fundamental building block. In Chapter 3, the mathematical design synthesis of the passband flattening filters is described along with the solution to have a zero dispersion filter. Chapter 4 contains the simulation results of the eye diagrams of the received data after being filtered. The last chapter, Chapter 5, contains the conclusions and recommendations of the project.

2 Digital Filter Descriptions of Mach-Zehnder Interferometers

In this project, digital signal processing approaches are applied to the design of the optical filters. The first section of this chapter explains the basic concepts of digital filters. Next, the theoretical background of the operation principle of a simple Mach-Zehnder interferometer as the fundamental building block of the ADM filters is described.

2.1 Digital Filter Basic Concepts

2.1.1 The *Z*-Transform

In digital filter concepts, the *z*-transform technique is widely used as a mathematical tool. The *z*-transform is an analytic extension of the discrete-time Fourier transform (DTFT) for discrete signals [2]. For a given sequence *h(n)*, its *z*-transform *H(z)* is defined as

$$H(z) = \mathcal{Z}\left\{h(n)\right\} = \sum_{n=-\infty}^{\infty} h(n) z^{-n} \tag{2.1}$$

where $z = \mathrm{Re}(z) + j\,\mathrm{Im}(z)$ is a complex variable that may have any magnitude and phase.

For $|z| = 1$ or $z = e^{j\omega}$, where ω here is the normalized angular frequency, the *z*-transform of *h*(*n*) is reduced to its discrete-time Fourier transform, provided that the latter exists. A circle of unit radius, $|z| = 1$, in the *z*-plane is called the *unit circle*, where the filter's frequency response is found by evaluating *H*(*z*) along $z = e^{j\omega}$. For the infinite series of Eq. (2.1) to be meaningful, a region of convergence must be specified. The set of values of *z* for which its *z*-transform attains a finite value is called the region of convergence, for example $R_- \le |z| \le R_+$, where R_- and R_+ are radii.

2.1.2 Poles and Zeros

Given the impulse response sequence $h(n)$ of a filter, its z-transform $H(z)$ is more commonly called the *transfer function* or the *system function*. Consider an input-output relation, where $y(n)$ and $x(n)$ are, respectively, the output and input sequences. If $Y(z)$, $X(z)$, and $H(z)$ denote the z-transforms of $y(n)$, $x(n)$, and $h(n)$, respectively, then the convolution resulting in the time domain reduces to its multiplication in the z domain [3].

$$Y(z) = H(z)X(z) \tag{2.2}$$

Thus, the transfer function $H(z)$ is obtained by dividing the output by the input in the z-domain.

$$H(z) = \frac{Y(z)}{X(z)} \tag{2.3}$$

The filter input and output are related by weighted sums of inputs and, if existing, previous outputs. The relation is described by the following equation [4]:

$$y(n) = -\sum_{k=1}^{N} a_k y(n-k) + \sum_{k=0}^{M} b_k x(n-k) \tag{2.4}$$

The weights are given by the coefficients a_k and b_k. The z-transform results in a rational transfer function in z^{-1}, i.e., it is a ratio of two polynomials in z^{-1}. The transfer function can be written as follows:

$$H(z) = \frac{\sum_{m=0}^{M} b_m z^{-m}}{1 + \sum_{n=1}^{N} a_n z^{-n}} = \frac{B(z)}{A(z)} \tag{2.5}$$

$A(z)$ and $B(z)$ are Nth and Mth-order polynomials respectively. An alternative way to represent the transfer function in Eq. (2.5) is to factor out the numerator and denominator polynomials leading to [3]:

$$H(z) = \Gamma \frac{\prod_{m=1}^{M}(1 - z_m z^{-1})}{\prod_{n=1}^{N}(1 - p_n z^{-1})} \tag{2.6}$$

or in terms of the roots of the polynomials as

$$H(z) = \Gamma z^{N-M} \frac{\prod_{m=1}^{M}(z - z_m)}{\prod_{n=1}^{N}(z - p_n)} \tag{2.7}$$

where Γ is the gain. A passive filter has a transfer function that can never be greater than 1, so the maximum value of Γ is determined by $\max\left\{\left|H(z)\right|_{z=e^{jw}}\right\} = 1$. The roots of the numerator polynomials in Eq. (2.6) and (2.7), designated by z_m, are called the *zeros* of $H(z)$, while the roots of the denominator polynomial which are designated by p_n are called the *poles* of $H(z)$. Provided that $z = e^{j\omega}$, a zero that happens on the unit circle, $|z_m| = 1$, results in zero transmission at that frequency.

A convenient graphical way to represent the transfer function is the *pole-zero plot* or *pole-zero diagram*. It shows the locations of each pole and zero in the complex plane. A zero is designated by *o* and a pole is designated by *x*. An example of a pole-zero diagram is depicted in Figure 2.1.

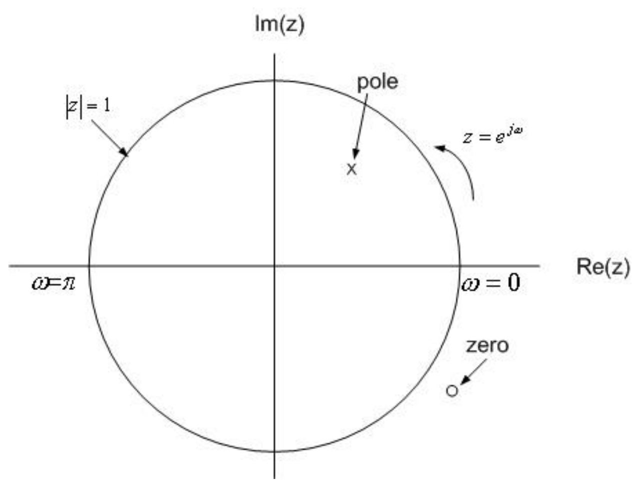

Figure 2.1. A pole-zero diagram with unit circle, one pole, and one zero

A filter that has only zeros in its transfer function is classified as a Moving Average (MA) filter and can be referred to as a Finite Impulse Response (FIR) filter. It has only feed-forward paths. An all-pole filter contains one or more feedback paths and is classified as an Autoregressive (AR) filter. A filter with both poles and zeros is classified as an Autoregressive Moving Average (ARMA) filter. A filter designated as Infinite

Impulse Response (IIR) filter contains at least one pole. The IIR filters may be either AR or ARMA types.

2.1.3 The Frequency Response

The Fourier transform relationship between the impulse response $h(n)$ and the frequency response function $H(\omega)$ is given by [4]:

$$H(\omega) = \sum_{n=-\infty}^{\infty} h(n) e^{-j\omega n} \tag{2.8}$$

The frequency response function $H(\omega)$ is a complex function of ω with a period of 2π. It is usually expressed in terms of its magnitude and phase.

$$H(\omega) = |H(\omega)| e^{j\Theta(\omega)} \tag{2.9}$$

The quantity $|H(\omega)|$ is called the *magnitude response* and the quantity $\Theta(\omega)$ is called the *phase response* where

$$\Theta(\omega) = \arg\{H(\omega)\} \tag{2.10}$$

The phase response can be extended for multiple zeros. The phase of the overall transfer function is the sum of the phases for each root, i.e. [2]:

$$H(\omega) = |H_{1z}(\omega)| \ldots |H_{Mz}(\omega)| e^{j[\Theta_{1z}(\omega)+\ldots+\Theta_{Mz}(\omega)]} \tag{2.11}$$

Sometimes, the magnitude is specified in decibels (dB) units as below:

$$|H(\omega)|_{\mathrm{dB}} = 20\log_{10}|H(\omega)| = 10\log_{10}|H(\omega)|^2 \tag{2.12}$$

If the region of convergence of $H(z)$ includes the unit circle, the frequency response of the system may be obtained by evaluating $H(z)$ on the unit circle, i.e.,

$$H(\omega) = H(e^{j\omega}) = H(z)\big|_{z=e^{j\omega}} \tag{2.13}$$

If the magnitude squared will be expressed in terms of $H(z)$, it is noted that [4]

$$|H(\omega)|^2 = H(\omega)H^*(\omega) \tag{2.14}$$

$H^*(\omega)$ is obtained by evaluating $H^*(1/z^*)$ on the unit circle. When the coefficients of the transfer function are real, then in this case, $H^*(1/z^*) = H(z^{-1})$ [4] and Eq. (2.14) becomes

$$|H(\omega)|^2 = H(\omega)H^*(\omega) = H(\omega)H(-\omega) = H(z)H(z^{-1})\Big|_{z=e^{j\omega}} \tag{2.15}$$

In particular, reciprocal zeros, which are mirror images of each other about the unit circle, have identical magnitude characteristics. Based on the pole-zero representation in $H(z)$, only the distance of each pole and zero from the unit circle, i.e. $|e^{j\omega} - p_n|$ or $|e^{j\omega} - z_m|$, affects the magnitude response. Hence the magnitude characteristic of a zero z_m will be identical with the magnitude characteristic of its reciprocal $1/z_m^*$, but they have different phase characteristics. Naming convention is used to distinguish both zeros. The zero with magnitude smaller than one, $|z_m| < 1$, is called *minimum-phase*, and the one with magnitude bigger than one, $|z_m| > 1$, is called *maximum-phase*. They will be explained in more details in Section 2.1.5.

2.1.4 Group Delay and Dispersion

Group delay is a measure of linearity of the phase response with respect to the frequency. The group delay is the local slope of the phase response curve, i.e., the slope of the phase at the frequency being evaluated. A filter's *group delay* or *envelope delay* is defined as the negative derivative of the phase response with respect to angular frequency as follows [4]:

$$\tau_g(\omega) = -\frac{\mathrm{d}\Theta(\omega)}{\mathrm{d}\omega} \tag{2.16}$$

For a sequence of discrete signals, each stage has a delay that is an integer multiple of a unit delay. If the angular frequency is normalized to the unit delay T such that $\omega' = \omega T$ then the normalized group delay, τ_g', is

$$\tau_g'(\omega') = -\frac{\mathrm{d}}{\mathrm{d}\omega'}\Theta(\omega') = -\frac{\mathrm{d}}{\mathrm{d}\omega'}\arg(H(z))\Big|_{z=e^{j\omega'}} \tag{2.17}$$

If the phase response is in radians and the angular frequency ω is in radians per second, then the absolute group delay is given in seconds. The normalized group delay is given in the number of the delay with respect to the unit delay T. The relation between the absolute group delay and the normalized group delay is given by [2]

$$\tau_g = T \cdot \tau_g' \tag{2.18}$$

It is important to notice the filter dispersion. *Dispersion* is the derivative of the group delay. For normalized frequency $f' = fT$, the normalized dispersion is [2]

$$D' \equiv \frac{\mathrm{d}\tau_g'}{\mathrm{d}f'} = 2\pi \frac{\mathrm{d}\tau_g'}{\mathrm{d}\omega'} \tag{2.19}$$

and the filter dispersion D in absolute units is [1]

$$D = -c_0 \left(\frac{T}{\lambda}\right)^2 D' \qquad \text{[ps/nm]} \tag{2.20}$$

In comparison, for optical fibers, dispersion D is typically defined as the derivative of the group delay with respect to wavelength (λ) and normalized with respect to length (L) [2],

$$D = \frac{1}{L}\frac{\mathrm{d}\tau_g}{\mathrm{d}\lambda} \qquad \text{[ps/nm/km]} \tag{2.21}$$

2.1.5 Linear Phase Filters

Of particular interest are the linear phase filters. Those filters have constant group delays and thus they are dispersion-less. A distortion-less filter has a magnitude response that is flat across the frequency band of the input signal and the phase response in the passband region is a linear function of frequency. Linear phase filters are important in applications where no phase distortion is allowed. A moving average or a FIR filter can be designed to have linear phase.

As mentioned in Section 2.1.3, two zeros that are reciprocally mirrored about the unit circle give identical magnitude characteristics. Consider two systems having transfer functions:

$$H_1(z) = 1 - \frac{1}{5} z^{-1} \tag{2.22}$$

$$H_2(z) = \frac{1}{5} - z^{-1} \tag{2.23}$$

$H_1(z)$ has a zero at $z_m = 1/5$, which is a minimum-phase, and $H_2(z)$ has a zero at $z_m = 5$, which is a maximum-phase. They both have identical magnitude characteristics but different phase responses as depicted by Figure 2.2. Note that these functions are just as examples, in fact passive device cannot have a transfer function greater than one. It can be observed from the phase responses, the first system having minimum-phase zero has a net phase change of zero at the frequency range of $\omega' = 0$ to $\omega' = \pi$. On the other hand, the system having maximum-phase zero has a net phase change of $-\pi$ radians at the frequency range of $\omega' = 0$ to $\omega' = \pi$. Figure 2.3 shows the normalized group delays and the normalized dispersion of both systems. The minimum-phase system implies a minimum delay function, while the maximum-phase system implies a maximum delay function.

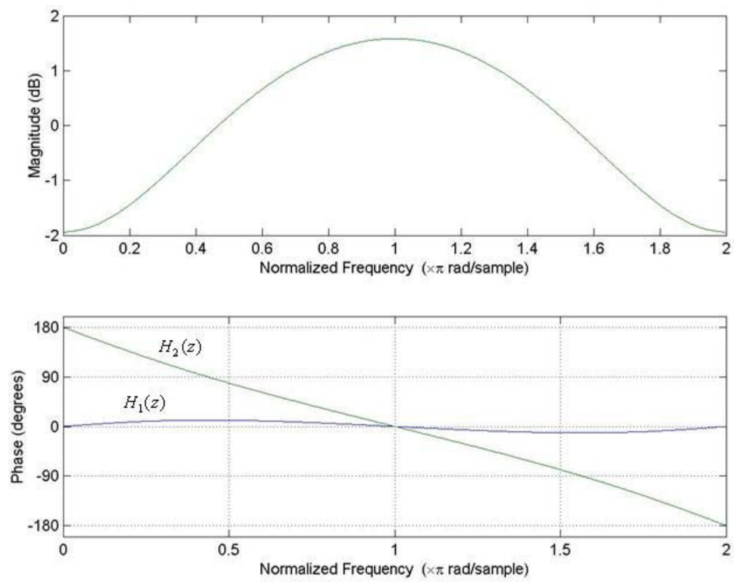

Figure 2.2. Magnitude response and phase response of a minimum-phase system and a maximum-phase system

Since the overall phase is additive for multiple zeros or a multistage filter, it is expected to have a linear phase response by placing a pair of zeros that is reciprocally mirrored about the unit circle. The group delay responses of two single-stage filters whose zeros are located at mirror image positions about the unit circle are related by [2]

$$\tau_{1z}\left(\frac{1}{r},\varphi\right) = 1 - \tau_{1z}(r,\varphi) \tag{2.24}$$

where τ_{1z} is the group delay of a single zero system, r is the magnitude of the zero, and φ is the phase of the zero. Eq. (2.24) shows that the two reciprocally mirrored zeros cancel each other's frequency dependence phase response and leave a constant group delay.

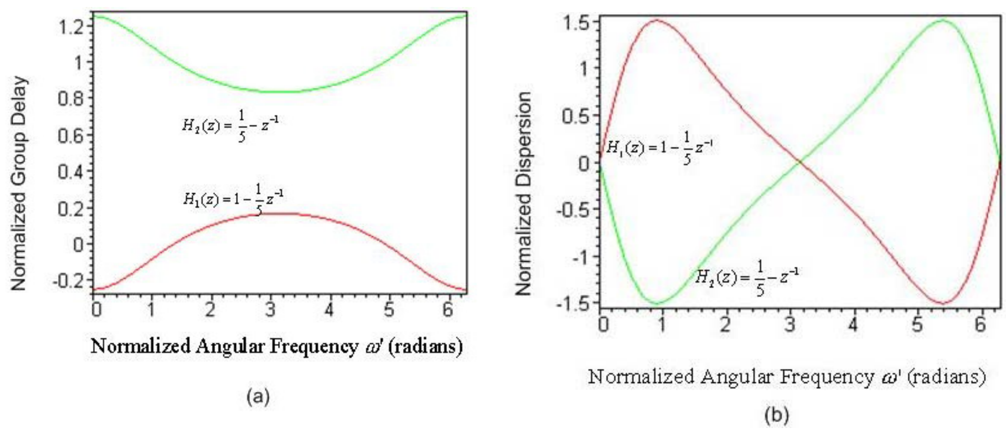

Figure 2.3. Normalized group delay (a) and normalized dispersion (b) of a minimum phase and a maximum phase system

The transfer function of a linear phase filter has a mirror–image polynomial form. This is due to the symmetry condition of the filter characteristic. The values of the unit sample response $h(n)$ of the filter or the filter coefficients of a filter with length N (with filter order of $N-1$) satisfy symmetric or antisymmetric conditions as below [5]:

$$h(n) = h(N-1-n) \tag{2.25}$$

$$h(n) = -h(N-1-n) \tag{2.26}$$

for $0 < n < N-1$. Appendix A describes this symmetry property of linear phase filters.

2.2 Single-Stage Mach-Zehnder Interferometer

The fundamental building block for the ADM filters is the Asymmetric Mach-Zehnder interferometer (MZI). In order to get an understanding of how the device works or possible advanced improvements for further filter design, the concepts of the transfer matrix method and the z-transform will be described.

2.2.1 Transfer Matrix Method

A single-stage MZI consists of two directional couplers with power coupling ratios κ_1 and κ_2, and one delay line as shown by Figure 2.4. The MZI is a 2×2 port device. It has two input ports and two output ports. $E_{1_{in}}$ and $E_{2_{in}}$ represent the coupler inputs complex field amplitudes, while $E_{1_{out}}$ and $E_{2_{out}}$ represent the coupler output complex field amplitudes. The delay section is formed by two independent waveguides having different lengths L_1 and L_2. In this work, it is assumed $L_1 > L_2$. Due to this delay line, the output intensity of the MZI has discrete delays and is wavelength dependent.

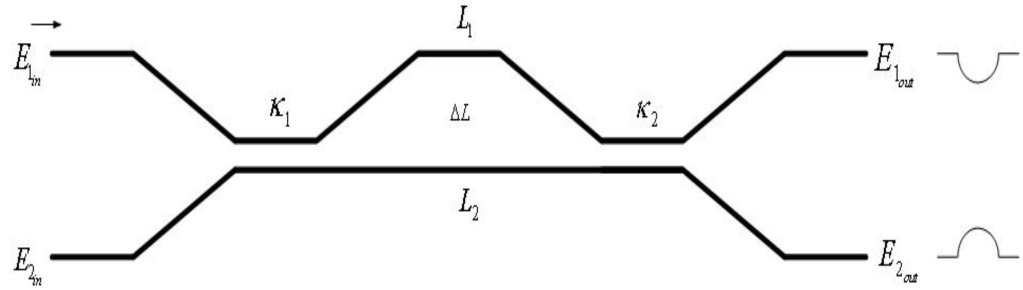

Figure 2.4. An asymmetric Mach-Zehnder Interferometer waveguide layout

The transfer matrix relates field quantities in one plane to those in another one. In this case, the quantities in input ports to those in output ports. Consider a device such as the above MZI, having two input ports each carrying electric fields having complex amplitudes $E_{1_{in}}$ and $E_{2_{in}}$ respectively, and two output ports with fields $E_{1_{out}}$ and $E_{2_{out}}$. The relation between the fields in input ports and output ports may be given by

$$\begin{pmatrix} E_{1_{out}} \\ E_{2_{out}} \end{pmatrix} = \mathbf{H} \begin{pmatrix} E_{1_{in}} \\ E_{2_{in}} \end{pmatrix} = \begin{pmatrix} H_{11} & H_{12} \\ H_{21} & H_{22} \end{pmatrix} \begin{pmatrix} E_{1_{in}} \\ E_{2_{in}} \end{pmatrix} \tag{2.27}$$

where the complex matrix **H** is the transfer matrix consisting of two bar transfer functions (H_{11} and H_{22}), or sometimes called the through transfer function, and two cross transfer functions (H_{12} and H_{21}).

The transfer matrix of the directional coupler is given by [2]

$$\mathbf{H}_{dc} = \begin{pmatrix} c & -js \\ -js & c \end{pmatrix} \tag{2.28}$$

The through and cross-port transmission, c and $-js$, are defined as

$$c = \sqrt{1-\kappa} \tag{2.29}$$

$$-js = -j\sqrt{\kappa} \tag{2.30}$$

where κ is the power coupling ratio. The above transfer matrix assumes that no excess loss is introduced. Hence the sum of the output powers equals the sum of the input powers.

At the delay line, it is assumed almost identical branches, in particular having the same attenuation coefficient α of the single guided mode, but if it is allowed for a small deviation from the average effective index N_{eff}, then an additional phase delay φ in branch 1 with respect to branch 2 is introduced. The transfer matrix of the delay lines is given by

$$\mathbf{H}_{delay} = \begin{pmatrix} e^{-\alpha L_1} e^{-jk_0 N_{eff} L_1} e^{-j\varphi} & 0 \\ 0 & e^{-\alpha L_2} e^{-jk_0 N_{eff} L_2} \end{pmatrix} \tag{2.31}$$

where $k_0 = \omega/c$ is the vacuum wave number, ω is the angular frequency of the guided wave, and c is the vacuum speed of light. The term $e^{-\alpha L_1} e^{-jk_0 N_{eff} L_1}$ is the propagation factor of the first waveguide branch. If the differential delay is defined as:

$$T = \frac{(L_1 - L_2) N_{eff}}{c} = \frac{\Delta L . N_{eff}}{c} \tag{2.32}$$

then taking branch 2 as the reference, the delay transfer matrix can be written in terms of T as:

$$\mathbf{H}_{delay} = \gamma \begin{pmatrix} \gamma_{\Delta L} e^{-j\omega T} e^{-j\varphi} & 0 \\ 0 & 1 \end{pmatrix} \tag{2.33}$$

where propagation constant $\gamma = e^{-\alpha L_2} e^{-j\beta L_2}$, comprising attenuation $|\gamma| = e^{-\alpha L_2}$ and an overall phase delay $e^{-j\beta L_2} = e^{-jk_0 N_{eff} L_2}$, while $\gamma_{\Delta L} = e^{-\alpha \Delta L}$ is the differential loss along the differential path length ΔL.

The relation between the free spectral range (FSR) and the delay T can be expressed as [Mad99]

$$FSR = \Delta f = \frac{c}{N_g L_U} = \frac{1}{T} \tag{2.34}$$

where L_U is the unit delay and N_g is the group index. The description above is slightly more in-depth then in Eq. (2.32) in the sense of the group index that can deviate considerably from the effective index N_{eff} for the used waveguides.

$$N_g = N_{eff}(f_0) + f_0 \left. \frac{dN_{eff}}{df} \right|_{f_0} = N_{eff}(\lambda_0) - \lambda_0 \left. \frac{dN_{eff}}{d\lambda} \right|_{\lambda_0} \tag{2.35}$$

It is useful to introduce the normalized angular frequency with respect to the free spectral range ($FSR_f = 1/T$). The delay section has a periodic angular frequency response with period $\Delta\omega = 2\pi/T$ or $\Delta f = 1/T$. The transfer function in terms of the normalized angular frequency $\omega' = \omega T$ or $f' = fT$ will be periodic with period $\Delta\omega' = 2\pi$ or $\Delta f' = 1$. Hence by making a substitution in the z-transform

$$e^{-j\omega'} = z^{-1} \tag{2.36}$$

the transfer matrix in Eq. (2.33) becomes

$$\mathbf{H}_{delay} = \gamma \begin{pmatrix} \gamma_{\Delta L} z^{-1} e^{-j\varphi} & 0 \\ 0 & 1 \end{pmatrix} \tag{2.37}$$

The total transfer matrix for a single stage MZI is then found by multiplication of each of the transfer matrix of the first directional coupler, delay section, and the second directional coupler.

$$\mathbf{H}_{\mathbf{MZI}} = \mathbf{H}_{dc_2} \mathbf{H}_{delay} \mathbf{H}_{dc_1} \tag{2.38}$$

Hence, the overall transfer matrix in z polynomials is

$$\mathbf{H}_{\mathbf{MZI}} = \begin{pmatrix} H_{11}(z) & H_{12}(z) \\ H_{21}(z) & H_{22}(z) \end{pmatrix} = \gamma \begin{pmatrix} -s_1 s_2 + c_1 c_2 \gamma_{\Delta L} z^{-1} e^{-j\varphi} & -j(c_1 s_2 + s_1 c_2 \gamma_{\Delta L} z^{-1} e^{-j\varphi}) \\ -j(s_1 c_2 + c_1 s_2 \gamma_{\Delta L} z^{-1} e^{-j\varphi}) & c_1 c_2 - s_1 s_2 \gamma_{\Delta L} z^{-1} e^{-j\varphi} \end{pmatrix} \tag{2.39}$$

If the common path length is neglected (since it only adds constant loss and linear phase to the frequency response) and the loss along the differential path length, $\gamma_{\Delta L}$, also neglected because typically $\Delta L << L_2$, then it comes to:

$$\mathbf{H}_{\mathbf{MZI}}(z) = \begin{pmatrix} -s_1 s_2 + c_1 c_2 z^{-1} e^{-j\varphi} & -j(c_1 s_2 + s_1 c_2 z^{-1} e^{-j\varphi}) \\ -j(s_1 c_2 + c_1 s_2 z^{-1} e^{-j\varphi}) & c_1 c_2 - s_1 s_2 z^{-1} e^{-j\varphi} \end{pmatrix} = \begin{pmatrix} A(z) & B^R(z) \\ B(z) & A^R(z) \end{pmatrix} \tag{2.40}$$

Figure 2.5 shows the z-transform schematic of the MZI where the additional phase delay φ is neglected. In the transfer matrix, z^{-1} can be reintroduced later by $z^{-1}e^{-j\varphi}$ if there is additional phase delay φ.

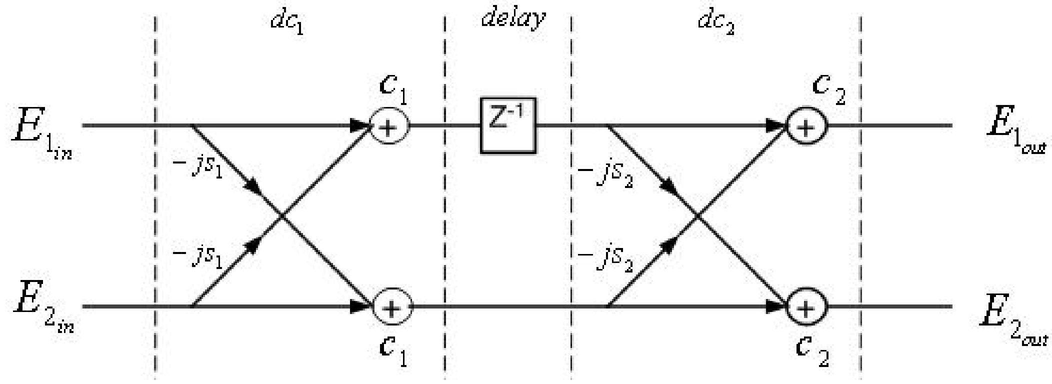

Figure 2.5. A single-stage Mach-Zehnder Interferometer z-transform schematic consisting of two directional couplers and one delay line

The coefficients of the polynomial of $H_{22}(z)$ are in reverse order compared to $H_{11}(z)$, and so thus for $H_{12}(z)$ and $H_{21}(z)$. $A(z)$ and $B(z)$ are the forward polynomials for the bar and cross transfer respectively, while $A^R(z)$ and $B^R(z)$ are the reverse polynomials. See Appendix B for the explanation of forward and reverse polynomials. The transfer matrix can also be written in terms of the roots of the polynomials as follows:

$$\mathbf{H_{MZI}}(z) = \begin{pmatrix} -s_1 s_2 z^{-1}(z - \frac{c_1 c_2}{s_1 s_2} e^{-j\varphi}) & -jc_1 s_2 z^{-1}(z - (-\frac{s_1 c_2}{c_1 s_2} e^{-j\varphi})) \\ -js_1 c_2 z^{-1}(z - (-\frac{c_1 s_2}{s_1 c_2} e^{-j\varphi})) & c_1 c_2 z^{-1}(z - \frac{s_1 s_2}{c_1 c_2} e^{-j\varphi}) \end{pmatrix} \tag{2.41}$$

The zeros and poles position in the z-plane depends on the coupling ratios and the phase φ. The behavior of a filter over its free spectral range can be investigated by evaluating its transfer matrix. A zero that occurs on the unit circle, $|z_m| = 1$, results in zero transmission at that frequency. Since passive devices never have an infinite transfer, possible poles will never occur on the unit circle.

When the two couplers are identical ($\kappa = \kappa_1 = \kappa_2$) and the additional phase delay is neglected for convenience, the transfer matrix becomes:

$$\mathbf{H_{MZI}}(z) = \begin{pmatrix} -s^2 z^{-1}(z - \frac{c^2}{s^2}) & -jscz^{-1}(z - (-1)) \\ -jscz^{-1}(z - (-1)) & c^2 z^{-1}(z - \frac{s^2}{c^2}) \end{pmatrix} \tag{2.42}$$

The cross transfers always have a zero on the unit circle. Bar transfers have a zero on the unit circle if $c^2 = s^2$. Hence, if $\kappa = \kappa_1 = \kappa_2 = 0.5$, both bar and cross transfers have a zero on the unit circle. So a 3 dB coupler has a zero transmission at the bar transfer at the normalized frequency of $\omega = 0$ and $\omega = 2\pi$, and at the cross transfer at the normalized frequency of $\omega = \pi$.

2.2.2 Frequency Responses of a Mach-Zehnder Interferometer

Referring to Section 2.1.3 and the transfer matrix obtained in Section 2.2.1, the magnitude responses of the bar and cross transfers of a single-stage MZI are calculated. The magnitude response of the bar transmission of an MZI with differential loss $\gamma_{\Delta L}$ in term of the normalized angular frequency is found as:

$$\left|H_{11}(\omega')\right|^2 = \left|H_{22}(\omega')\right|^2 = \kappa_1\kappa_2 + (1-\kappa_1)(1-\kappa_2)\gamma_{\Delta L}^2 - 2\sqrt{\kappa_1\kappa_2}\sqrt{(1-\kappa_1)(1-\kappa_2)}\gamma_{\Delta L}\cos\omega' \quad (2.43)$$

For identical couplers, it reduces to

$$\left|H_{11}(\omega')\right|^2 = \left|H_{22}(\omega')\right|^2 = \kappa^2 + (1-\kappa)^2\gamma_{\Delta L}^2 + 2(\kappa^2 - \kappa)\gamma_{\Delta L}\cos\omega' \quad (2.44)$$

For a 3 dB coupler, $\kappa = 0.5$, hence

$$\left|H_{11}(\omega')\right|^2 = \left|H_{22}(\omega')\right|^2 = \gamma_{\Delta L}\sin^2\left(\frac{\omega'}{2}\right) + \frac{1}{4}\left(1-\gamma_{\Delta L}\right)^2 \quad (2.45)$$

If the differential loss is neglected, $\alpha = 0$ hence $\gamma_{\Delta L} = 1$, then

$$\left|H_{11}(\omega')\right|^2 = \left|H_{22}(\omega')\right|^2 = \sin^2(\frac{\omega'}{2}) \quad (2.46)$$

The magnitude response of the cross transmission of an MZI with differential loss $\gamma_{\Delta L}$ is found as:

$$\left|H_{12}(\omega')\right|^2 = \left|H_{21}(\omega')\right|^2 = (\kappa_2 - \kappa_1\kappa_2)\gamma_{\Delta L}^2 + \kappa_1 - \kappa_1\kappa_2 + 2\sqrt{\kappa_2(1-\kappa_1)}\sqrt{\kappa_1(1-\kappa_2)}\gamma_{\Delta L}\cos\omega' \quad (2.47)$$

For identical couplers, it reduces to

$$\left|H_{12}(\omega')\right|^2 = \left|H_{21}(\omega')\right|^2 = \gamma_{\Delta L}4(\kappa - \kappa^2)\cos^2\left(\frac{\omega'}{2}\right) + (\kappa - \kappa^2)(1-\gamma_{\Delta L})^2 \quad (2.48)$$

For 3 dB coupler, $\kappa = 0.5$, hence

$$\left|H_{12}(\omega')\right|^2 = \left|H_{21}(\omega')\right|^2 = \gamma_{\Delta L}\cos^2\left(\frac{\omega'}{2}\right) + \frac{1}{4}(1-\gamma_{\Delta L})^2 \quad (2.49)$$

If the differential loss is neglected, $\alpha = 0$ hence $\gamma_{\Delta L} = 1$, then

$$\left|H_{12}(\omega')\right|^2 = \left|H_{21}(\omega')\right|^2 = \cos^2\left(\frac{\omega'}{2}\right) \tag{2.50}$$

The transfer matrix satisfies the power conservation (see Appendix C). The sum of the power of bar transfer and the power of the cross transfer is equal to one. For instance, a lossless 3 dB coupler, will satisfy the conditions:

$$\left|H_{11}(\omega')\right|^2 + \left|H_{12}(\omega')\right|^2 = \sin^2(\frac{\omega'}{2}) + \cos^2(\frac{\omega'}{2}) = 1 \tag{2.51}$$

$$\left|H_{21}(\omega')\right|^2 + \left|H_{22}(\omega')\right|^2 = \cos^2(\frac{\omega'}{2}) + \sin^2(\frac{\omega'}{2}) = 1 \tag{2.52}$$

The phase response is found from the argument term of the transfer function as explained in Section 2.1.3. The phase response for bar transmission of a lossless MZI and identical power coupling ratio, $\kappa = \kappa_1 = \kappa_2 = 0.5$, is

$$\Theta_{11}(\omega') = \Theta_{22}(\omega') = \tan^{-1}\left[\frac{\sin\omega'}{1-\cos\omega'}\right] \tag{2.53}$$

and the phase response for the cross transfer is

$$\Theta_{12}(\omega') = \Theta_{21}(\omega') = \tan^{-1}\left[\frac{1+\cos\omega'}{\sin\omega'}\right] \tag{2.54}$$

Figure 2.6 shows the magnitude and phase responses of the MZI for various differential losses. Note that the magnitude curves are sine shaped and they have very narrow stopbands. The stopband width at the stopband rejection of –25 dB is only about 4% of the FSR or 8% of the channel spacing. The phase response calculated starts from -90° and continues linearly across the passband until reaches near -180°. The phase response shows a discontinuity when the intensity is zero at the normalized angular frequency of $\omega = \pi$. The phase value is calculated again slightly after $\omega = \pi$. The intensity of the 1 dB loss curve is shallower at the transmission nulls and the phase response is not as steep as the zero loss curve at the stopband.

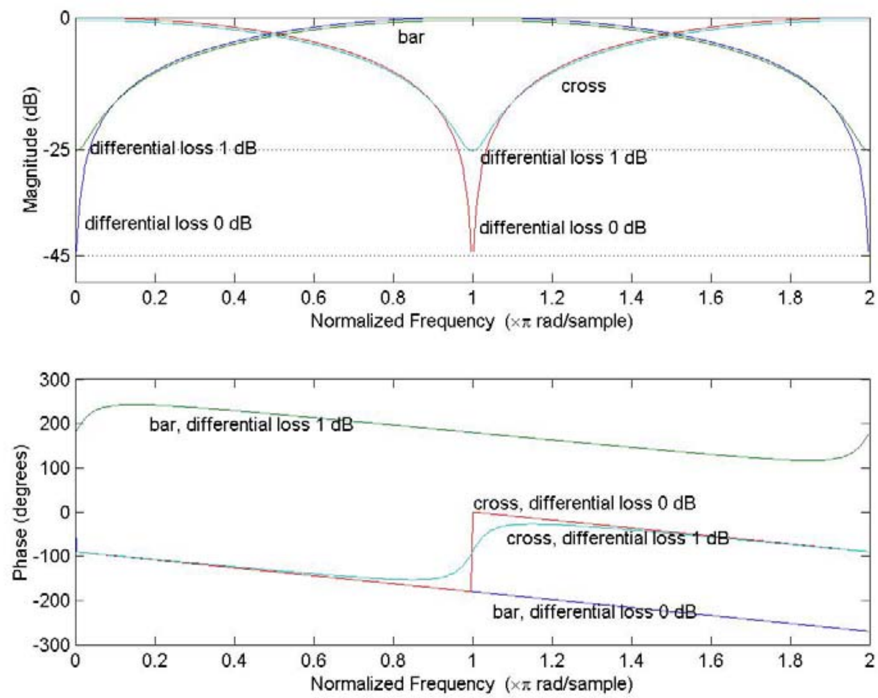

Figure 2.6. Magnitude and phase responses of a single-stage Mach-Zehnder Interferometer with differential loss of 0 and 1 dB

2.2.3 Group Delay and Dispersion of the Mach-Zehnder Interferometer

As has been explained in Section 2.1.4, the group delay is derived from the negative derivative of the phase response with respect to the angular frequency. Figure 2.7 shows the normalized group delay of the bar transmission for various power coupling ratios. Each curve shows the values of the normalized group delay versus normalized angular frequency for different power coupling ratios.

Figure 2.8 shows the normalized dispersion of the bar transmission of the MZI for various power coupling ratios. The dispersion sweeps from the stopband region to the passband region where in the passband the dispersion is lower. Note from the figures that the ideal MZI, $\kappa = 0.5$ and zero $\left|z_m\right| = 1$, has a constant group delay and thus zero dispersion. The group delay and dispersion go to infinite when κ goes to 0.5, but they go higher in the stopband region where the intensity transfer goes to zero.

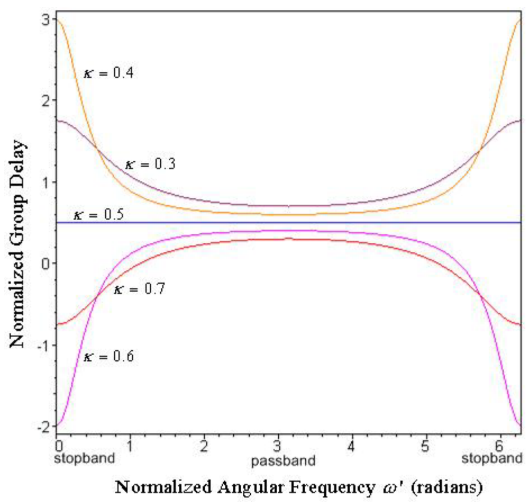

Figure 2.7. Normalized group delay of the bar transmission of Mach-Zehnder Interferometer for various coupling ratios

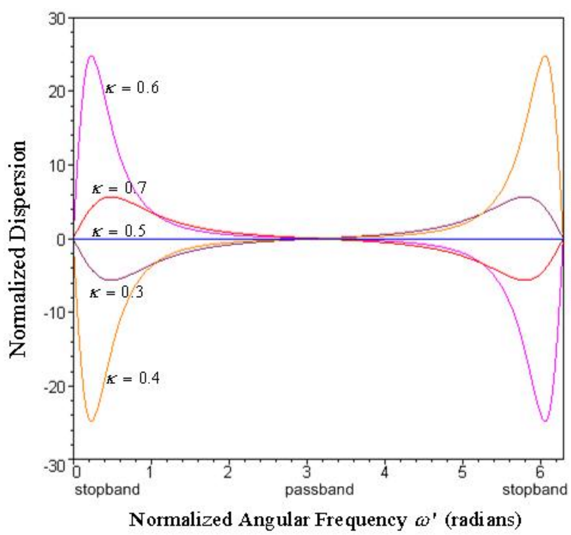

Figure 2.8. Normalized dispersion of the bar transmission of Mach-Zehnder Interferometer for various coupling ratios

2.3 Lattice Filters of Mach-Zehnder Interferometer

As noted from previous sections, the frequency response of the transfer function of a single-stage MZI filter has a very narrow stopband and a non-flattened passband. Sometimes some applications need a broader stopband or passband width. One way to improve the filter performance is to realize a multistage filter by concatenating the MZIs in a lattice structure. This is also called Multi-Stage Moving Average filter or resonant coupler. Figure 2.9 shows an example of a two-stage lattice filter. It is a 2×2 port device with two input ports and two output ports. It consists of three directional couplers and two delay lines.

In general, an *N* stage filter has *N*+1 directional couplers and *N* delay lines. An *N*-th order filter can be made with this multistage configuration. Using the *z*-transformation, the filter response can be represented by the polynomial form in *z*. A synthesis algorithm that can calculate the optical filter parameters from a desired filter response has been presented successfully in literatures [6], [2]. This algorithm uses recursion equations to map the filter coefficients designed with digital filter tools to the power coupling ratios of each directional coupler and the phase of each delay line. Note that although a polynomial filter of a very high order, e.g. order of one hundred, can be realized in digital filters, it is still not possible to realize an optical filter device with a larger number of delay lines due to the chip space restriction and optical losses [1]. Moreover it adds complexity since every additional delay section needs an independent tuning element.

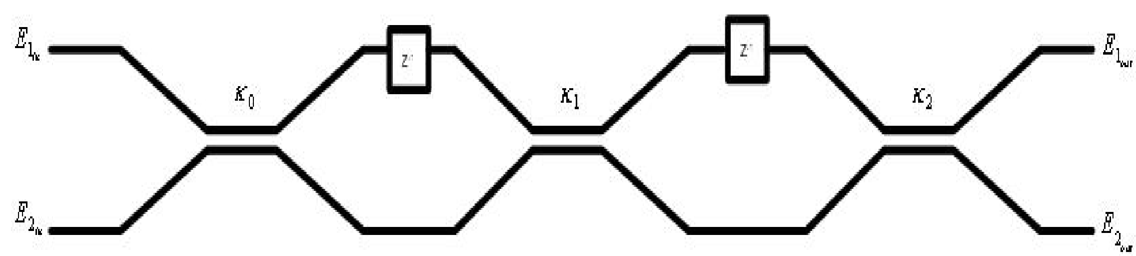

Figure 2.9. A 2×2 port two-stage lattice filter

3 Passband Flattened Filters Design

This chapter describes the mathematical design of the passband flattened interleaver including linear phase filters using Mach-Zehnder interferometer based lattice filters.

3.1 Filter Requirements

Bandpass optical filters can be used in the binary tree add-drop multiplexer. The filters have to fulfill some requirements. Since the filters are to be used as slicers or interleavers, some specific requirements need to be fulfilled. Below are the desired properties of the slicers:

1. They must have broad passband and stopband so that the available bandwidth can be used as efficiently as possible
2. The passband width must be equal to the stopband width since the wavelength channels are sent to the cross and bar port
3. They must have linear phase response functions in the passband region and hence zero dispersion
4. They have minimal loss at the passband
5. The cross and bar ports fulfill the power conservation rule since the MZI is a passive device
6. Good isolation or stopband rejection; to be noted, it is difficult to fabricate filters having better isolation than 25 dB [Roe02]

3.2 Filter Design Synthesis

In this work, four types of filters are designed. First, a third order passband flattened filter with non-linear phase response is designed followed by a fourth order linear phase passband flattened filter. A fifth order filter with broader stopband width but still having non-linear phase response is built then followed by a seventh order passband flattened filter with linear phase response.

Figure 3.1 summarizes the filters design synthesis process. There are four general steps in the process as described below.

3.2.1 Definition of the Filter Order

In this first step, Figure 3.1(a), the number of zeros, which is equal to the order of the filter, is defined. The number of zeros that can be chosen is three, four, five, or seven depending on the filter order. The number of zeros is related with the desired filter response. The desired filter response can be approximated by placing the zeros on the complex *z*-plane.

3.2.2 Generation of the Cross Port Transfer Function

This step is as depicted by Figure 3.1(b)-(e). To generate the cross transfer function, the positions of the zeros on the unit circle are described first. These zeros give zero intensity transfer at their normalized frequencies and thus define the stopband width. There are side-lobes in between each zero. Increasing the distance between each zero means that the stopband is broadened, but the side-lobe level also rises. Hence it gives limitation on the stopband width. The zeros are chosen such that the maximum side lobe level is -25 dB.

The rest of the zeros for each filter are defined using the condition that the passband width is equal to the stopband width. Referring to Eq. (2.15), the magnitude squared of a cross transfer function, *B(z)*, with real coefficients is

$$\left|B(z)\right|^2 = B(z)B(z^{-1})\Big|_{z=e^{j\omega'}} \tag{2.55}$$

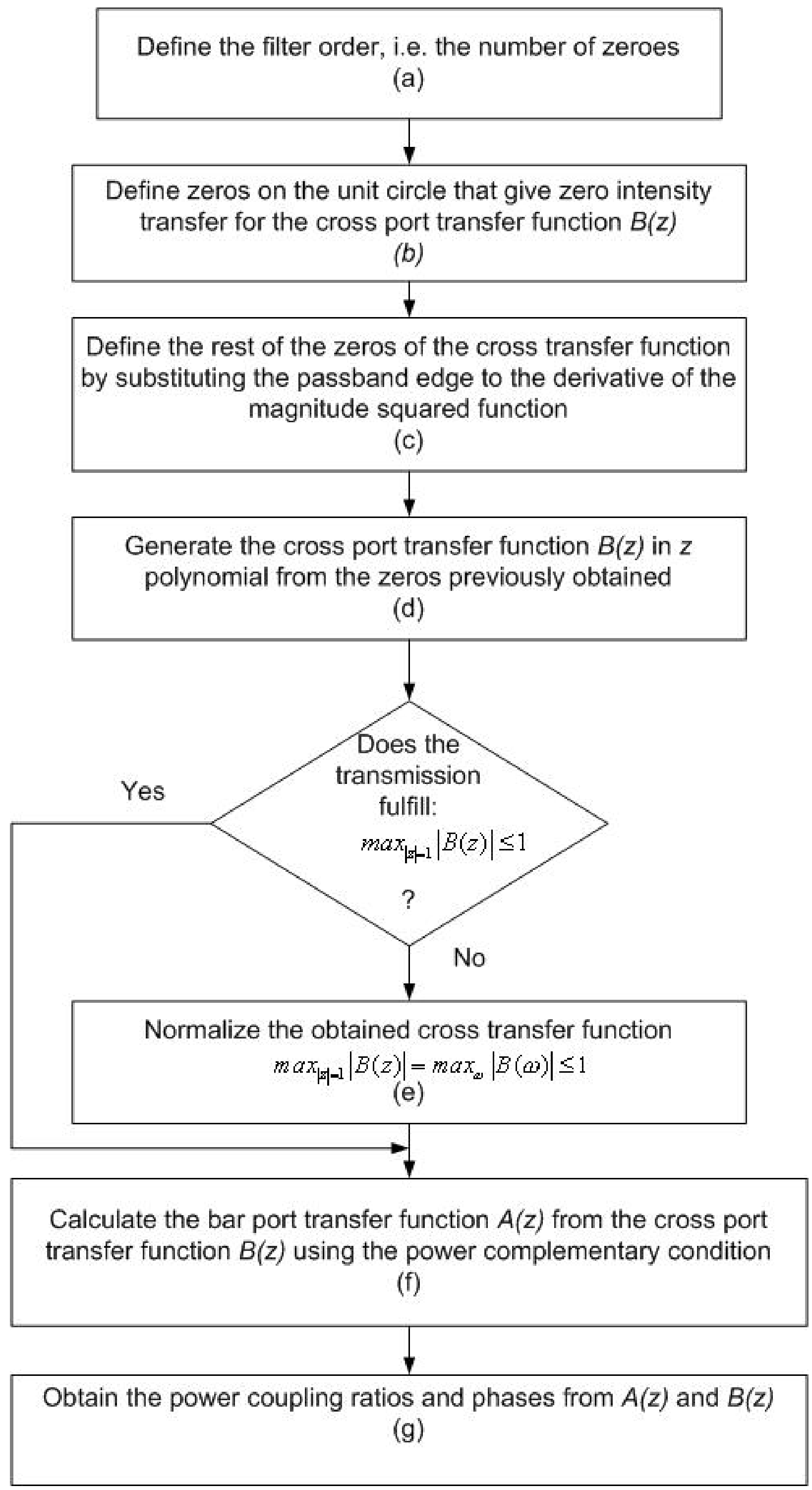

Figure 3.1. Passband flattened filters design synthesis flowchart

while the transfer function can be written in terms of its roots as

$$B(z) = \Gamma \prod_{m=1}^{M} (1 - z_m z^{-1}) \tag{2.56}$$

Substituting the unity zeros to Eq. (3.2) and applying Eq. (3.1), the magnitude squared function can be represented in terms of the unknown zeros and gain Γ. Note that linear phase filters have at least a pair of zeros that is reciprocally mirrored about the unit circle. The maxima of the magnitude squared curve are at the passband edges.

Taking the derivative of Eq. (3.1) with respect to the normalized angular frequency ω' as zero at the passband edge point, the constant Γ could be eliminated and the unknown zeros can be determined. From Eq. (3.1) and (3.2),

$$\begin{aligned}
\left|B(z)\right|^2\Big|_{z=e^{j\omega'}} &= \Gamma \prod_{m=1}^{M} (1 - z_m z^{-1}) \cdot \Gamma \prod_{m=1}^{M} (1 - z_m z)\Big|_{z=e^{j\omega'}} \\
\frac{\mathrm{d}\left|B(z)\right|^2\Big|_{z=e^{j\omega'}}}{\mathrm{d}(\omega')} &= \Gamma^2 \prod_{m=1}^{M} \frac{\mathrm{d}[(1 - z_m z^{-1})(1 - z_m z)\big|_{z=e^{j\omega'}}]}{\mathrm{d}(\omega')} \\
0 &= \Gamma^2 \prod_{m=1}^{M} \frac{\mathrm{d}[(1 - z_m z^{-1})(1 - z_m z)\big|_{z=e^{j\omega'}}]}{\mathrm{d}(\omega')} \\
0 &= \prod_{m=1}^{M} \frac{\mathrm{d}[(1 - z_m z^{-1})(1 - z_m z)\big|_{z=e^{j\omega'}}]}{\mathrm{d}(\omega')}
\end{aligned} \tag{2.57}$$

The derivations of calculations in more details will be explained in next sections for each filter type.

The third order filter has two zeros on the unit circle and one unknown zero. Meanwhile, the fourth order linear phase filter has two zeros on the unit circle and two unknown zeros, but still has one degree of freedom left since the two unknown zeros are the mirror of each other in order to have a linear phase response. The fifth order filter has three zeros on the unit circle and two unknown zeros, while the seventh order linear phase filter has three zeros on the unit circle and four unknown zeros but also still have two unknown variables since the four unknown zeros are two pairs of mirrored zeros. For the fifth and seventh order filters, the analysis of zero derivative of Eq. (3.1) with respect to the normalized angular frequency are taken at two points, one is at the passband edge point and the other is at half-width of the passband which is related with the side lobe position in the stopband.

Figure 3.2 shows the positions of zeros of each filter. For the third order filter, the position of the third zero, z_3, can be replaced by its reciprocal mirror $1/z_3^*$ since both zeros give same magnitude response. The same condition applies to the fifth order filter whose unknown fourth and fifth zeros inside the unit circle can be replaced by their mirrors outside the unit circle.

After obtaining all the zeros, the cross transfer function *B(z)* is calculated using Eq. (3.2) with the gain Γ is first considered as equal to one. Then the frequency response of the cross transfer function is calculated. Since the transmission of a passive device such as this Mach-Zehnder interferometer cannot exceed one, the transfer function should be normalized such that the maximum transmission cannot be greater than one. Below is the normalization process performed,

$$max_{|z|=1}\left|B(z)\right| = max_{\omega}\left|B(\omega)\right| \le 1 \tag{2.58}$$

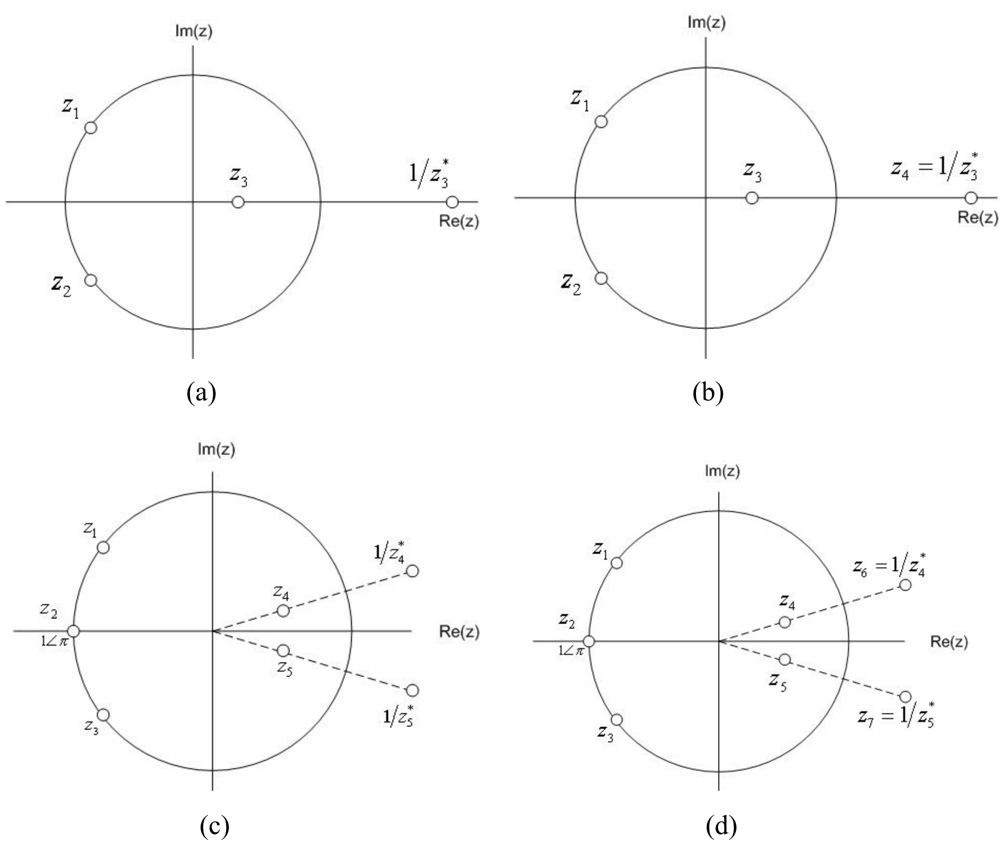

Figure 3.2. Zero diagram of the cross transfer function of the designed (a) third (b) fourth (c) fifth, and (d) seventh order filters

3.2.3 Calculation of the Bar Port Transfer Function

Once the cross transfer function has been obtained, the bar transfer function can be calculated using the power complementary condition. In this step, Figure 3.1(f), the bar transfer function *A*(*z*) is calculated by substituting the normalized cross transfer function *B*(*z*) to the power conservation rule. Recall from Eq. (2.14), the squared magnitude of the bar transfer function can be expressed as

$$\left|A(\omega)\right|^2 = A(\omega)A^*(\omega) \tag{2.59}$$

$$\left|A(z)\right|^2 = A(z)A^*(1/z^*) \tag{2.60}$$

From the power conservation rule, the sum of the power of the bar transfer and the cross transfer should be equal to one. Eq. (3.6) can be written as

$$\begin{aligned}\left|A(z)\right|^2 = A(z)A^*(1/z^*) &= a_0a_0^*\prod_{k=1}^{N}(z-\alpha_k)(\frac{1}{z}-\alpha_k^*)\\ &=1-B(z)B^*(1/z^*)\end{aligned} \tag{2.61}$$

where a_0 is the 0-th complex coefficient or the gain of *A*(*z*). If the transfer functions have real coefficients then Eq. (3.7) can be written as

$$\begin{aligned}\left|A(z)\right|^2 = A(z)A(z^{-1}) &= a_0a_0\prod_{k=1}^{N}(z-\alpha_k)(\frac{1}{z}-\alpha_k^*)\\ &=1-B(z)B(z^{-1})\end{aligned} \tag{2.62}$$

2*N* zeros of $1-B(z)B(z^{-1})$ appears as pairs of $(\alpha_k, 1/\alpha_k^*)$ for $k=1\sim N$. To obtain the bar transfer function *A*(*z*), the *N* zeros of *A*(*z*) must be calculated from (3.8).

Using spectral factorization, each zero of $A(z)$ is defined by selecting one from each pair of zero of $1-B(z)B^*(z^{-1})$. There are 2^N selections to obtain the zeroes of *A*(*z*). Thus, 2^N different kinds of *A*(*z*) can be obtained from one known *B*(*z*). They have the same amplitude characteristics but different phase characteristics.

3.2.4 Obtaining the Optical Parameters

The last step is the generation of power coupling ratios and phases of each directional coupler and delay line of the filters from the bar and cross ports transfer functions. A simulation tool based on an algorithm derived by Jinguji [6] that can map the coefficients of the filter transfer function in a z polynomial to the optical parameters is used. The algorithm uses recursion equations to calculate the power coupling ratios of each directional coupler and the phase of each delay line.

3.3 Third Order Filter

3.3.1 The Cross Transfer of the Third Order Filter

In order to have a broader stopband width and hence also broader passband width, one zero on the unit circle is added to the single-stage MZI which has only one zero in its transfer function. Now the filter has two zeros, namely z_1 and z_2, that lie on the unit circle and hence the stopband is broadened. There is a side-lobe between the two zeros. But the passband is still not flat. The third zero z_3 should be placed at a distance in between the first two zeros but at the other side of the origin of the complex z-plane and not on the unit circle to get a passband flattened. The zeros' positions of the third order filter are as has been depicted by Figure 3.2(a).

The positions of the two zeros on unit circle are chosen first such that the side-lobe level is -30 dB. Suppose z_1 and z_2 are chosen as (the angles are given in radians)

$$\begin{aligned} z_1 &= -0.9509 + j0.3094 = 1\angle 2.827 \\ z_2 &= -0.9509 - j0.3094 = 1\angle -2.827 \end{aligned} \tag{2.63}$$

z_3 is the unknown zero and since in this case is real, it can be represented as

$$z_3 = x + j0 \tag{2.64}$$

The stopband determined by the two zeros on the unit circle lies from normalized angular frequency of 0.9π to 1.1π. Note that the angles are given in radians.

From Eq. (3.2), the cross transfer function can be written as follows

$$B(z) = \Gamma(1 - z_1 z^{-1})(1 - z_2 z^{-1})(1 - z_3 z^{-1}) \tag{2.65}$$

or in expanded version:

$$B(z) = \Gamma - \Gamma(z_1 + z_2 + z_3)z^{-1} + \Gamma(z_3(z_1 + z_2) + z_1 z_2)z^{-2} - \Gamma(z_1 z_2 z_3)z^{-3} \tag{2.66}$$

The transfer function can also be written in terms of its coefficients as

$$B(z) = c_0 + c_1 z^{-1} + c_2 z^{-2} + c_3 z^{-3} \tag{2.67}$$

Now definitions are made for the part of each coefficient as following

$$\begin{aligned} \breve{c}_0 &= 1 \\ \breve{c}_1 &= -(z_1 + z_2 + z_3) \\ \breve{c}_2 &= (z_3(z_1 + z_2) + z_1 z_2) \\ \breve{c}_3 &= -(z_1 z_2 z_3) \end{aligned} \tag{2.68}$$

Note that $c_n = \Gamma \cdot \breve{c}_n$ for $n = 0 \sim N$. Since z_1 and z_2 are known and recalling Eq. (3.10), equations in (3.14) are represented in terms of x. Defining back Eq. (3.12) in terms of Eq. (3.14) and applying Eq. (3.1), the magnitude squared of the cross transfer function can be represented as following

$$\begin{aligned} \left|B(z)\right|^2_{z=e^{j\omega'}} &= \Gamma^2 \sum_{k=0}^{3} \sum_{l=0}^{3} \breve{c}_k \breve{c}_l z^{-(k-l)} \\ &= \Gamma^2 \sum_{k=0}^{3} \sum_{l=0}^{3} \breve{c}_k \breve{c}_l e^{-(k-l)j\omega'} \end{aligned} \tag{2.69}$$

where $\breve{c}_k$ and $\breve{c}_l$ are coefficients components as defined by (3.14) of $B(z)$ and $B(z^{-1})$ respectively. The derivative of Eq. (3.15) with respect to the normalized angular frequency is as follows

$$\begin{aligned} \frac{\mathrm{d}\left|B(e^{j\omega'})\right|^2}{\mathrm{d}(\omega')} &= \Gamma^2 \sum_{k=0}^{3} \sum_{l=0}^{3} \breve{c}_k \breve{c}_l \frac{\mathrm{d}(e^{-(k-l)j\omega'})}{\mathrm{d}(\omega')} \\ &= \Gamma^2 \sum_{k=0}^{3} \sum_{l=0}^{3} \breve{c}_k \breve{c}_l (-(k-l)) e^{-(k-l)j\omega'} \end{aligned} \tag{2.70}$$

Since the stopband edges are at normalized angular frequencies of 0.9π and 1.1π, the passband edges are found at normalized angular frequencies of 0.1π and 1.9π. Taking Eq. (3.16) as zero at one of those points, x can be found and hence z_3 can be determined.

Table 3.1 shows the zeros of the cross transfer function of the third order filter. The third zero can be chosen either as z_3 or its mirror $1/z_3^*$ since both of them give same magnitude response although they have different phase responses. Thus two cross transfer functions can be obtained. The possible solutions of the cross transfer function after being normalized is shown in Table 3.2.

z_1	$1\angle 2.827$
z_2	$1\angle -2.827$
z_3	$0.2841\angle 0$
$1/z_3^*$	$3.5200\angle 0$

Table 3.1. Zeros of the cross transfer third order filter

z_1	$1\angle 2.827$	z_1	$1\angle 2.827$
z_2	$1\angle -2.827$	z_2	$1\angle -2.827$
z_3	$0.2841\angle 0$	z_3	$3.5200\angle 0$
$B_1(z) = 0.3577 + 0.5786z^{-1} + 0.1644z^{-2} - 0.1016z^{-3}$		$B_2(z) = 0.1016 - 0.1644z^{-1} - 0.5786z^{-2} - 0.3577z^{-3}$	

Table 3.2. Cross transfer functions of the third order filter

The magnitude squared response of the obtained cross transfer function for $B_1(z)$ is shown by Figure 3.3 and the phase response is shown by Figure 3.4. The stopband width at –25 dB is 15.2% of the FSR or 30.4% of the channel spacing. The side-lobe level is –26.92 dB. The *ripple level* in the passband is very small, $-8.69\cdot 10^{-3}$ dB, thus the passband can still be considered as flat. The phase response shows the non-linear phase function. Thus it has a non-constant group delay and hence a non-zero dispersion. The normalized group delay and dispersion of the designed filter are shown by Figure 3.5. Note the dispersion sweeps in the passband region.

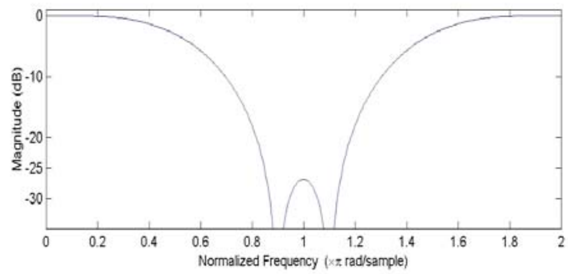

(a)

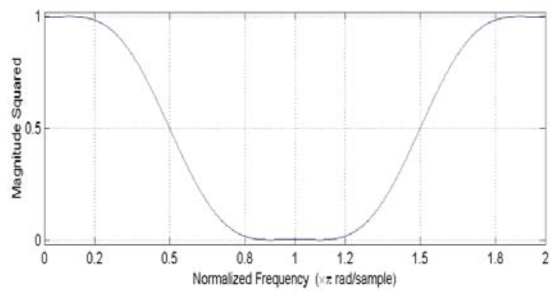

(b)

Figure 3.3. Magnitude squared response of the cross port transfer function of the third order filter (a) in decibel scale and (b) in linear scale

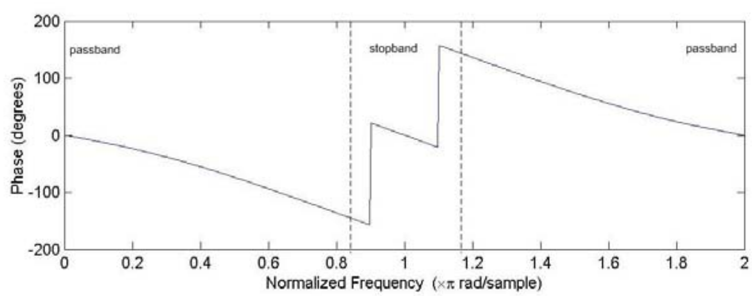

Figure 3.4. Phase response of the cross port transfer function of the third order filter

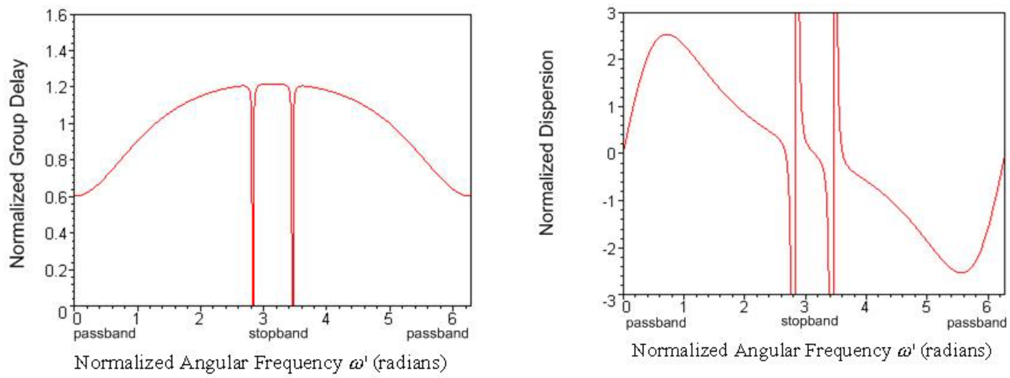

(a) (b)

Figure 3.5. Normalized (a) group delay and (b) dispersion of the cross port transfer function of the third order filter

3.3.2 The Bar Transfer of the Third Order Filter

From Figure 3.3(b), the cross transfer function magnitude squared curve is symmetric within one period. The zeros of the bar transfer can be found referring to Section 3.2.3. using Eq. (3.8) which are actually can be found also by rotating the zero diagram of the cross transfer by π radians since the cross transfer is symmetric. The zero diagram of the bar transfer of the third order filter is depicted by Figure 3.6. Table 3.3 gives the possible two bar transfer functions for two different zero configurations.

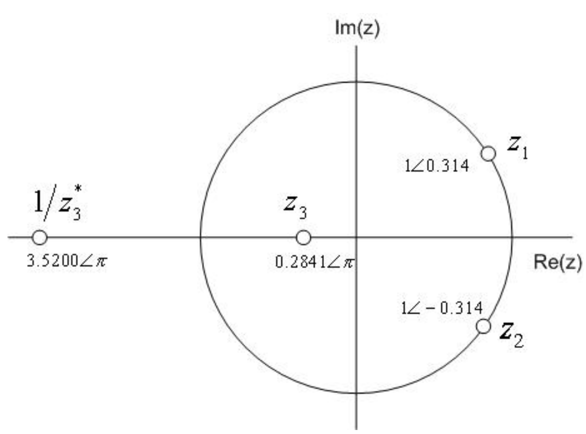

Figure 3.6. Zero diagram of the bar transfer third order filter

z_1	$1\angle 0.314$	z_1	$1\angle 0.314$
z_2	$1\angle -0.314$	z_2	$1\angle -0.314$
z_3	$0.2841\angle \pi$	z_3	$3.5200\angle \pi$
$A_1(z) = 0.3577 - 0.5786z^{-1} + 0.1644z^{-2} + 0.1016z^{-3}$		$A_2(z) = 0.1016 + 0.1644z^{-1} - 0.5786z^{-2} + 0.3577z^{-3}$	

Table 3.3. Bar transfer functions and their zeros of the third order filter

Figure 3.7(a) shows the magnitude response of the bar transfer in decibel scale and Figure 3.7(b) shows the magnitude squared response of both cross, $B_1(z)$, and bar transfer $A_1(z)$ for comparison. Figure 3.8 shows the phase response of the bar transfer. The phase response also shows a non-linear function. The curves satisfy the power conservation. The normalized group delay and dispersion are shown by Figure 3.9. Note that the responses are the shifted version of those of the cross transfer.

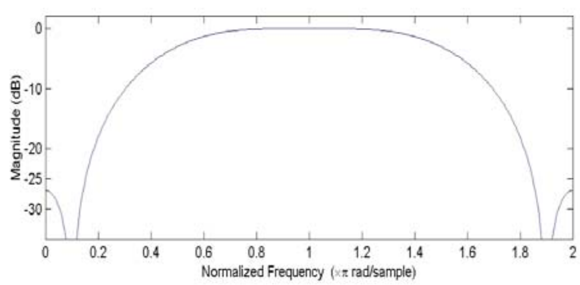

(a)

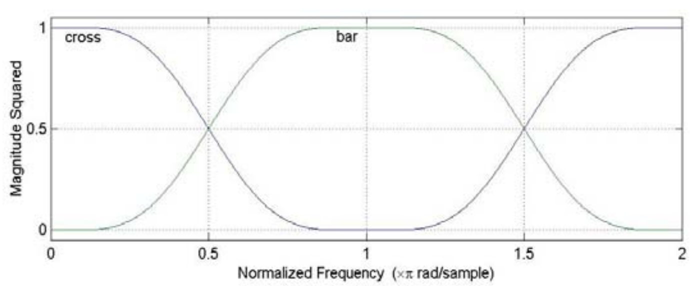

(b)

Figure 3.7. Magnitude response of the bar transfer function third order filter in decibel scale (a) and magnitude squared response of the bar and cross transfer of the third order filter (b)

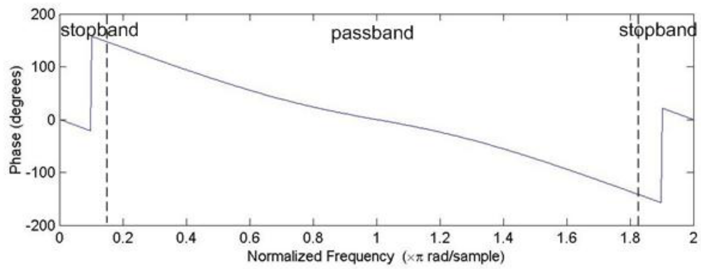

Figure 3.8. Phase response of the bar port transfer function of the third order filter

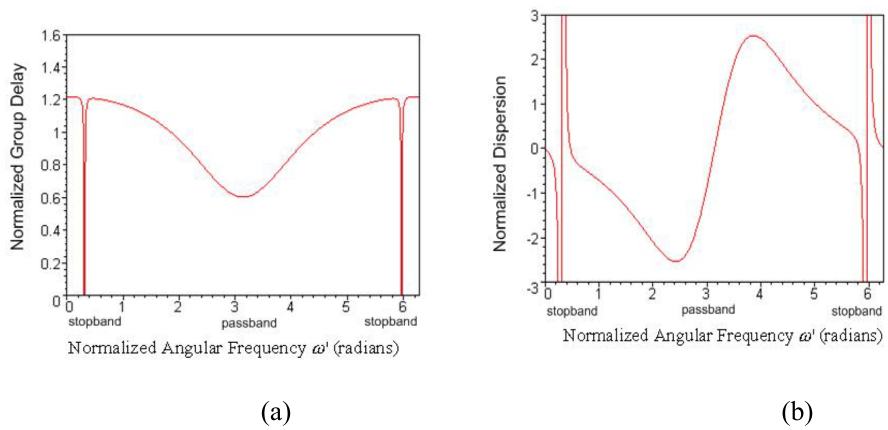

Figure 3.9. Normalized (a) group delay and (b) dispersion of the bar port transfer function of the third order filter

3.3.3 The Optical Parameters of the Third Order Filter

From the cross and bar transfer obtained, a three-stage optical filter can represent the third order filter slicer. Appendix D gives the possible configurations of the power coupling constants of each directional coupler and the phases of each delay line calculated using the available simulation tools. For the third order filter, since there are two possible solutions for each bar and cross transfer, there are four possible configurations.

For every configuration, it turns out that one coupler has a power coupling constant of zero. It means that the associated coupler can be removed and the neighbouring delay lines can be combined into one with doubled delay. The filter is reduced into a two-stage filter. The better configuration may be the one that consists of the coupler with $\kappa = 0.07$ since it is the shortest coupler.

3.4 Fourth Order Filter

3.4.1 The Cross Transfer of the Fourth Order Filter

As seen previously, the third order filter still has a non-linear phase response and non-zero dispersion in the passband. As explained in the previous chapter, a linear phase filter has at least a pair of zeros that are mirrored about the unit circle. The zeros positions of the fourth order filter are as has been depicted by Figure 3.2(b). The filter will be built with a similar algorithm as for the third order filter.

Suppose now the zeros on the unit circle are still as same as the third order filter:

$$\begin{aligned} z_1 &= -0.9509 + j0.3094 = 1\angle 2.827 \\ z_2 &= -0.9509 - j0.3094 = 1\angle -2.827 \end{aligned} \tag{2.71}$$

Now the rest two unknown zeros are defined as

$$\begin{aligned} z_3 &= x + j0 \\ z_4 &= \frac{1}{x} + j0 \end{aligned} \tag{2.72}$$

The stopband also lies from normalized angular frequency of 0.9π to 1.1π where the transfers are zero at both of those points. The fourth order cross transfer function can be written in terms of its roots as

$$\begin{aligned} B(z) = \Gamma - \Gamma(z_1 + z_2 + z_3 + z_4)z^{-1} + \Gamma[z_3 z_4 + z_4(z_1 + z_2) + z_3(z_1 + z_2) + z_1 z_2]z^{-2} \\ -\Gamma[(z_1 + z_2)z_3 z_4 + (z_3 + z_4)z_1 z_2]z^{-3} + \Gamma(z_1 z_2 z_3 z_4)z^{-4} \end{aligned} \tag{2.73}$$

or in terms of its coefficients as

$$B(z) = c_0 + c_1 z^{-1} + c_2 z^{-2} + c_3 z^{-3} + c_4 z^{-4} \tag{2.74}$$

The following definitions are made:

$$\begin{aligned} \breve{c}_0 &= 1 \\ \breve{c}_1 &= -(z_1 + z_2 + z_3 + z_4) \\ \breve{c}_2 &= z_3 z_4 + z_4(z_1 + z_2) + z_3(z_1 + z_2) + z_1 z_2 \\ \breve{c}_3 &= -[(z_1 + z_2)z_3 z_4 + (z_3 + z_4)z_1 z_2] \\ \breve{c}_4 &= z_1 z_2 z_3 z_4 \end{aligned} \tag{2.75}$$

Substituting the zeros in (3.17) and (3.18) to Eq. (3.21) and defining Eq. (3.19) in terms of (3.21) then taking the squared magnitude of the function, the following equation emerges

$$\begin{aligned}\left|B(z)\right|^2_{z=e^{j\omega'}} &= \Gamma^2 \sum_{k=0}^{4}\sum_{l=0}^{4} \breve{c}_k \breve{c}_l z^{-(k-l)} \\ &= \Gamma^2 \sum_{k=0}^{4}\sum_{l=0}^{4} \breve{c}_k \breve{c}_l e^{-(k-l)j\omega'}\end{aligned} \tag{2.76}$$

The derivative of the magnitude squared with respect to the normalized angular frequency is as follows

$$\begin{aligned}\frac{\mathrm{d}\left|B(e^{j\omega'})\right|^2}{\mathrm{d}(\omega')} &= \Gamma^2 \sum_{k=0}^{4}\sum_{l=0}^{4} \breve{c}_k \breve{c}_l \frac{\mathrm{d}(e^{-(k-l)j\omega'})}{\mathrm{d}(\omega')} \\ &= \Gamma^2 \sum_{k=0}^{4}\sum_{l=0}^{4} \breve{c}_k \breve{c}_l (-(k-l)) e^{-(k-l)j\omega'}\end{aligned} \tag{2.77}$$

As done with the third order filter, z_3 and z_4 can be found by substituting the normalized angular frequency that defines the passband edge to Eq. (3.23) and taking the value of (3.23) as zero. The passband edges are found at normalized angular frequencies of 0.1π and 1.9π. Zeros found for the fourth order filter are:

$$\begin{aligned} z_1 &= 1\angle 2.827 \\ z_2 &= 1\angle -2.827 \\ z_3 &= 0.1810\angle 0 \\ z_4 &= 5.5250\angle 0 \end{aligned} \tag{2.78}$$

The cross transfer function obtained with zeros in (3.24) is

$$B(z) = 0.0691 - 0.2629z^{-1} - 0.6118z^{-2} - 0.2629z^{-3} + 0.0691z^{-4} \tag{2.79}$$

Note that the transfer function is a mirror-image polynomial as referred to Chapter 2 or Appendix A.

The magnitude squared response of the obtained cross transfer function $B(z)$ is shown by Figure 3.10 and the phase response is shown by Figure 3.11. The stopband width at –25 dB is 14.6% of the FSR or 29.2% of the channel spacing. The side-lobe level is –25.63 dB. Seems that addition of a zero at the passband increases the side-lobe level and hence decreases the –25 dB stopband width compared to the third order filter. The ripple level in the passband is $-6.08 \cdot 10^{-3}$ dB. The phase response is linear at the passband. Hence the normalized group delay of the fourth order filter is constant and the dispersion is zero.

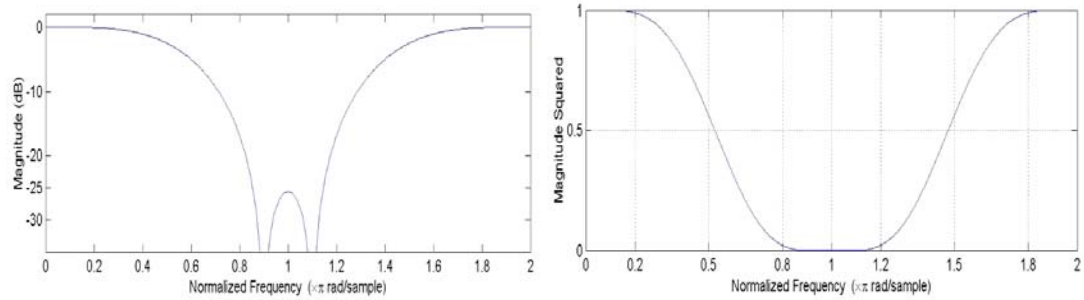

(a) (b)

Figure 3.10. Magnitude squared response of the cross port transfer function of the fourth order filter in (a) decibel scale and (b) linear scale

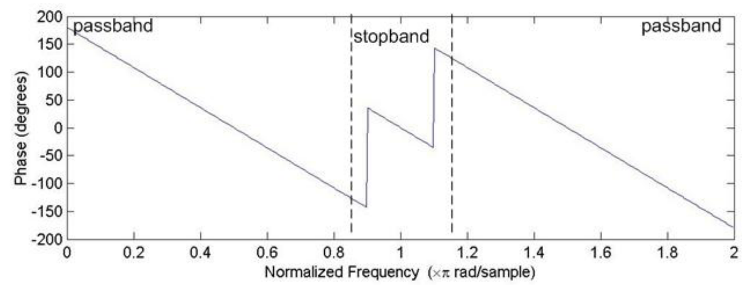

Figure 3.11. Phase response of the cross port transfer function of the fourth order filter

3.4.2 The Bar Transfer of the Fourth Order Filter

The bar port transfer function can be calculated from the cross transfer function by applying the power conservation rule as explained previously in Section 3.2.3. By substituting the cross transfer $B(z)$ to the Eq. (3.8), the four zeros of bar transfer $A(z)$ can be obtained using spectral factorization. The zero diagram of the bar transfer of the fourth order filter is depicted by Figure 3.12. The third zero can be chosen from two different zeros that is a pair of zeros mirrored to each other about the unit circle. The same condition happens to the fourth zero.

Given zeros:

$$\begin{aligned} z_1 &= 1\angle 3.14 \\ z_2 &= 1\angle -0.314 \\ z_3 &= 3.1618\angle \pi \\ z_4 &= 7.1500\angle 0 \end{aligned} \tag{2.80}$$

the bar transfer obtained is

$$A(z) = 0.0145 - 0.0856z^{-1} - 0.2037z^{-2} + 0.5666z^{-3} - 0.3284z^{-4} \tag{2.81}$$

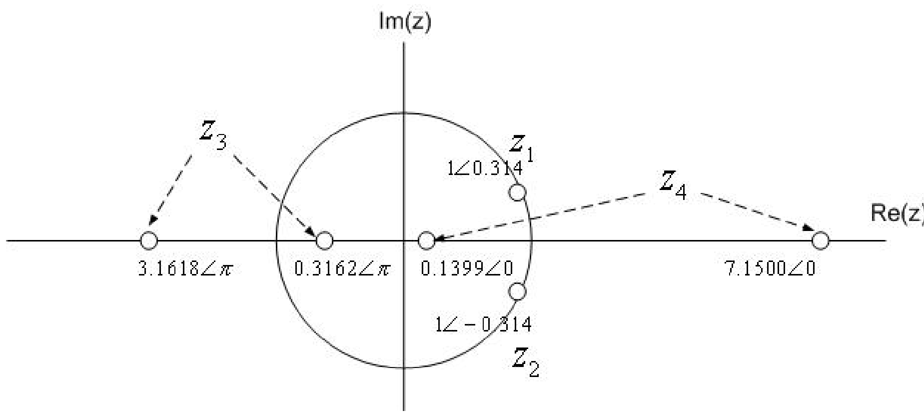

Figure 3.12. Zero diagram of the bar transfer fourth order filter

Figure 3.13(a) shows the magnitude response of the bar transfer in decibel scale while Figure 3.13(b) shows the magnitude squared response of both cross transfer $B(z)$ and bar transfer $A(z)$ for comparison. Figure 3.14 shows the phase response of the bar transfer. Since the zeros do not comprise of zeros that are mirrored each other about the unit circle anymore, it has a non-linear phase response. Hence the group delay is not constant and the dispersion is not zero.

Recalling the ADM building blocks as depicted by Figure 1.2, the dispersion of the bar transfer from the splitting part can be compensated at the combining part by the negative version of that dispersion. It can be realized by applying at the combining part the bar transfer function that is the reverse function of its associated bar transfer function at the splitting part. See Appendix B for the explanation of the reverse polynomial.

For the bar transfer function as defined by Eq. (3.27), the reverse polynomial is

$$A^R(z) = -0.3284 + 0.5666z^{-1} - 0.2037z^{-2} - 0.0856z^{-3} + 0.0145z^{-4} \qquad (2.82)$$

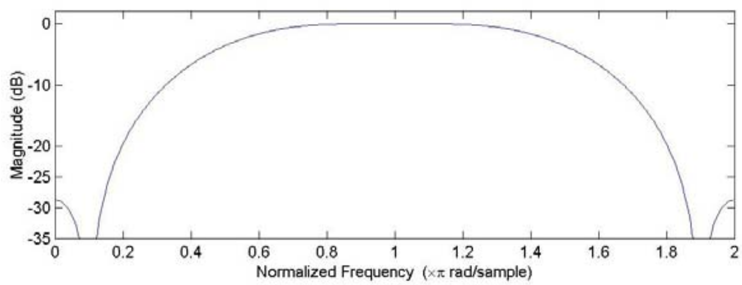

(a)

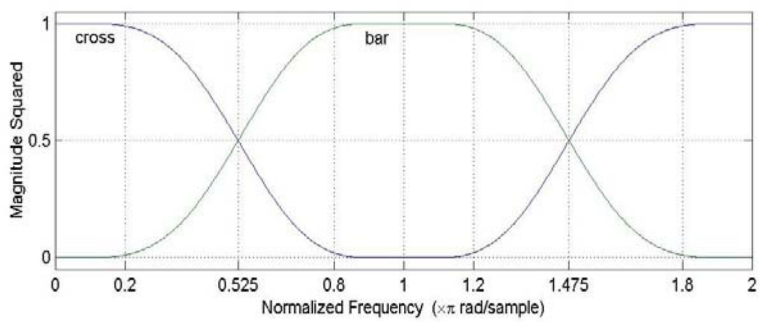

(b)

Figure 3.13. Magnitude response of the bar transfer function fourth order filter in decibel scale (a) and magnitude squared response of the bar and cross transfer of the fourth order filter (b)

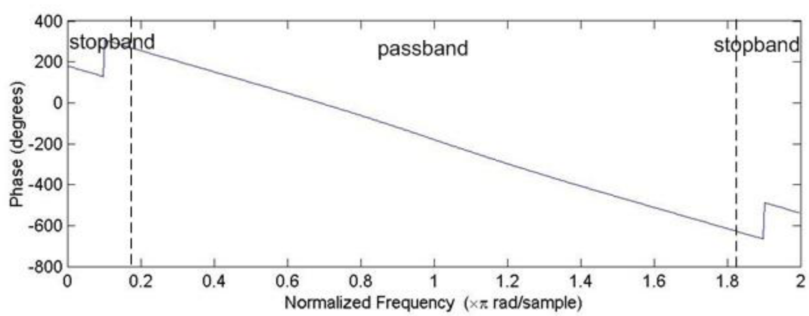

Figure 3.14. Phase response of the bar port transfer function of the fourth order filter

The normalized group delay and dispersion calculated for the obtained bar transfer and its reverse function are shown by Figure 3.15. As can be seen from the graphs, although the dispersion of each function is not equal to zero, but they are compensates each other. Hence they may produce a zero dispersion at the bar output port.

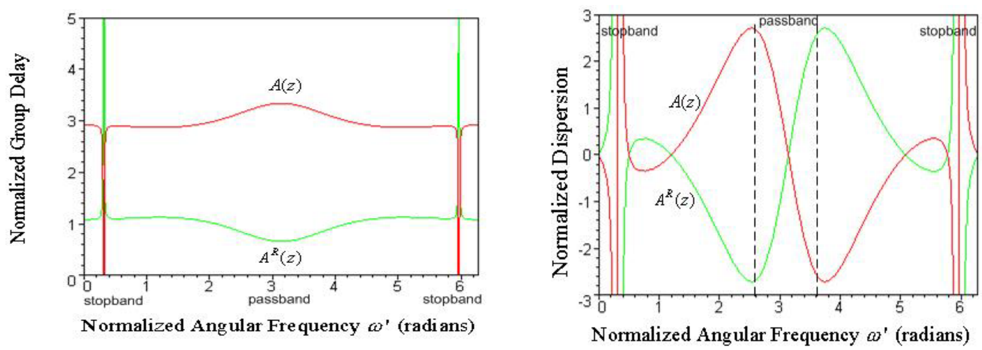

(a) (b)

Figure 3.15. Normalized (a) group delay and (b) dispersion of the bar port transfer function of the fourth order filter and its reverse polynomial

3.4.3 The Optical Parameters of the Fourth Order Filter

The optical filter parameters are obtained from the generated bar transfer and cross transfer $A(z)$ and $B(z)$. Note that $B^R(z) = B(z)$. In Appendix D, Table D.2 gives the power coupling constant of each directional coupler and the phase of each delay line. It gives two configurations, one is for the splitting part and the other is for the combining part with the reverse bar transfer function. The filter coefficients can be mapped to a four-stage optical filter with five couplers and four delay lines.

3.5 Fifth Order Filter

3.5.1 The Cross Transfer of the Fifth Order Filter

The fifth order filter zero diagram is as has been shown by Figure 3.2(c). In order to have a broader stopband width compared to the third and fourth order filters, three zeros are put on the unit circle. They are, namely z_1, z_2, and z_3. The fourth and fifth zeroes, namely z_4 and z_5, are not on the unit circle and will be placed at the opposite side of the origin in the passband region to obtain passband flattening.

At first, the positions of the three zeroes on the unit circle are chosen, then the fourth and fifth zeroes will be found through calculation. The calculation algorithm is similar with the previous filter designs. If the three zeroes on the unit circle are chosen first such that the side lobe level in between is –30 dB, the result with the five zeroes is shown a rising of the side lobe level of 12 dB. Hence the positions of the three zeroes are chosen first such that the maximum side lobe level is –40 dB in order to anticipate the final response with five zeroes will have side lobe level not greater than –25 dB. Moreover the addition of two more zeroes to design the next seventh order filter should be anticipated to have a side lobe level also not greater than –25 dB.

The zeros on unit circle are chosen as

$$\begin{aligned} z_1 &= -0.8265 + j0.5629 = 1\angle 2.544 \\ z_2 &= -1 + j0 = 1\angle \pi \\ z_3 &= -0.8265 - j0.5629 = 1\angle -2.544 \end{aligned} \tag{2.83}$$

The remaining two unknown zeros are defined as

$$\begin{aligned} z_4 &= x + jy \\ z_5 &= x - jy \end{aligned} \tag{2.84}$$

with x and y are the real and imaginary parts of z_4 and z_5.

The stopband determined by the three zeros on the unit circle lies from the normalized angular frequency of 0.81π to 1.19π. The fifth order cross transfer function can be written in terms of its roots as

$$\begin{aligned} B(z) = {} & \Gamma - \Gamma(z_1 + z_2 + z_3 + z_4 + z_5)z^{-1} + \Gamma(z_4z_5 + z_3z_5 + z_3z_4 + z_2z_5 + z_2z_4 + z_2z_3 + z_1z_5 + z_1z_4 \\ & + z_1z_3 + z_1z_2)z^{-2} - \Gamma(z_3z_4z_5 + z_2z_4z_5 + z_2z_3z_5 + z_2z_3z_4 + z_1z_4z_5 + z_1z_3z_5 + z_1z_3z_4 + z_1z_2z_5 \\ & + z_1z_2z_4 + z_1z_2z_3)z^{-3} + \Gamma(z_2z_3z_4z_5 + z_1z_3z_4z_5 + z_1z_2z_4z_5 + z_1z_2z_3z_5 + z_1z_2z_3z_4)z^{-4} - \\ & \Gamma(z_1z_2z_3z_4z_5)z^{-5} \end{aligned} \tag{2.85}$$

The following definitions are made,

$$
\begin{aligned}
\breve{c}_0 &= 1 \\
\breve{c}_1 &= -(z_1 + z_2 + z_3 + z_4 + z_5) \\
\breve{c}_2 &= (z_4 z_5 + z_3 z_5 + z_3 z_4 + z_2 z_5 + z_2 z_4 + z_2 z_3 + z_1 z_5 + z_1 z_4 + z_1 z_3 + z_1 z_2) \\
\breve{c}_3 &= -(z_3 z_4 z_5 + z_2 z_4 z_5 + z_2 z_3 z_5 + z_2 z_3 z_4 + z_1 z_4 z_5 + z_1 z_3 z_5 + z_1 z_3 z_4 + z_1 z_2 z_5 + z_1 z_2 z_4 + z_1 z_2 z_3) \\
\breve{c}_4 &= (z_2 z_3 z_4 z_5 + z_1 z_3 z_4 z_5 + z_1 z_2 z_4 z_5 + z_1 z_2 z_3 z_5 + z_1 z_2 z_3 z_4) \\
\breve{c}_5 &= z_1 z_2 z_3 z_4 z_5
\end{aligned}
\tag{2.86}
$$

Substituting (3.29) and (3.30) to Eq. (3.32) and defining Eq. (3.31) in terms of (3.32), then taking the magnitude squared of the cross transfer function, the following equation emerges

$$
\begin{aligned}
\left|B(z)\right|^2_{z=e^{j\omega'}} &= \Gamma^2 \sum_{k=0}^{5}\sum_{l=0}^{5} \breve{c}_k \breve{c}_l z^{-(k-l)} \\
&= \Gamma^2 \sum_{k=0}^{5}\sum_{l=0}^{5} \breve{c}_k \breve{c}_l e^{-(k-l)j\omega'}
\end{aligned}
\tag{2.87}
$$

The derivative of the magnitude squared with respect to the normalized angular frequency is as follows

$$
\begin{aligned}
\frac{\mathrm{d}\left|B(e^{j\omega'})\right|^2}{\mathrm{d}(\omega')} &= \Gamma^2 \sum_{k=0}\sum_{l=0} \breve{c}_k \breve{c}_l \frac{\mathrm{d}(e^{-(k-l)j\omega'})}{\mathrm{d}(\omega')} \\
&= \Gamma^2 \sum_{k=0}^{5}\sum_{l=0}^{5} \breve{c}_k \breve{c}_l (-(k-l)) e^{-(k-l)j\omega'}
\end{aligned}
\tag{2.88}
$$

For the fifth order filter, z_4 and z_5 can be found by taking the value of (3.33) as zero at two points, one is at the passband edge point and the other is at half-width of the passband which is related with the side lobe position in the stopband. Table 3.4 shows the zeros of the cross transfer function of the fifth order filter. The fourth zero can be chosen between z_4 and its mirror $1/z_4^*$ since both of them give identical magnitude response although they have different phase responses, and so can the fifth zero be chosen between z_5 and its mirror $1/z_5^*$. It results into four possible cross transfer functions that can be chosen.

z_1	$1\angle 2.544$
z_2	$1\angle \pi$
z_3	$1\angle -2.544$
z_4	$0.3724\angle 0.511$
$1/z_4^*$	$2.6859\angle 0.511$
z_5	$0.3724\angle -0.511$
$1/z_5^*$	$2.6859\angle -0.511$

Table 3.4. Zeros of the cross transfer fifth order filter

Taking zeros of:

$$\begin{aligned} z_1 &= 1\angle 2.544 \\ z_2 &= 1\angle \pi \\ z_3 &= 1\angle -2.544 \\ z_4 &= 2.6859\angle 0.511 \\ z_5 &= 2.6859\angle -0.511 \end{aligned} \tag{2.89}$$

the cross transfer calculated is:

$$B(z) = 0.0388 - 0.0788z^{-1} - 0.0994z^{-2} + 0.2988z^{-3} + 0.5604z^{-4} + 0.2797z^{-5} \tag{2.90}$$

The magnitude squared response of the obtained cross transfer function $B(z)$ is shown by Figure 3.16 and the phase response is shown by Figure 3.17. The stopband width at –25 dB is 23.5% of the FSR or 47% of the channel spacing. The side lobe level is –28.31 dB. The ripple level in the passband is $-8.69 \cdot 10^{-3}$ dB.

The normalized group delay and the dispersion of the designed filter are shown by Figure 3.18. Since the phase response is a non-linear function, the filter has a non-constant group delay and hence a non-zero dispersion. Note the dispersion sweeps in the passband region.

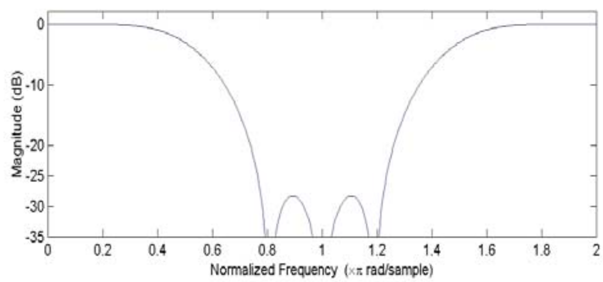

(a)

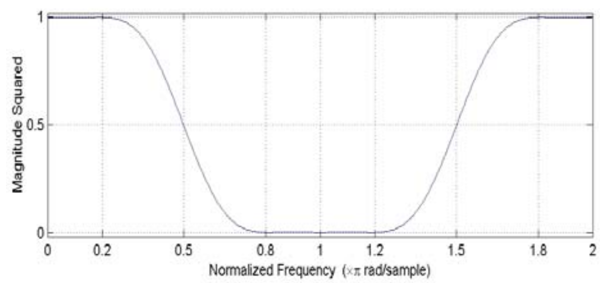

(b)

Figure 3.16. Magnitude squared response of the cross port transfer function of the fifth order filter in (a) decibel scale and (b) linear scale

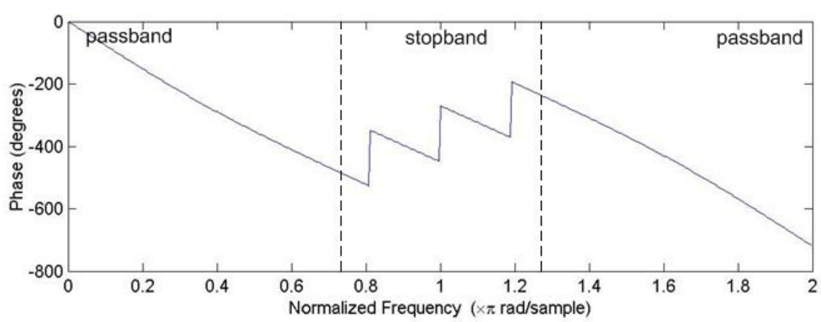

Figure 3.17. Phase response of the cross port transfer function of the fifth order filter

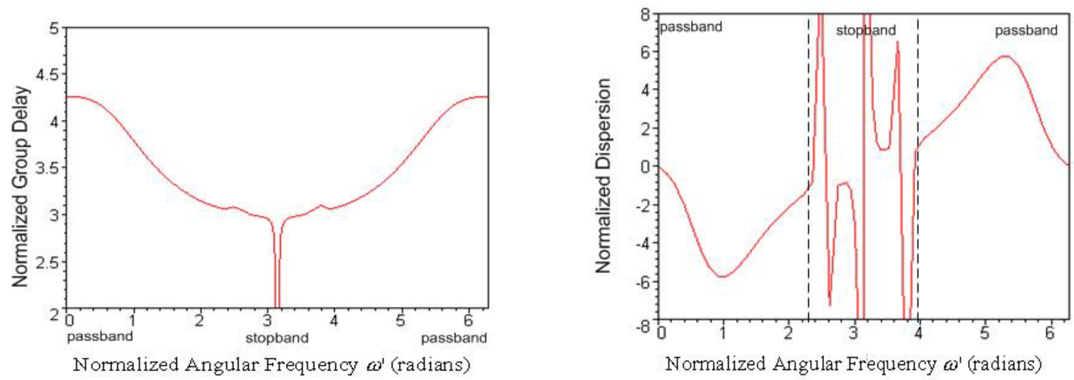

(a) (b)

Figure 3.18. Normalized (a) group delay and (b) dispersion of the cross port transfer function of the fifth order filter

3.5.2 The Bar Transfer of the Fifth Order Filter

The zeros of the bar transfer can be found referring to Section 3.2.3 using Eq. (3.8). From Figure 3.16(b), the cross transfer function magnitude squared curve is symmetric within one period, thus the bar transfer function can be found also by rotating the zero diagram of the cross transfer by π radians. The zero diagram of the bar transfer of the fifth order filter is depicted by Figure 3.19.

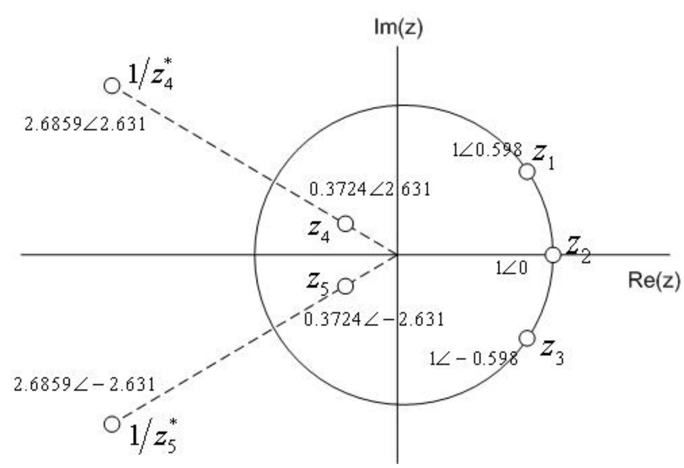

Figure 3.19. Zero diagram of the bar transfer fifth order filter

Given the cross transfer function as in Eq. (3.36), the zeros found are

$$
\begin{aligned}
z_1 &= 1\angle 0.598 \\
z_2 &= 1\angle 0 \\
z_3 &= 1\angle -0.598 \\
z_4 &= 2.6859\angle 2.631 \\
z_5 &= 2.6859\angle -2.631
\end{aligned}
\tag{2.91}
$$

and the bar transfer function calculated is

$$A(z) = 0.0388 + 0.0788z^{-1} - 0.0994z^{-2} - 0.2988z^{-3} + 0.5604z^{-4} - 0.2797z^{-5} \tag{2.92}$$

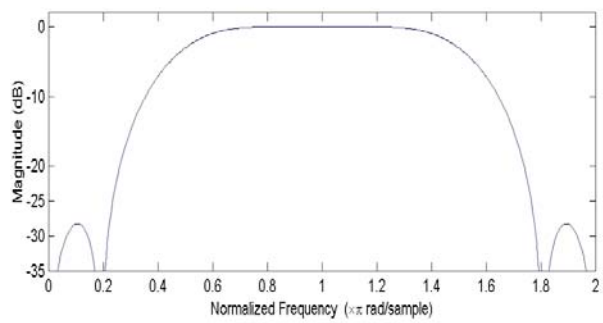

(a)

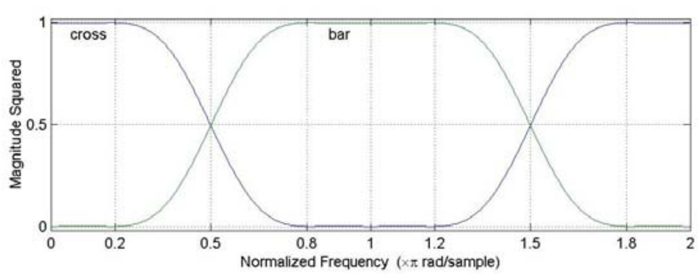

(b)

Figure 3.20. Magnitude response of the bar transfer function fifth order filter in decibel scale (a) and magnitude squared response of the bar and cross transfer of the fifth order filter (b)

Figure 3.20(a) shows the magnitude response of the bar transfer in decibel scale while Figure 3.20(b) shows the magnitude squared response of both cross transfer $B(z)$ and bar transfer $A(z)$. Figure 3.21 shows the phase response of the bar transfer. The phase response also shows a non-linear function. As a consequence, the normalized group delay is not a constant function and the normalized dispersion is not equal to zero as can be seen in Figure 3.22.

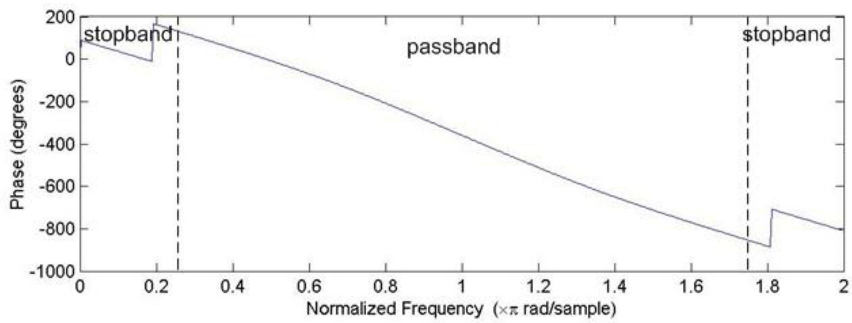

Figure 3.21. Phase response of the bar port transfer function of the fifth order filter

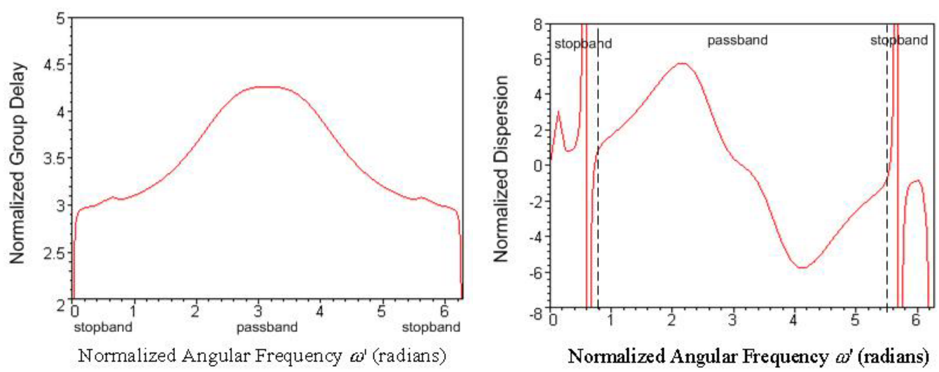

(a) (b)

Figure 3.22. Normalized (a) group delay and (b) dispersion of the bar port transfer function of the fifth order filter

3.5.3 The Optical Parameters of the Fifth Order Filter

From the cross and bar transfer obtained, a five-stage optical filter can represent the fifth order filter slicer. In Appendix D, Table D.3 gives the possible configurations of the power coupling constants of each directional coupler and the phases of each delay line calculated using the available simulation tools. Since there are four possible solutions for each bar and cross transfer, there are sixteen possible configurations.

The configurations of the two first rows, A_1B_1 and A_1B_2, give the shortest coupling and have one coupler with $\kappa = 0$ which means that one coupler can be removed and the associated neighbouring delay lines can be combined into one with doubled delay.

3.6 Seventh Order Filter

3.6.1 The Cross Transfer of the Seventh Order Filter

Although the fifth order filter has a broader stopband compared to the third and fourth order filter, it still has a non-linear phase response and non-zero dispersion in the passband. Further improvement of the filter in the sense of the linear phase response can be made. The three zeroes on the unit circle are fixed as the fifth order filter. Figure 3.2(d) shows the zero diagram of the seventh order filter. The fourth and fifth zeros are located inside the unit circle and are related as a complex conjugate pair. The sixth and seventh zeros are actually the mirrors of their pair inside the unit circle.

Given zeros on the unit circle as same as the ones for fifth order filter, see Eq. (3.28), the remaining four unknown zeros are defined as

$$\begin{aligned} z_4 &= x + jy \\ z_5 &= x - jy \\ z_6 &= 1/z_4^* = \frac{x + jy}{x^2 + y^2} \\ z_7 &= 1/z_5^* = \frac{x - jy}{x^2 + y^2} \end{aligned} \tag{2.93}$$

There are only two degrees of freedom since z_6 is equal to $1/z_4^*$ and z_7 is equal to $1/z_5^*$. The stopband determined by the three zeros on the unit circle also lies from normalized angular frequency of 0.81π to 1.19π.

Definitions are made for the part of each coefficient of the cross transfer function as given in Appendix E, Table E.1. Substituting all the zeros values including the unknown zeros in Eq. (3.39) to the equations in Table E.1, then defining Eq. (3.2) in terms of equations in Table E.1, the squared magnitude of the function is defined in terms of the gain Γ, x, and y variables.

$$\begin{aligned} \left|B(z)\right|^2_{z=e^{j\omega'}} &= \Gamma^2 \sum_{k=0}^{7}\sum_{l=0}^{7} \breve{c}_k \breve{c}_l z^{-(k-l)} \\ &= \Gamma^2 \sum_{k=0}^{7}\sum_{l=0}^{7} \breve{c}_k \breve{c}_l e^{-(k-l)j\omega'} \end{aligned} \tag{2.94}$$

The derivative of the magnitude squared with respect to the normalized angular frequency is as follows

$$\begin{aligned} \frac{\mathrm{d}\left|B(e^{j\omega'})\right|^2}{\mathrm{d}(\omega')} &= \Gamma^2 \sum_{k=0}^{7}\sum_{l=0}^{7} \breve{c}_k \breve{c}_l \frac{\mathrm{d}(e^{-(k-l)j\omega'})}{\mathrm{d}(\omega')} \\ &= \Gamma^2 \sum_{k=0}^{7}\sum_{l=0}^{7} \breve{c}_k \breve{c}_l (-(k-l)) e^{-(k-l)j\omega'} \end{aligned} \tag{2.95}$$

The variables x and y can be found by taking the value of (3.41) as zero at two points. One is at the passband edge point and the other is at half-width of the passband which is related with the side lobe position in the stopband. Hence z_4, z_5, z_6, and z_7 are determined. Table 3.6 shows the zeros of the cross transfer function of the fifth order filter. The zeros found for the seventh order filter are:

$$\begin{aligned} z_1 &= 1\angle 2.544 \\ z_2 &= 1\angle \pi \\ z_3 &= 1\angle -2.544 \\ z_4 &= 0.2644\angle 0.660 \\ z_5 &= 0.2644\angle -0.660 \\ z_6 &= 3.7827\angle 0.660 \\ z_7 &= 3.7827\angle -0.660 \end{aligned} \tag{2.96}$$

The cross transfer function generated, after normalization, with zeros in (3.41) is

$$\begin{aligned} B(z) = 0.0225 - 0.0842z^{-1} + 0.0576z^{-2} + 0.5040z^{-3} + 0.5040z^{-4} \\ +0.0576z^{-5} - 0.0842z^{-6} + 0.0225z^{-7} \end{aligned} \tag{2.97}$$

The magnitude squared response of the obtained cross transfer function $B(z)$ is shown by Figure 3.23 and the phase response is shown by Figure 3.24. The filter has a stopband width at –25 dB as 22.5% of the FSR or 45% of the channel spacing. The side lobe level is –25.35 dB. The ripple level in the passband is very small, it is only $-3.48\cdot 10^{-3}$ dB. The phase response is linear at the passband. Since the phase response is linear, now the normalized group delay has a constant value. As the consequence, the filter has zero dispersion.

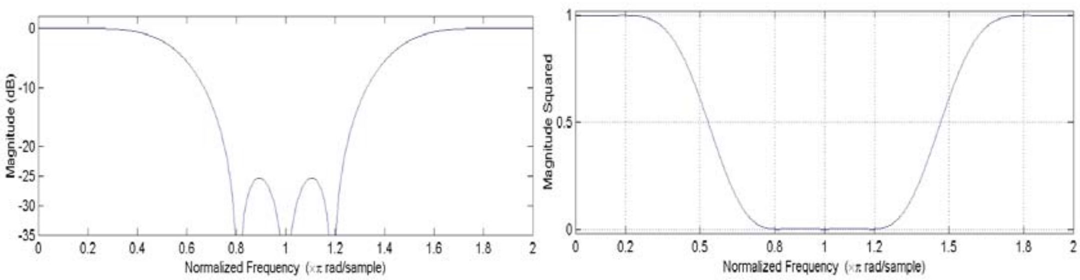

(a) (b)

Figure 3.23. Magnitude squared response of the cross port transfer function of the seventh order filter (a) in decibel scale and (b) in linear scale

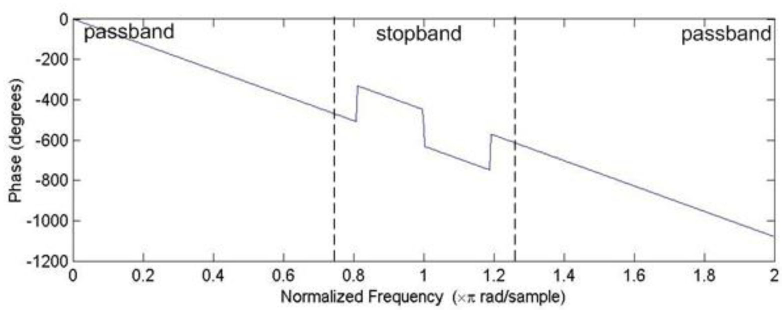

Figure 3.24. Phase response of the cross port transfer function of the seventh order filter

3.6.2 The Bar Transfer of the Seventh Order Filter

Once the linear phase cross transfer function has been obtained, the bar transfer function is obtained using the power conservation rule. By substituting the cross transfer $B(z)$ to the Eq. (3.8), the seven zeros of bar transfer $A(z)$ can be obtained using spectral factorization. The zeros position of the bar transfer of the seventh order filter obtained are depicted by Figure 3.25.

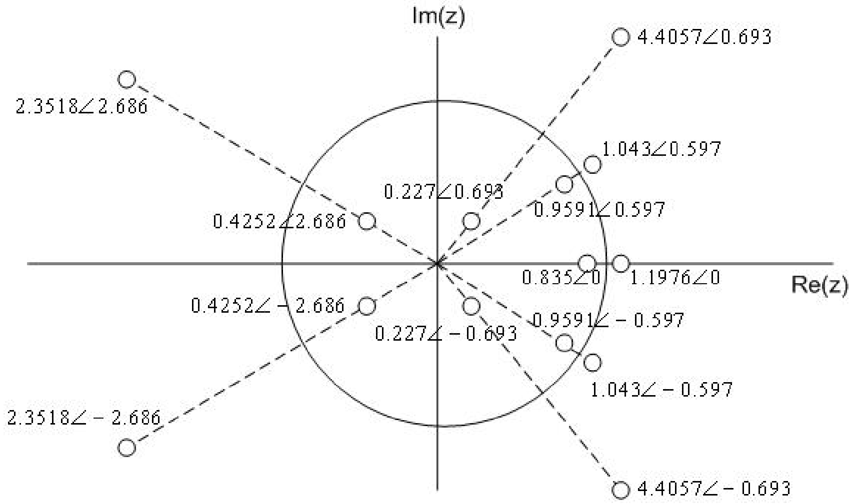

Figure 3.25. Zero diagram of the bar transfer seventh order filter

There are seven pairs of zeros $(\alpha_k, 1/\alpha_k^*)$ that appear. Seven zeros of the bar transfer are chosen one from each pair. Note that three pairs of zeros are very near to the unit circle. They are actually the "rotated" version of their counterpart zeros at the other side of the origin, which are the zeros of the cross transfer.

Given zeros:

$$\begin{aligned} z_1 &= 0.9591\angle 0.597 \\ z_1 &= 0.9591\angle -0.597 \\ z_3 &= 0.8350\angle 0 \\ z_4 &= 0.2270\angle 0.693 \\ z_5 &= 0.2270\angle -0.693 \\ z_6 &= 0.4252\angle 2.686 \\ z_7 &= 0.4252\angle -2.686 \end{aligned} \tag{2.98}$$

the bar transfer obtained is

$$\begin{aligned} A(z) = 0.2660 - 0.5338z^{-1} + 0.3210z^{-2} + 0.0589z^{-3} - 0.0874z^{-4} \\ -0.0132z^{-5} + 0.0104z^{-6} - 0.0019z^{-7} \end{aligned} \tag{2.99}$$

Figure 3.26 shows the magnitude response in decibel scale of the bar transfer and magnitude squared of both cross and bar transfer functions. Figure 3.27 shows the phase response of the bar transfer. Note that the intensity in the stopband does not go to zero anymore, but the side lobe level and the intensity are still low enough, they are below –30 dB. Since the zeros do not comprise of zeros that are mirrored to each other about the unit circle anymore, it has a non-linear phase response. Hence the group delay expected is not constant and the dispersion is not zero.

As done with the fourth order linear phase filter, the dispersion of the bar transfer from the splitting part of the ADM can be compensated at the combining part by the negative version of that dispersion. By applying at the combining part the bar transfer function that is the reverse function of its associated bar transfer function at the splitting part, the dispersion can be compensated. For the bar transfer function as defined by Eq. (3.45), the reverse polynomial is

$$\begin{aligned} A^R(z) = &-0.0019 + 0.0104z^{-1} - 0.0132z^{-2} - 0.0874z^{-3} + 0.0589z^{-4} + 0.3210z^{-5} \\ &-0.5338z^{-6} + 0.2660z^{-7} \end{aligned} \tag{2.100}$$

The normalized group delay and dispersion calculated for the bar transfer obtained and its reverse function are shown by Figure 3.28. As can be seen from the graphs, although the dispersion of each function is not equal to zero, they compensate each other. Hence they will produce a zero dispersion at the bar output port.

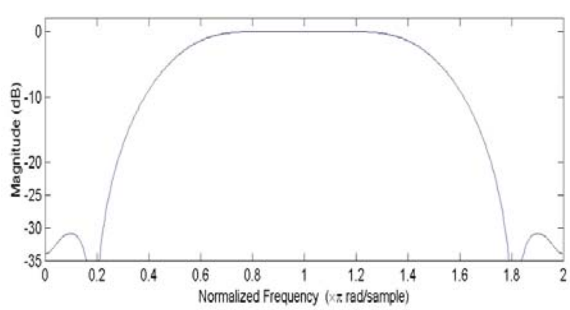

(a)

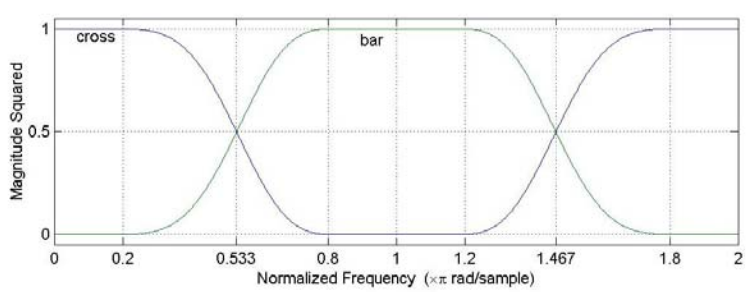

(b)

Figure 3.26. Magnitude response of the bar transfer function seventh order filter in decibel scale (a) and magnitude squared response of the bar and cross transfer of the seventh order filter (b)

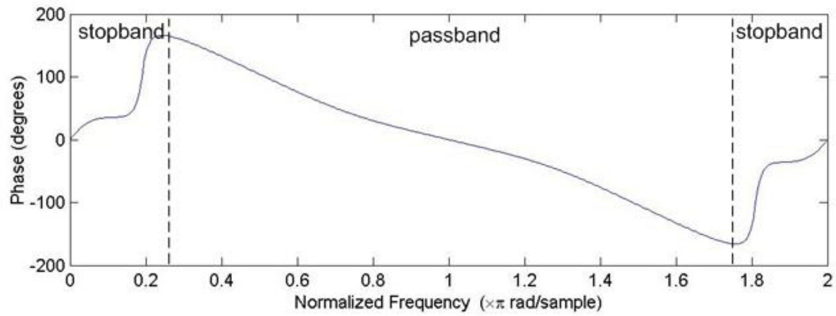

Figure 3.27. Phase response of the bar port transfer function of the seventh order filter

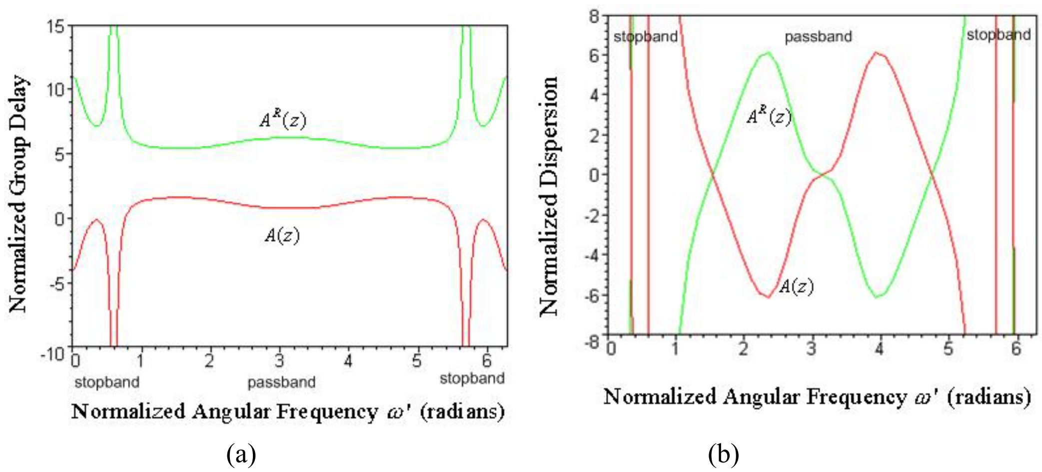

Figure 3.28. Normalized (a) group delay and (b) dispersion of the bar port transfer function of the seventh order filter and its reverse polynomial

3.6.3 The Optical Parameters of the Seventh Order Filter

From the generated bar transfer and cross transfer $A(z)$ and $B(z)$, the optical filter parameters are obtained. In Appendix D, Table D.4 gives the power coupling constant of each directional coupler and the phase of each delay line. It gives two configurations, one is for the splitting part and the other is for the combining part with the reverse bar transfer function. The filter coefficients are mapped to a seven-stage optical filter with eight couplers and seven delay lines.

3.7 Summary

In this chapter, two kinds of lattice filter that have linear phase response of the transfer function and hence zero dispersion have been designed. They are made as an improvement to the non-linear phase filters. The non-linear phase filters are the third and fifth order filters, while the linear phase filters are the fourth and seventh order filters.

The third order filter, which has three zeros in its polynomials, is improved by adding one zero in the passband region which results in a fourth order filter that has a linear phase response characteristic. To have a broader stopband width and hence broader passband width, two zeros are added to the third order filter resulting in a fifth order filter. It has three zeros on the unit circle. The fourth and fifth zeroes are not on the unit circle and are placed at the opposite side of the origin in the passband region to obtain passband flattening. The fifth order filter is improved by adding two more zeros which results in a seventh order filter that has a linear phase response characteristic. All the filters are designed such as they have a passband flattened amplitude response.

Chapter 4

4 Eye Diagram Simulation

In a digital transmission system, one form of distortion of the received signal called intersymbol interference may rise. Dispersion in the channel may cause the interference. The interference caused by the time response of the channel has temporal spreading and consequent overlapping from one symbol into another. This has the effect of potentially introducing deviations between the data sequence reconstructed at the receiver and the original data sequence applied to the transmitter input since the receiver cannot reliably distinguish changes between states. The intersymbol interference may be studied using the eye diagram or eye pattern. The eye diagram is constructed by overlaying plots of the waveform from successive unit time intervals.

4.1 Complex Low-Pass Representation of a Narrow-Band System

Typically, the incoming signal and the system of interest are both narrow-band with a common midband frequency. In this system, the center wavelength used is 1550 nm and the midband frequency used is 193.548 THz. The band-pass transmission of a signal may be analysed using an equivalent low-pass transmission model.

The frequency shifting property of the Fourier transform suggests that we may express the pre-envelope $x_+(t)$ in the form [7]

$$x_+(t) = \tilde{x}(t)\exp(j2\pi f_c t) \tag{4.1}$$

where $\tilde{x}(t)$ is the complex envelope of $x(t)$. Given the narrow-band signal $x(t)$, the real part of the product of (4.1) is equal to $x(t)$, as shown by

$$x(t) = \mathrm{Re}[\tilde{x}(t)\exp(j2\pi f_c t)] \tag{4.2}$$

The narrow-band signal $x(t)$ may be expressed as

$$x(t) = x_\mathrm{I}(t)\cos(2\pi f_c t) - x_\mathrm{Q}(t)\sin(2\pi f_c t) \tag{4.3}$$

The complex envelope $\tilde{x}(t)$ is defined in terms of the in-phase component $x_I(t)$ and the quadrature component $x_Q(t)$ as follows:

$$\tilde{x}(t) = x_{\mathrm{I}}(t) + jx_{\mathrm{Q}}(t) \tag{4.4}$$

Suppose a narrow-band signal

$$x(t) = m(t)\cos(2\pi f_c t) \tag{4.5}$$

where $m(t)$ is an information-bearing signal. From Eq. (4.3) and (4.4), then the complex envelope is

$$\tilde{x}(t) = m(t) \tag{4.6}$$

Consider next a narrow-band system defined by the impulse response $h(t)$ or equivalently, the transfer function $H(f)$. Accordingly, from analogy with the complex low-pass representation of a narrow-band signal, the desired complex low-pass representation of the narrow-band system may be developed by retaining the positive-frequency half of the transfer function $H(f)$ centered on f_{c} and shifting it to the left by f_{c}.

The Fourier transform of the output of the narrow-band system is given by

$$Y(f) = H(f)X(f) \tag{4.7}$$

Accordingly, the Fourier transform of the output of the complex low-pass system is given by [Hay89]

$$\tilde{Y}(f) = \tilde{H}(f)\tilde{X}(f) \tag{4.8}$$

Suppose a transfer function:

$$H(f) = \sum_{n=0}^{N} c_n z^{-n} = \sum_{n=0}^{N} c_n \,\mathrm{e}^{-(j2\pi fT)n} \tag{4.9}$$

with its impulse response:

$$h(t) = \sum_{n=0}^{N} c_n \delta(t - nT) \tag{4.10}$$

If it is shifted to the left by the carrier frequency f_{c}, then

$$\begin{aligned}
\tilde{h}(t) &= \mathcal{F}^{-1}[H(f+f_c)] \\
&= \sum_{n=0}^{N} c_n \int \mathrm{e}^{-n(j2\pi(f+f_c)T)}\, e^{j2\pi ft} df \\
&= \sum_{n=0}^{N} c_n \int e^{j2\pi f(t-nT)} e^{-j2\pi f_c nT} df \\
&= \sum_{n=0}^{N} c_n e^{-j2\pi f_c nT} \int e^{j2\pi f(t-nT)} df \\
&= \sum_{n=0}^{N} c_n e^{-j2\pi f_c nT} \delta(t-nT) \\
&= \sum_{n=0}^{N} \tilde{c}_n \delta(t-nT)
\end{aligned} \tag{4.11}$$

with the term $c_n e^{-j2\pi f_c nT}$ is now the new coefficient term, namely $\tilde{c}_n$.

Figure 4.1 shows the schematic layout of the real system. c_n is the filter coefficient, while T is the unit delay of the filter. Figure 4.2, 4.3, 4.4, and 4.5 show the complex low-pass equivalent models used for the simulation for the cross transfer of the third, fourth, fifth, and seventh order filters respectively with a pseudonoise sequence generator. The center wavelength used is 1550 nm center wavelength, or 193.548 THz carrier frequency, and an FSR of 100 GHz (unit delay T=10 ps). Since in the cross transfer the carrier frequency is lying on the stopband, in order to check the transmission of the signal, the transfer function is shifted by half the FSR, i.e. shifting 50 GHz, to get the passband.

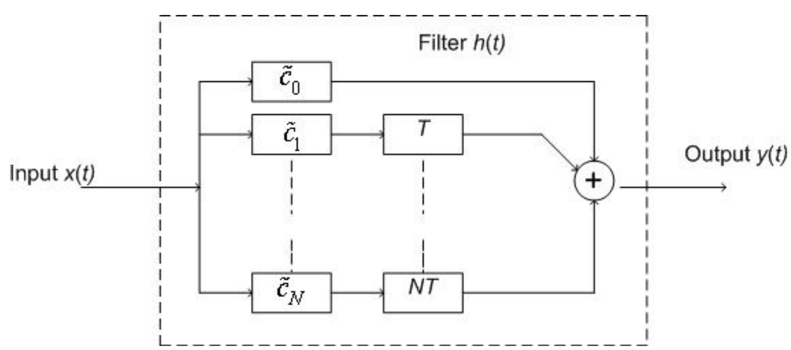

Figure 4.1. Schematic layout of the system

To understand the working principle of the model, take Figure 4.2 as an example. The PN Sequence generator block generates a sequence of random binary numbers. The block actually produces a sequence of binary data in on-off signalling format. The Gain block is the filter coefficient. Each stage of the filter gives a delay equals to nT (see Eqs. 4.9 to 4.11) where T is the filter unit delay. After being delayed and gained, the input is multiplied by an exponential constant (refer to Eq. 4.11). Each stage value is added together, and then the magnitude squared value is displayed by the scope and eye diagram blocks. The coefficients of the filters are taken from results in Chapter 3. The third order coefficients are taken from Table 3.2, the fourth order coefficients are taken from Eq. (3.25), the fifth order from Eq. (3.36), and the seventh order from Eq. (3.43).

To get an impression of the responses of the filter models, a complex input $e^{j2\pi ft}$ is given first to the systems and the magnitude and phase responses are checked for each frequency. Examples of the responses are shown in Appendix F. The responses show the similarity with the ones previously obtained in Chapter 3, although there is some slight deviation. The deviation may come from the numerical error by the simulator.

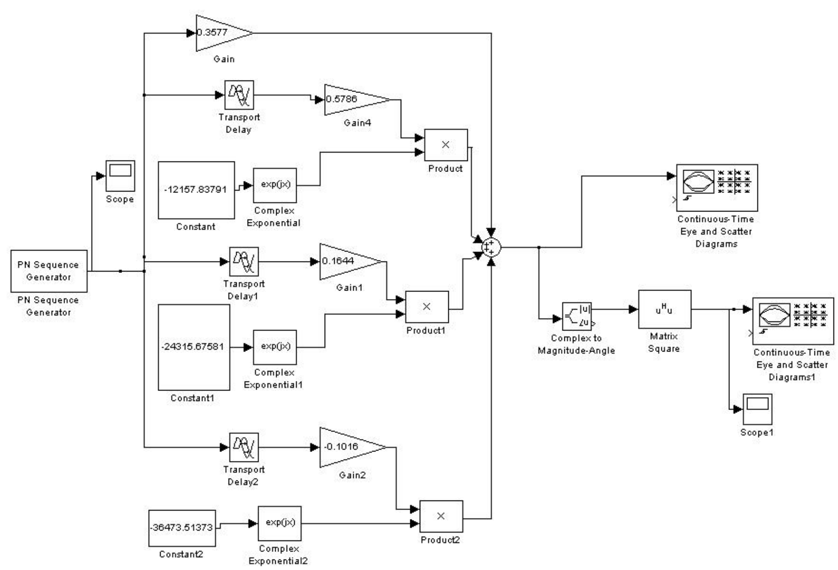

Figure 4.2. Low- pass equivalent model for the third order filter

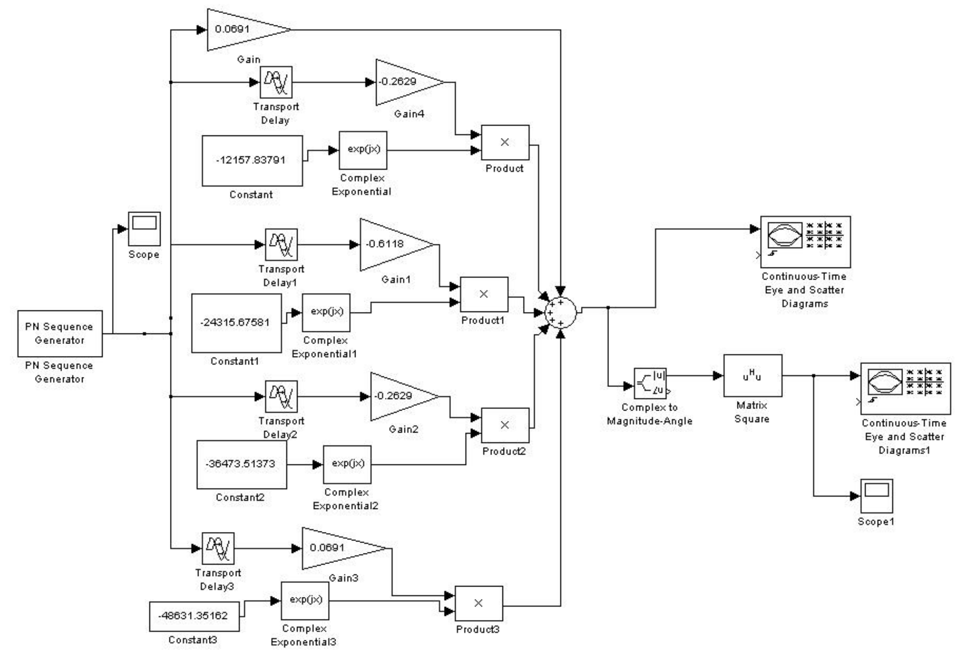

Figure 4.3. Low- pass equivalent model for the fourth order filter

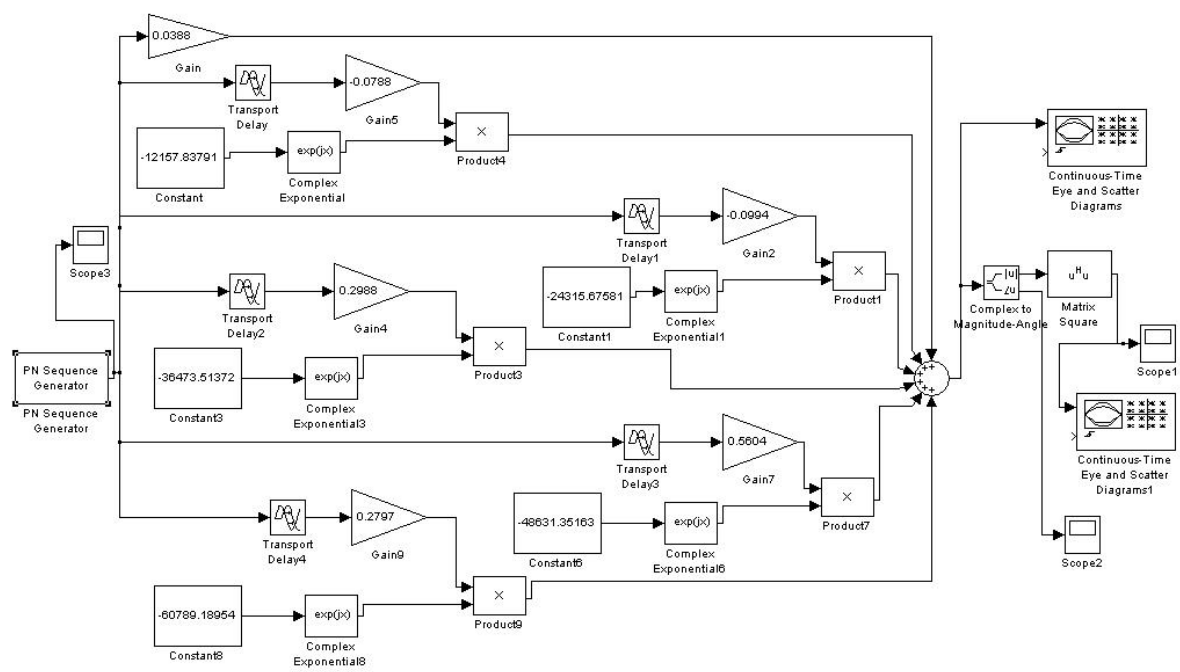

Figure 4.4. Low-pass equivalent model for the fifth order filter

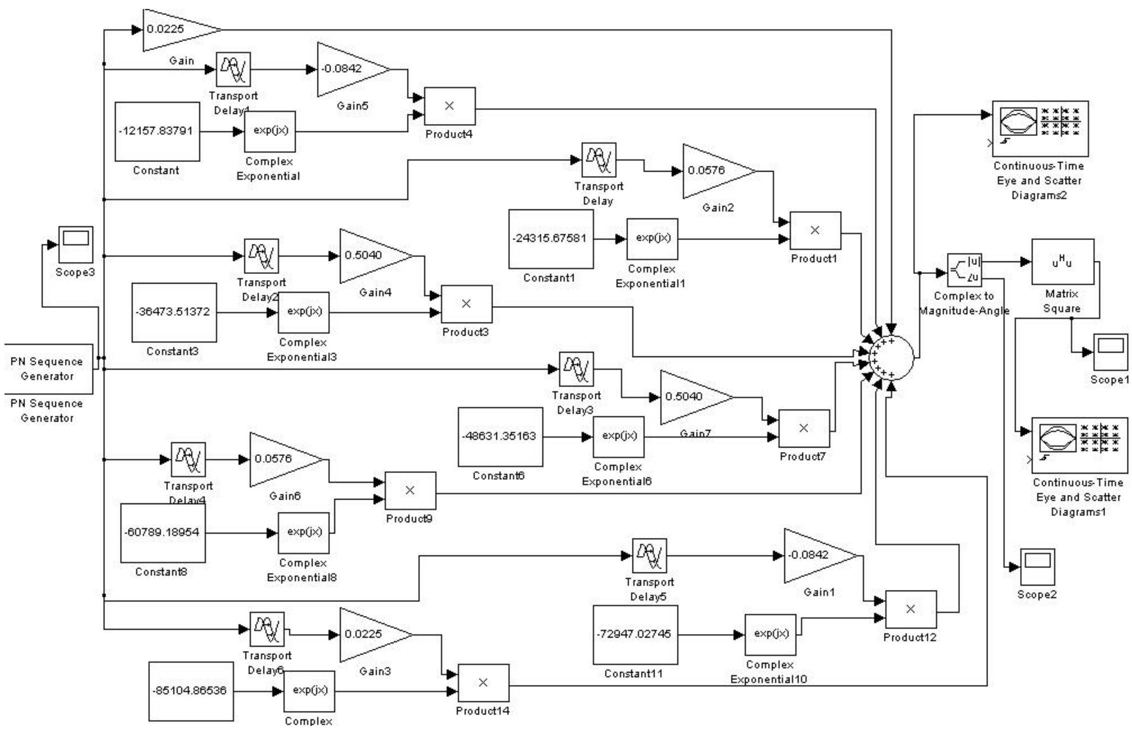

Figure 4.5. Low- pass equivalent model for the seventh order filter

4.2 Simulation Results

4.2.1 Third Order Filter

Figure 4.6 describes the magnitude squared output for one bit pulse input with bit rate 5 Gbps or bit time T_b 0.2 ns at the center of the passband for the third order filter. The output shows that the pulse is broadened compared to the original input bit time due to the delay lines of the filter. It has a "stairs-alike" shape with the stairs width equals to the filter unit delay *T*. In this case the unit delay is 10 ps. The relation between the number of stair levels and the filter stages is as follows

$$\#\text{stair-levels} = 2(N+1) \tag{4.12}$$

with *N* is the number of filter stages or filter order. For this third order filter, there are eight stair-levels where the last level has a value of zero magnitude. The stair-level or the transition value depends on the filter coefficients. The input is delayed as much as an integer multiple of the unit delay *T* and gained by the coefficients. There is a level that is higher than one. This is due to the discrete response of the system that is caused by the delay lines of the filter. As obtained in Chapter 3, the cross transfer function of the third order filter is

$$B(z) = 0.3577 + 0.5786z^{-1} + 0.1644z^{-2} - 0.1016z^{-3} \tag{4.13}$$

For instance, the third stair-level has a value resulted from addition of the 0-th, 1^{st}, and 2^{nd} coefficients which is higher than one.

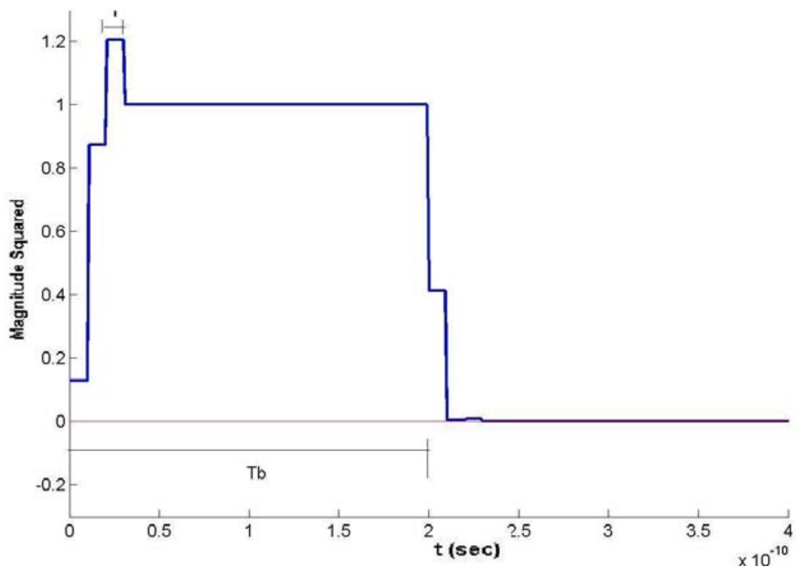

Figure 4.6. Output of the third order filter for one bit pulse 5 Gbps

Figure 4.7 describes the eye diagrams of an output sequence of the third order filter for bit rates of 5, 7.6, 25, 30, 40, and 50 Gbps for system working at the center of the passband. From the eye diagrams obtained, the pulse is broadened due to the delay line of the filter. If the input bit rate is smaller than or the same as the filter bandwidth, then the output will still have a good eye diagram. In this case, the third order filter with an FSR of 100 GHz has an equivalent low-pass bandwidth of 7.6 GHz (as confirmed from Chapter 3), consider it corresponds with –25 dB stop-band width.

As can be seen from the eye openings of Figure 4.7 (c) and (d), for bit rate up to 40 Gbps, there are still wide enough time intervals over which the pulse can be sampled without error from intersymbol interference. If the bit rate is increased then the pulse is broadened more, overlapping may occur, and the width of the eye opening is getting narrower. Figure 4.8 describes the system output for one bit pulse input with bit rate 50

Gbps or bit time 20 ps. It can be seen that besides the response is overlapping much into the next symbol time interval, the amplitude has decreased. The stair-level is not eight anymore since the delay is half of the bit time, thus previous delayed input terms may had finished before other terms come.

Suppose that the center wavelength shifts, or example if there is drift of the laser, such that the system is not at the center of the passband anymore. The output of the filter for an 11 GHz frequency shift is shown by Figure 4.9. At that frequency, from previous results, the dispersion is the highest. Comparing Figure 4.9 to Figure 4.7(a) and (c) where the system is at the center of the passband, the pulse width remains the same, only the magnitude that differs slightly at the sides of the pulse. The same condition applies if the shift is increased, say as much as 25 GHz (Figure 4.10). If the system shifts such as it works in the stopband region (Figure 4.11), the amplitude goes to zero. Thus only amplitude decreases when the center wavelength or carrier frequency shifts. Although there is still some intensity, but it is very small. The isolation is –25 dB as obtained from Chapter 3.

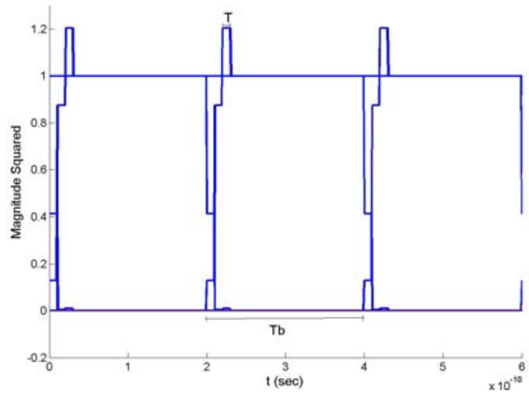

(a)

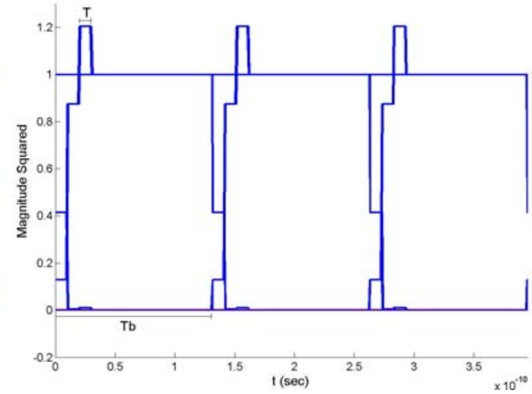

(b)

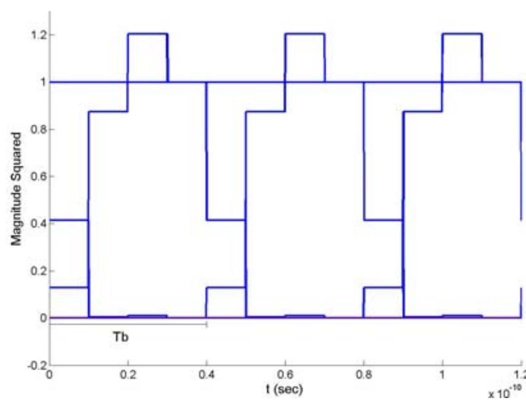

(c)

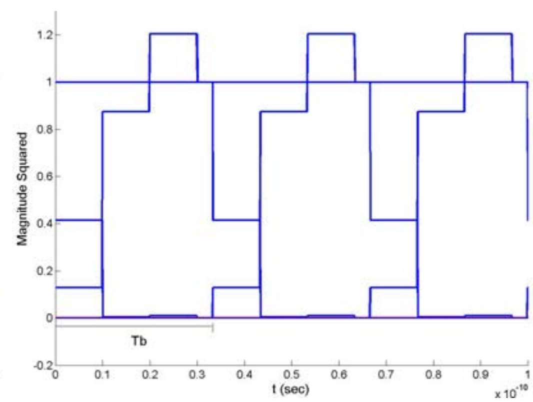

(d)

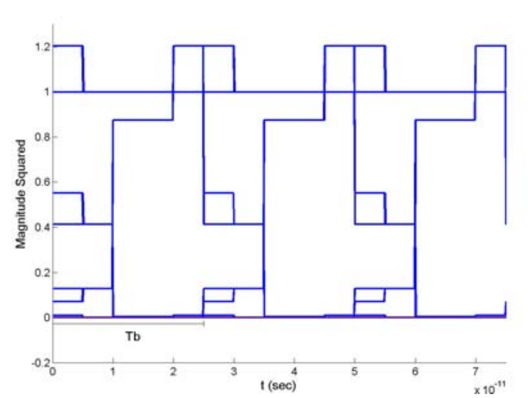

(e)

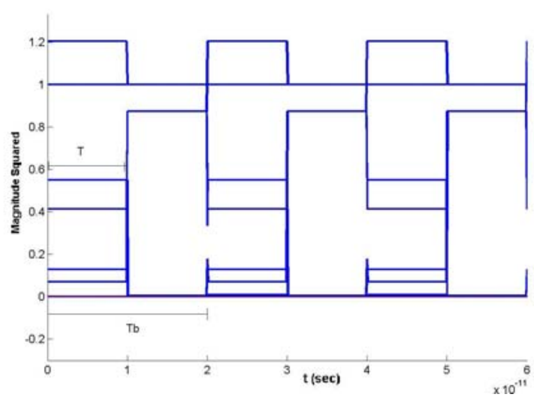

(f)

Figure 4.7. Output eye diagrams of (a) 5 Gbps, (b) 7.6 Gbps (c) 25 Gbps, (d) 30 Gbps, (e) 40 Gbps, and (f) 50 Gbps input at the center of the passband of the third order filter

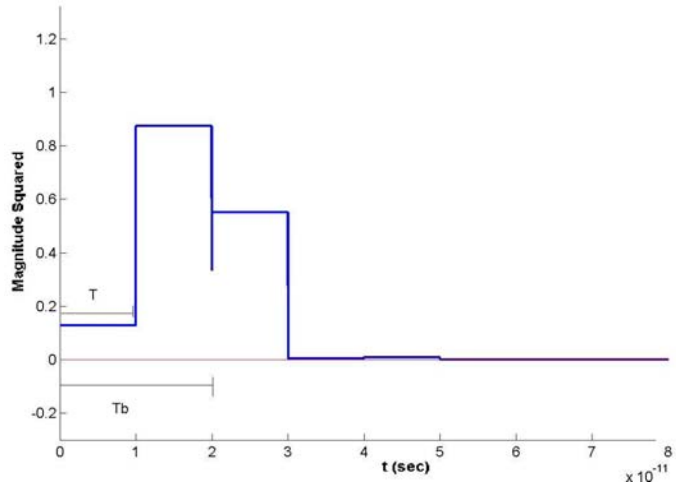

Figure 4.8. Output of the third order filter for one bit pulse 50 Gbps

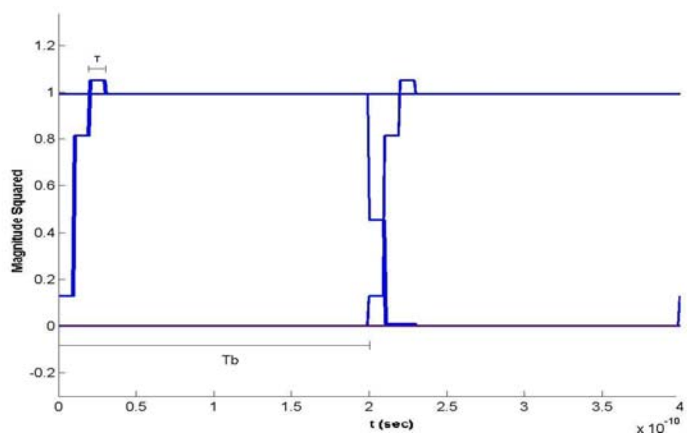

(a)

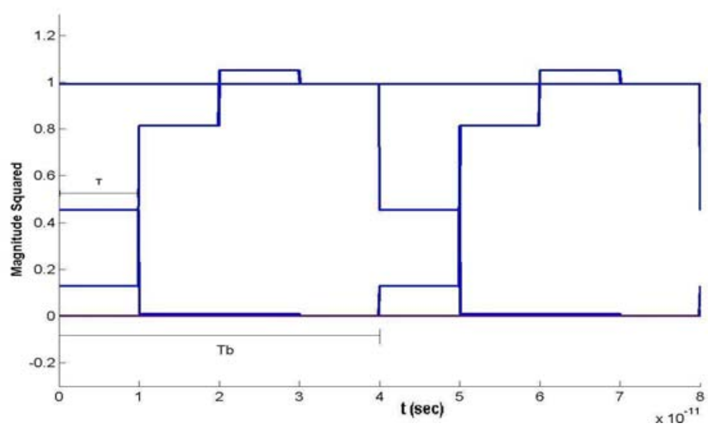

(b)

Figure 4.9. Output eye diagrams of the third order filter for frequency shift of 11 GHz (a) 5 Gbps, (b) 25 Gbps

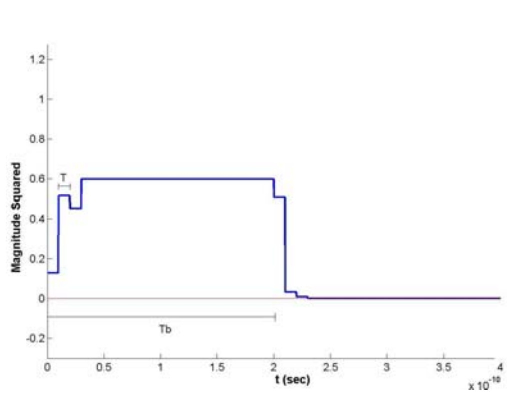

(a) (b)

Figure 4.10. Output eye diagrams for two bit times of the third order filter for frequency shift of 25 GHz for 5 Gbps input (a) one bit input and (b) sequence input

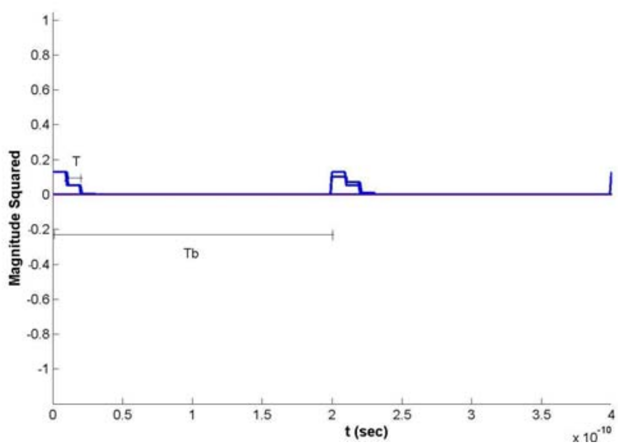

Figure 4.11. Output eye diagrams for two bit times of 5 Gbps input at the stopband region of the third order filter

4.2.2 Fourth Order Filter

Figure 4.12 describes the magnitude squared output for one bit pulse input with bit rate 5 Gbps or bit time $T_b = 0.2$ ns at the center of the passband for the fourth order filter. The unit delay is the same as the previous filter, T = 10 ps. For this fourth order filter there are ten stair-levels where the last level has a zero magnitude. Each stair width equals to the filter unit delay. As obtained in Chapter 3, the cross transfer function of the fourth order filter is

$$B(z) = 0.0691 - 0.2629z^{-1} - 0.6118z^{-2} - 0.2629z^{-3} + 0.0691z^{-4} \qquad (4.14)$$

As in the third order case, the pulse also broadens due to the delays it receives, but there is and extra delay compared to the third order filter since it has more delay lines. The value of each stair-level depends on the filter coefficients and the delays. For this fourth order filter, the output pulse shows symmetry.

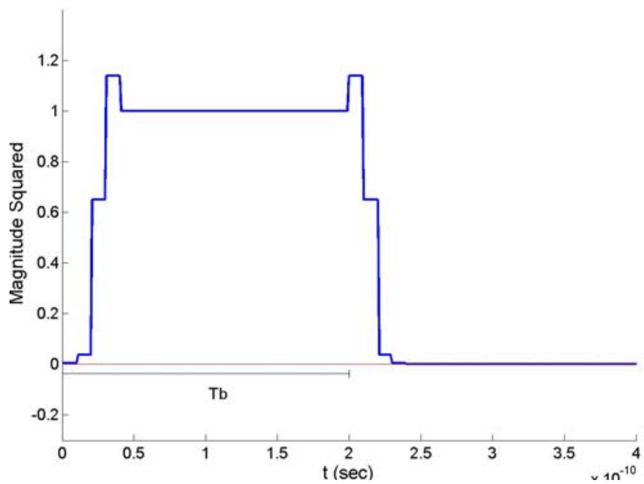

Figure 4.12. Output of the fourth order filter for one bit pulse 5 Gbps

Figure 4.13 shows the eye diagrams obtained from an output sequence of the fourth order filter for bit rate of 5, 7.3, 25, 30, 40, and 50 Gbps for a system working at the center of the passband. If the input bit rate is smaller than or as the same as the filter bandwidth, then the output will still have a good eye diagram. As can be seen from Figure 4.13, bit rates up to 7.3 Gbps, or at the filter bandwidth, still gives good eye diagram. In this case, the fourth order filter with FSR 100 GHz has an equivalent low-pass bandwidth of 7.3 GHz (as confirmed from Chapter 3 result), consider it corresponds with –25 dB stop-band width. As can be seen from the eye openings of Figure 4.13, bit rate up to 40 Gbps still gives wide enough time intervals over which the pulse can be sampled. If the bit rate is increased then the pulse is spreading more, overlapping may occur, and the width of the eye opening is getting smaller.

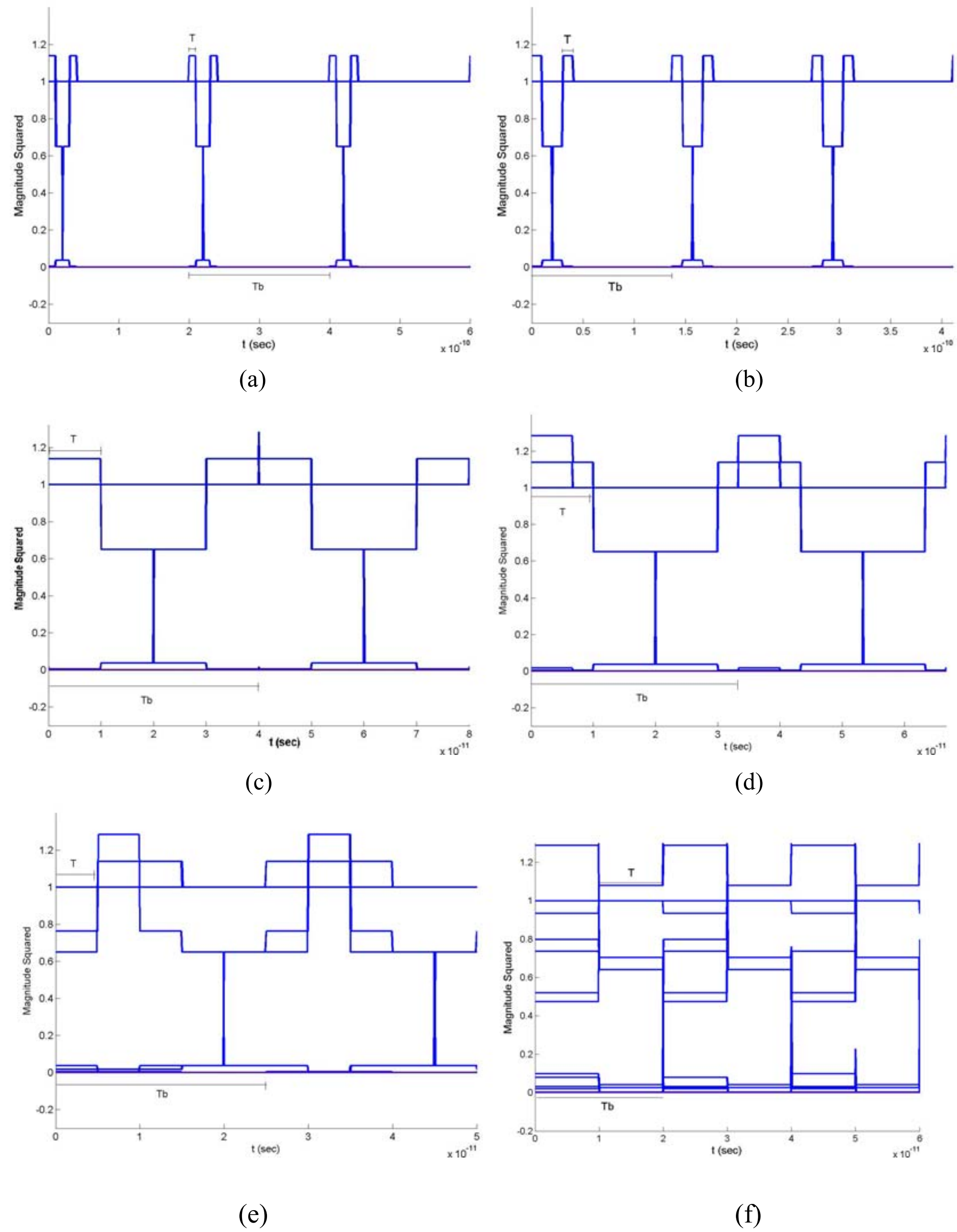

Figure 4.13. Output eye diagrams of (a) 5 Gbps, (b) 7.3 Gbps (c) 25 Gbps, (d) 30 Gbps, (e) 40 Gbps and (f) 50 Gbps input at the center of the passband of the fourth order filter

Figure 4.14 describes the system output for one bit pulse input with bit rate 50 Gbps or bit time 20 ps. It can be seen that the response is overlapping much into the next symbol time interval and the amplitude is less then one. A small dip can be observed, which is actually an artefact resulting from the limited sampling time of the simulator. At simulation time 30 ps, two coefficient terms has finished. The simulator still holds the value. Slightly after the sampling time interval, when a new coefficient term has been added, the simulator software then displays the new value.

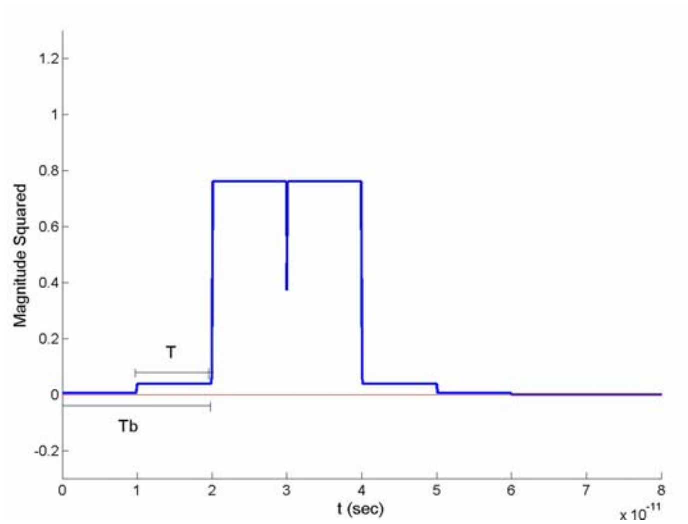

Figure 4.14. Output of the fourth order filter for one bit pulse 50 Gbps

Suppose the center wavelength shifts such that the system is not at the center of the passband anymore. The output of the filter for a 7.3 GHz frequency shifts is shown by Figure 4.15. Comparing the results obtained with the ones previously obtained where the system is at the center of the passband, the output pulse width remains the same. The symmetry property also remains the same. Only the magnitude that differs, but in this case there is only a slight difference that happens at the sides of the pulse. The amplitude decreasing is worse if the shift is increasing as can be seen in Figure 4.16 where the frequency shift is 25 GHz and in Figure 4.17 where the system is at the stopband.

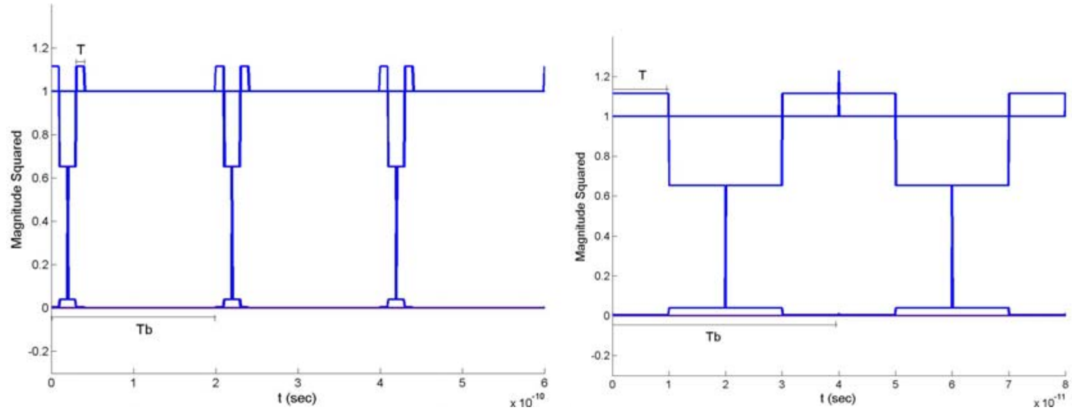

(a) (b)

Figure 4.15. Output eye diagrams of the fourth order filter for frequency shift of 7.3 GHz (a) 5 Gbps, (b) 25 Gbps

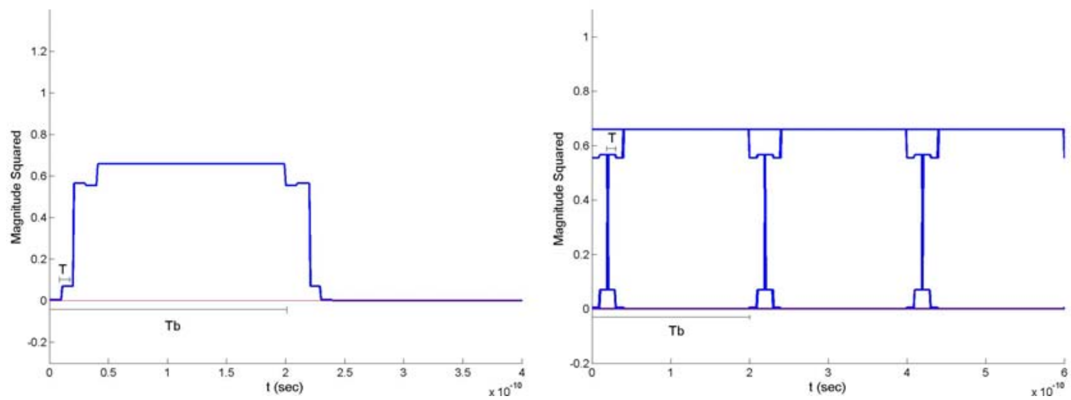

(a) (b)

Figure 4.16. Output eye diagrams of the fourth order filter for frequency shift of 25 GHz for 5 Gbps input (a) one bit input and (b) sequence input

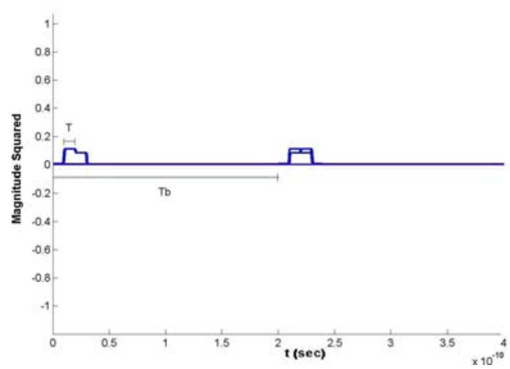

Figure 4.17. Output eye diagrams for two bit times of 5 Gbps input at the stopband region of the fourth order filter

4.2.3 Fifth Order Filter

Figure 4.18 describes the magnitude squared output for one bit pulse input with bit rate 5 Gbps or bit time $T_b = 0.2$ ns at the center of the passband for the fifth order filter. The unit delay is the same as the previous filter, T = 10 ps. For this fifth order filter there are twelve stair-levels where the last level has a zero magnitude. As obtained in Chapter 3, the cross transfer function of the fifth order filter is

$$B(z) = 0.0388 - 0.0788z^{-1} - 0.0994z^{-2} + 0.2988z^{-3} + 0.5604z^{-4} + 0.2797z^{-5} \quad (4.15)$$

As in previous filters, the pulse also broadens due to the delays it receives and there are extra delays compared to the third and fourth order filters since it has more delay lines. It also has a “stairs-alike” shape. The value of each stair-level depends on the filter coefficients. The input is delayed as much as an integer multiple of the unit delay T and gained by the coefficients.

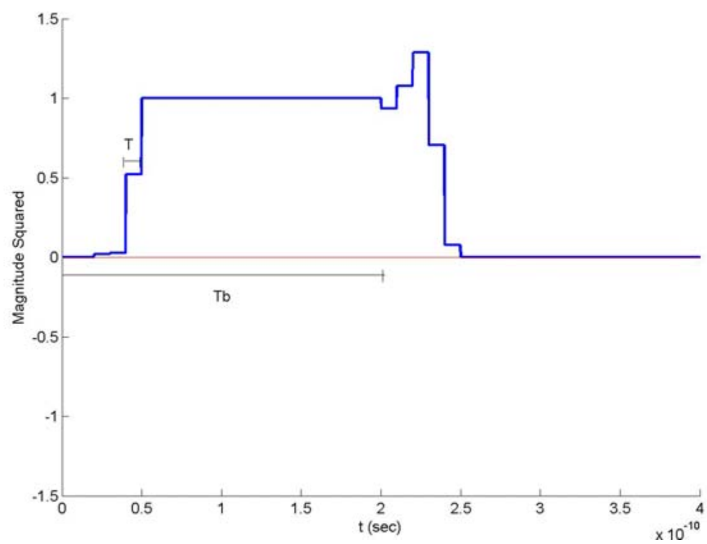

Figure 4.18. Output of the fifth order filter for one bit pulse 5 Gbps

Figure 4.19 describes the eye diagrams of an output sequence of the fifth order filter for bit rates of 5, 11.75, 25, 30, 40, and 50 Gbps for a system working at the center of the passband. From the eye diagrams obtained, the pulse is broadened due to the delay lines of the filter. If the input bit rate is smaller than the filter bandwidth, the output will still have a good eye diagram. The FSR of the fifth order filter remains 100 GHz with an

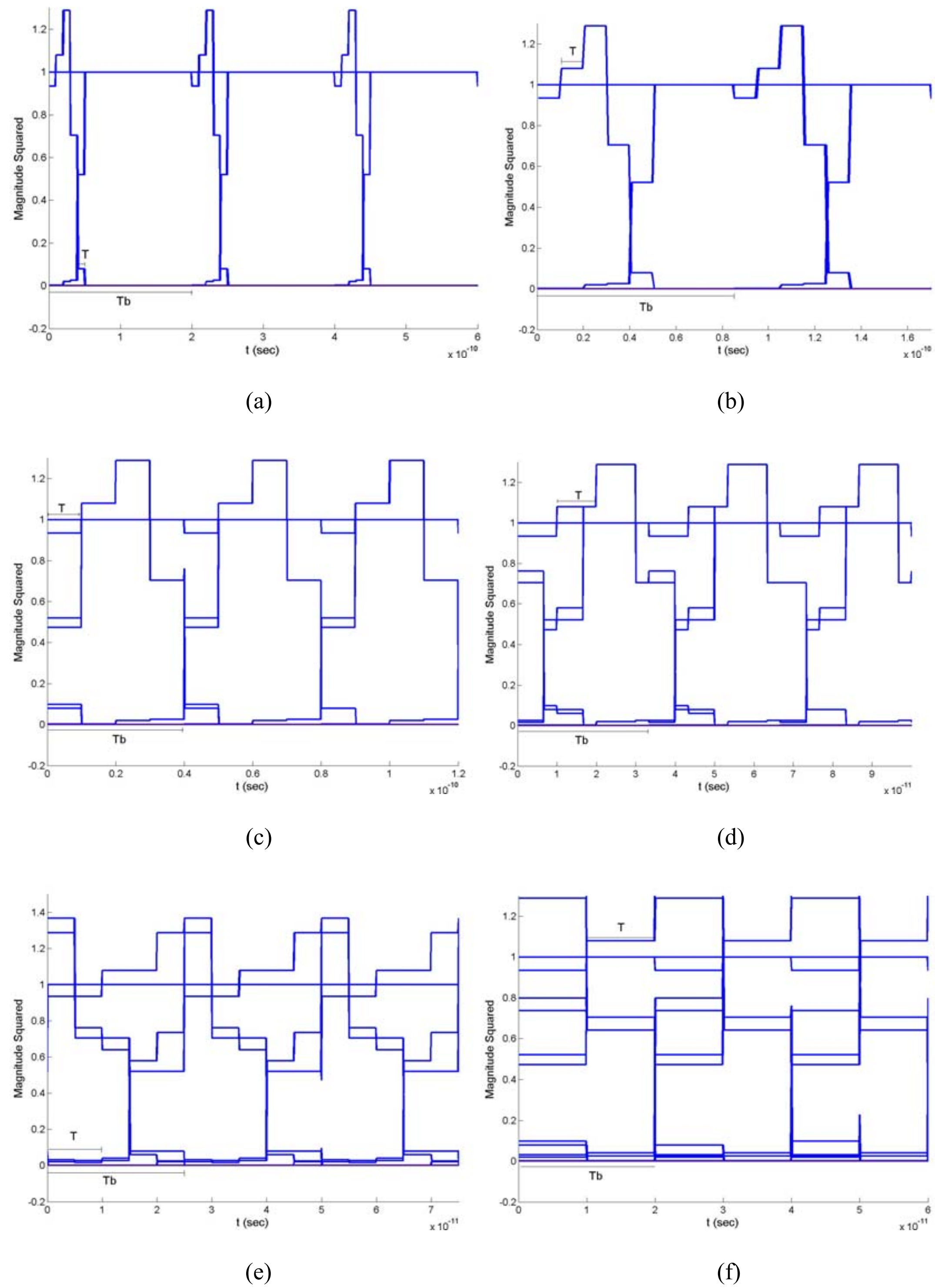

Figure 4.19. Output eye diagrams of (a) 5 Gbps, (b) 11.75 Gbps (c) 25 Gbps, (d) 30 Gbps, (e) 40 Gbps, and (f) 50 Gbps input at the center of the passband of the fifth order filter

equivalent low-pass bandwidth of 11.75 GHz (as confirmed from Chapter 3 result), consider it corresponds with –25 dB stop-band width. As can be seen from Figure 4.19, at bit rates up to 30 Gbps still give wide enough time intervals over which the pulse can be sampled. Figure 4.20 describes the system output for one bit pulse input with bit rate 50 Gbps or bit time 20 ps. It is seen that the output amplitude is not one anymore.

The output of the filter for a 15.9 GHz frequency shifts is shown by Figure 4.21. At that frequency for an FSR of 100 GHZ, from previous results, the dispersion is the highest (refer to Figure 3.18(b)). Comparing Figure 4.21 to Figure 4.19(a) and (c) where the system is at the center of the passband, the pulse width remains the same, only the magnitude that differs slightly. The amplitude distortion is worse if the shift is increasing as can be seen in Figure 4.22 where the frequency shift is 25 GHz and in Figure 4.23 where the system is at the stopband.

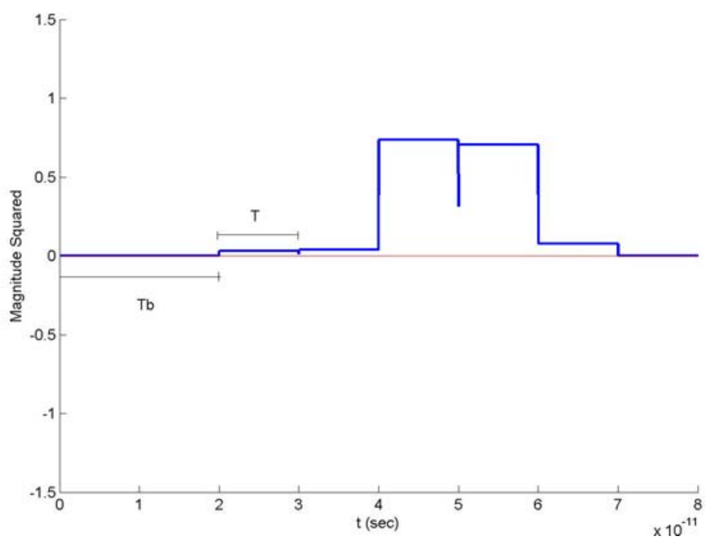

Figure 4.20. Output of the fifth order filter for one bit pulse 50 Gbps

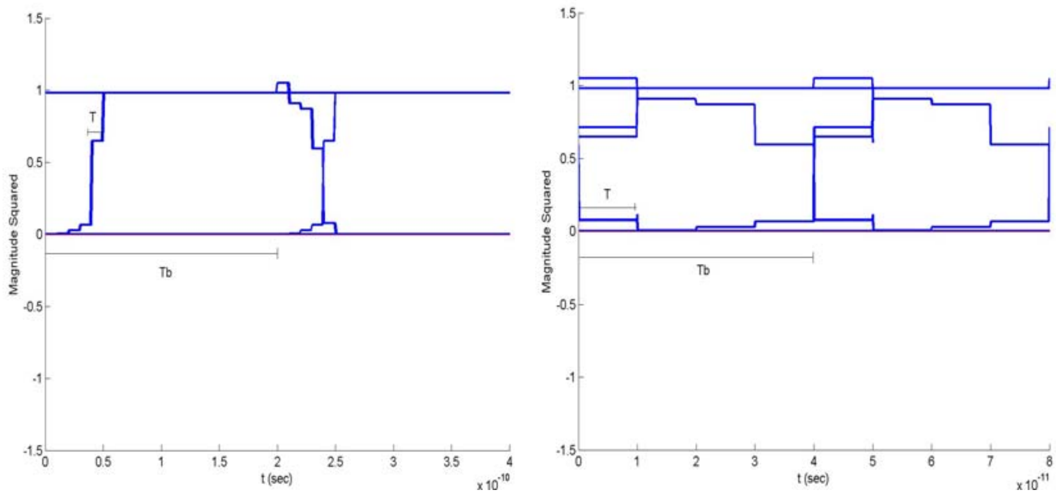

(a) (b)

Figure 4.21. Output eye diagrams for two bit times of the fifth order filter for frequency shift of 15.9 GHz (a) 5 Gbps, (b) 25 Gbps

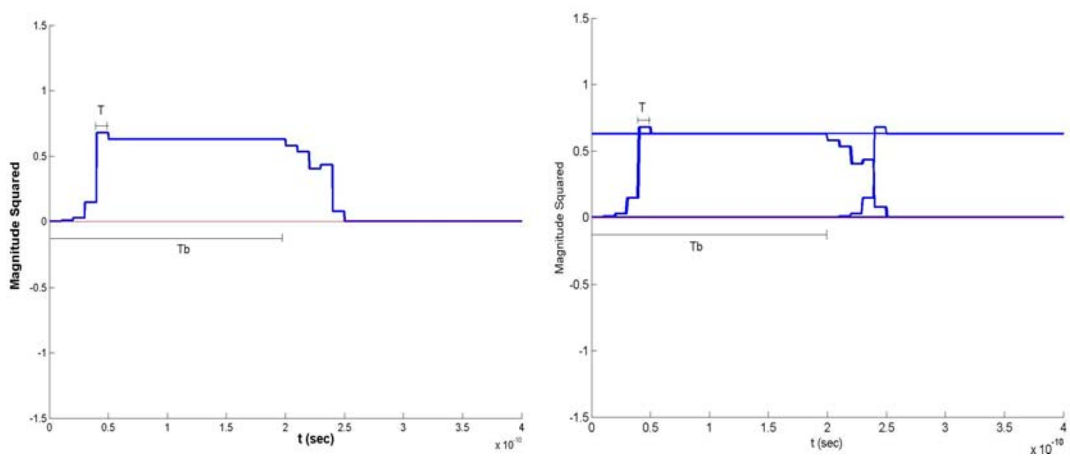

(a) (b)

Figure 4.22. Output eye diagrams for two bit times of the fifth order filter for frequency shift of 25 GHz for 5 Gbps input (a) one bit input and (b) sequence input

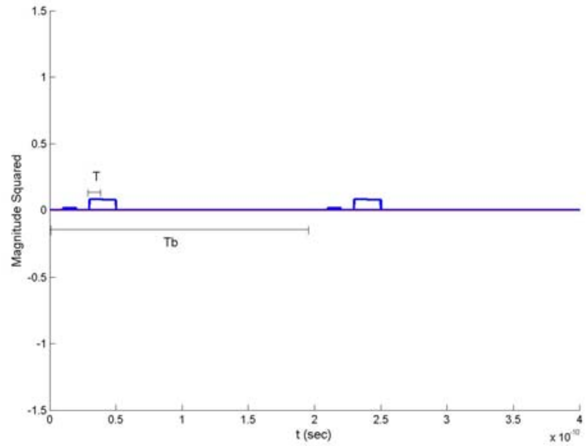

Figure 4.23. Output eye diagrams for two bit times of 5 Gbps input at the stopband region of the fifth order filter

4.2.4 Seventh Order Filter

Figure 4.24 describes the magnitude squared output for one bit pulse input with bit rate 5 Gbps or bit time T_b = 0.2 ns at the center of the passband for the seventh order filter. The unit delay is the same as the previous filters, T = 10 ps. For this seventh order filter there are sixteen stair-levels where the last level has a zero magnitude. As obtained in Chapter 3, the cross transfer function of the seventh order filter is

$$\begin{aligned}B(z) = 0.0225 - 0.0842z^{-1} + 0.0576z^{-2} + 0.5040z^{-3} + 0.5040z^{-4} \\ +0.0576z^{-5} - 0.0842z^{-6} + 0.0225z^{-7}\end{aligned} \tag{4.16}$$

As in previous filters, the pulse also broadens due to the delays it receives and there are extra delays compared to the previous filters since it has more delay lines. It also has a "stairs-alike" shape. The value of each stair-level depends on the filter coefficients. The input is delayed as much as an integer multiple of the unit delay T and gained by the coefficients.

Figure 4.25 describes the eye diagrams of an output sequence of the seventh order filter for bit rates of 5, 25, 40, and 50 Gbps for a system working at the center of the passband. As with the previous filters, the output pulse of the seventh order filter also broadened due to the delays it receives. The delays are seven times the unit delay. If the input bit rate is smaller than the filter bandwidth, the output has a good eye diagram. The FSR of the seventh order filter remains 100 GHz with an equivalent low-pass bandwidth of 11.25 GHz (as confirmed from Chapter 3 result), consider it corresponds with –25 dB stop-band width. As can be seen from Figure 4.25, bit rates up to 40 Gbps still gives wide enough time intervals over which the pulse can be sampled. Higher bit rate gives a narrower eye opening.

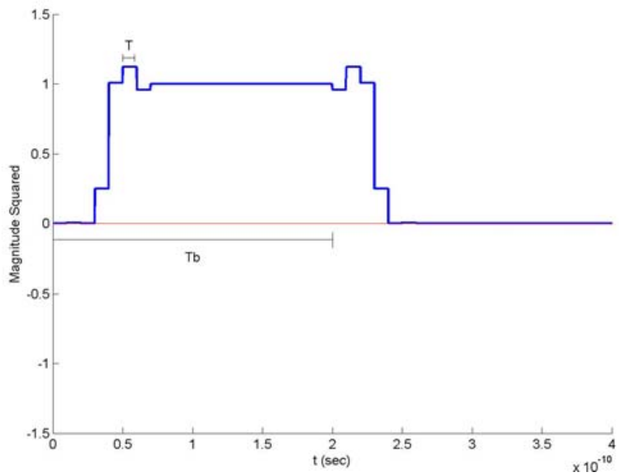

Figure 4.24. Output of the seventh order filter for one bit pulse 5 Gbps

Results after filtering for a shift in the center wavelength, i.e. the carrier frequency, are shown by figure 4.26. Suppose the shift is 11.25 GHz. Comparing the results obtained with the ones previously obtained where the system is at the center of the passband, as seen in Figure 4.25(a) and (c), the output pulse width remains the same, only the amplitude that differs slightly. The amplitude decreasing is worse if the shift is increasing as can be seen in Figure 4.27 where the frequency shift is 25 GHz. The amplitude is below one. The amplitude goes to zero in the stopband as can be seen in Figure 4.28.

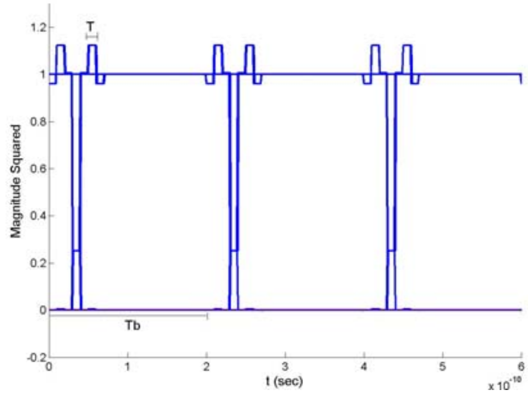

(a)

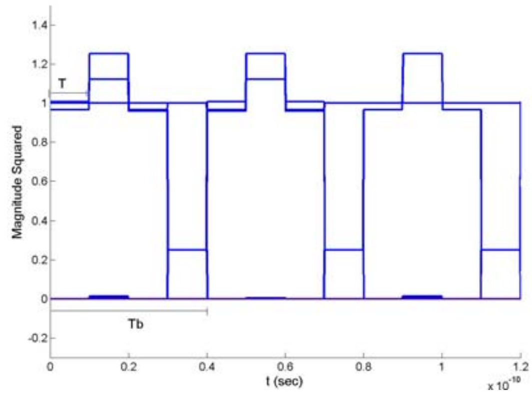

(b)

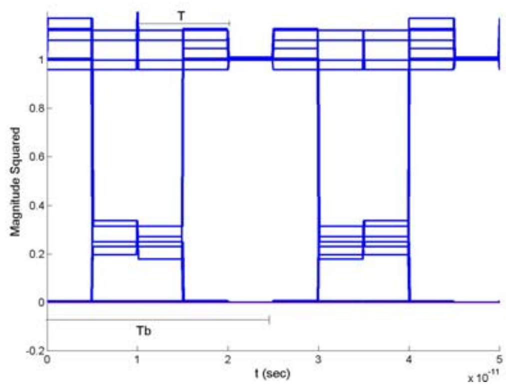

(e)

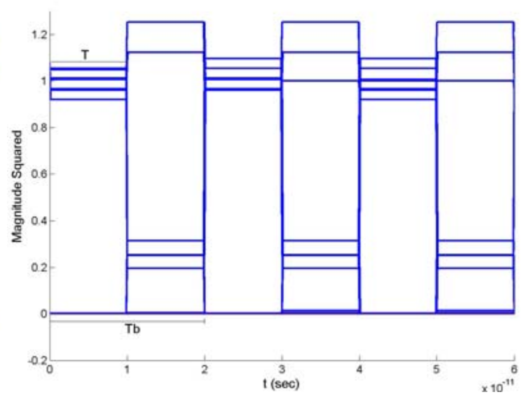

(f)

Figure 4.25. Output eye diagrams of (a) 5 Gbps, (b) 25 Gbps, (c) 40 Gbps, and (d) 50 Gbps input at the center of the passband of the seventh order filter

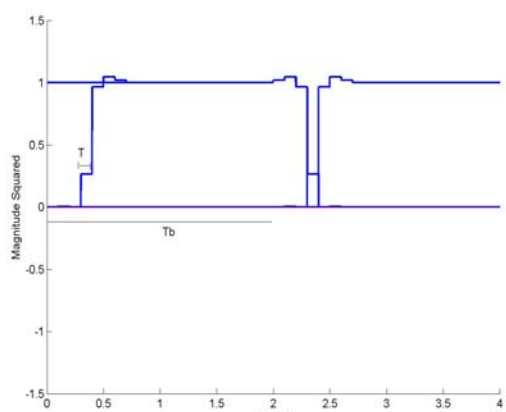

(a)

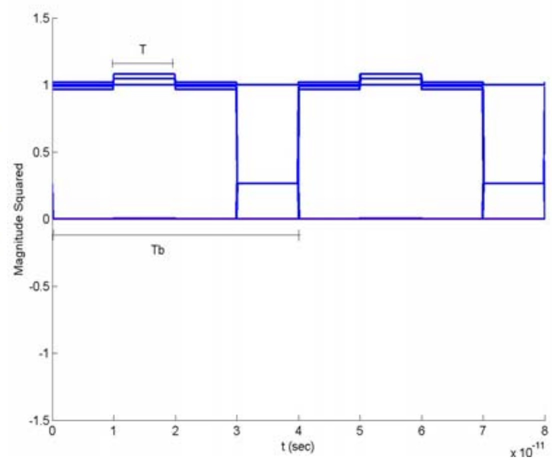

(b)

Figure 4.26. Output eye diagrams for two bit times of the seventh order filter for frequency shift of 11.25 GHz (a) 5 Gbps, (b) 25 Gbps

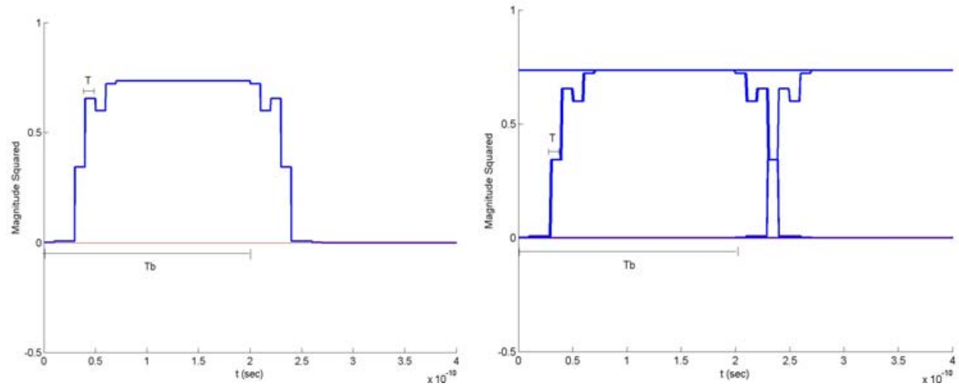

(a) (b)

Figure 4.27. Output eye diagrams for two bit times of the seventh order filter for frequency shift of 25 GHz for 5 Gbps input (a) one bit input and (b) sequence input

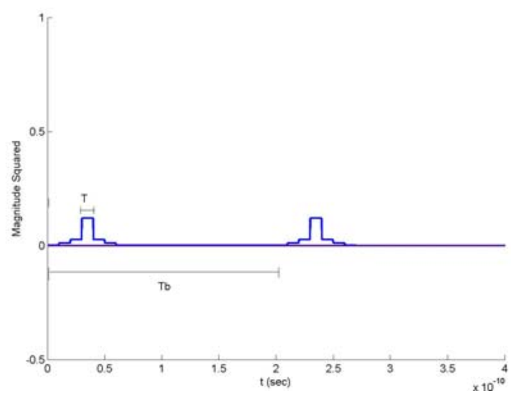

Figure 4.28. Output eye diagrams for two bit times of 5 Gbps input at the stopband region of the seventh order filter

4.3 Summary

In this chapter, eye diagram simulations are made to study intersymbol interference in binary data transmission using the proposed filters. From the results obtained, the time response depends on the delay stages. Both filters that have non-linear phase characteristic at the frequency response, i.e. the third and fifth order filters, and filters that have linear phase response, i.e. the fourth and seventh order filters, give output responses that are spreading out due to the delay lines.

The output pulse spreading or broadening depends on the number of delay lines of the filters, i.e. the filter order. The higher is the filter order the wider is the spreading. The maximum bit rate of third, fourth, fifth, and seventh order filters are 40 Gbps, 40 Gbps, 30 Gbps, and 40 Gbps respectively. One typical characteristic of the linear phase filters is that the output pulse shape is symmetric, in contrary with the non-linear phase filters whose output pulse is asymmetric. If there is a shift on the center wavelength or the midband frequency, the amplitude may decrease. Only the magnitude response influences the received pulse.

5 Conclusions and Recommendations

5.1 Conclusions

In this report, four kinds of filters are designed. Two types of them have a linear phase response and hence zero dispersion. They are made as an improvement to the non-linear phase filters. The other two filters have a non-linear phase response and hence non-zero dispersion. The non-linear phase filters are the third and fifth order FIR type filters, while the linear phase filters are the fourth and seventh order FIR filters. The linear-phase responses are for the cross transfer of the fourth and seventh order filters, not for the bar transfers. All the filters are designed such that they have a passband flattened amplitude response.

The third order non-linear phase filter, which has three zeros in its polynomial, is added one zero which results in a fourth order filter that has a linear phase response characteristics. The third order filter has a -25 dB stopband width of 15.2% of the Free Spectral Range (FSR), while the fourth order filter has a -25 dB stopband width of 14.6% of the FSR. To have a broader stopband width and hence broader passband width, two zeros are added to the third order filter resulting in a fifth order filter. The fifth order filter has a -25 dB stopband width of 23.5% of the FSR. It is wider than the third and fourth order filters. The fifth order filter is added two more zeros resulting in a seventh order filter that has a linear phase response characteristics. The seventh order filter has -25 dB stopband width of 22.5% of the FSR.

Dispersion of the third and fifth order filters is zero at the center of the passband. For the third order filter, the highest dispersion at the passband is at the frequency shifting from the center of the passband as much as 11% of the FSR, while for the fifth order filter it is as much as 15.9% of the FSR.

The fundamental building block for the ADM filters used in multiwavelength communication systems is the Asymmetric Mach-Zehnder interferometer (MZI). Once a filter has been designed, the coefficients of the filter can be mapped to the power coupling ratios of each directional coupler and the phase of each delay line of the MZI. The filter order corresponds with the number of the delays of the lattice filter of the cascaded MZI. If it turns out that one coupler has a power coupling constant of zero, then the associated coupler can be removed and the neighbouring delay lines can be combined into one with doubled delay.

In order to study the performance of the designed filters in the time domain, pulse response eye diagram simulations are made to study the possible intersymbol interference in binary data transmission using the designed filters. Simulations are made for on-off keying. Simulations are made with the same FSR and hence equal unit delay for each filter.

From the results obtained, it can be concluded that the time response depends on the delay stages. Both filters that have non-linear phase characteristic at the frequency response, i.e. the third and fifth order filters, and filters that have linear phase response, i.e. the fourth and seventh order filters, give output responses that spread out due to the delay lines. One typical characteristic of the linear phase filters is that the output pulse shape is symmetric, in contrary with the non-linear phase filters whose output pulse is asymmetric.

The output pulse spreading or broadening depends on the number of delay lines of the filters, i.e. the filter order. The higher is the filter order the wider is the spreading. The broadening of the pulse for each type of filter is as much as each filter's order times the unit delay. If the bit rate is small compared to the filter bandwidth, then the eye diagram shows a wide eye opening that the received pulse sequence can be sampled without error from intersymbol interference. The maximum bit rate of the third, fourth, fifth, and seventh order filters before intersymbol interference occurs are 40 Gbps, 40 Gbps, 30 Gbps, and 40 Gbps respectively. If there is a shift on the center wavelength or the midband frequency, the amplitude may decrease, but the width of the output pulse remains the same with that of the input pulse. Only the magnitude response influences the received pulse.

5.2 Recommendations

Firstly, since the time response of the filters results in broadening of the received bit pulse, further research may be made to get better results. Additional criteria may be needed such as how to have a smooth output bit while still having zero dispersion and passband flattened in magnitude response or how to compensate the pulse broadening.

Secondly, as the designs are done with the FIR filter, in this case an MZI lattice filter, an alternative form of interleaver such as an MZI plus ring resonator could be investigated.

Thirdly, the on-off keying modulation is considered in this report. Other modulation methods may be considered and are left for further research.

Fourthly, the simulations are made based on rectangular input pulse with one frequency. Chirped pulses may arise due to the imperfection of the modulator resulting in different frequency components in one pulse. It may be worth to investigate the response of the filters to the chirped pulse.

Fifthly, the eye diagram simulations are made directly after the filter. The use of the matched filter prior to the receiver, which involves a filter matched to the signal component of the received signal, may be worth to investigate.

Finally, the eye diagram simulation is studied for one transfer function of one interleaver, so not for the complete ADM system yet. A more comprehensive impression of the ADM system performance may be made with a more detailed analysis on the interleaver at both the splitting part and the combining part. Also measurement of the intensity and phase transfers of the ADM may be worth to do.

References

[1] C. Roeloffzen. *Passband Flattened Binary-Tree Structured Add-Drop Multiplexers Using SiON Waveguide Technology*. University of Twente, Enschede, The Netherlands, 2002.

[2] C.K. Madsen and J.H. Zhao. *Optical Filter Design and Analysis: A Signal Processing Approach*. John Wiley & Sons, Inc., New York, 1999.

[3] S.K. Mitra. *Digital Signal Processing: A Computer-Based Approach*. 2^{nd} edition. The McGraw-Hill Companies, Inc., New Delhi, 2001.

[4] J.G. Proakis and D.G. Manolakis. *Digital Signal Processing: Principles, Algorithms, and Applications*. 2^{nd} edition. Macmillan Publishing company, New York, 1992.

[5] D.J. DeFatta, J.G. Lukas, and W.S. Hodgkiss. *Digital Signal Processing: A System Design Approach*. John Wiley & Sons Inc., New York, 1988.

[6] K. Jinguji and M. Kawachi. ”Synthesis of Coherent Two-Port Lattice-Form Optical Delay-Line Circuit”. *J. Lightwave Technol*., vol. 13, no. 1, pp. 73-82, 1995.

[7] S.S. Haykin. *An Introduction to Analog and Digital Communications*. John Wiley & Sons Inc., New York, 1989.

[8] P.P. Vaidyanathan. “On Power-Complementary FIR Filters”. *IEEE Trans. On Circuits and Systems*, vol. CAS-32, no. 12, pp. 1308-1310, 1985.

Appendix A

Symmetry Property of Linear Phase Filters

The following explanations are as referred to DeFatta (1988). The transfer function of a FIR causal filter of length N is given by:

$$H(z) = \sum_{n=0}^{N-1} h(n) z^{-n} \tag{A.1}$$

The phase delay and group delay are defined as follows,

$$\tau_p = -\frac{\theta(\omega)}{\omega} \quad \text{and} \quad \tau_g = -\frac{d\theta(\omega)}{d\omega} \tag{A.2}$$

For the phase response to be linear, it requires

$$\theta(\omega) = -\tau\omega \tag{A.3}$$

where τ is a constant phase delay in samples.

The discrete-time Fourier transform of the finite sequence $h(n)$ for a unit delay T is given by

$$H(e^{j\omega T}) = \sum_{n=0}^{N-1} h(n) e^{-j\omega nT} = \left|H(e^{j\omega T})\right| e^{j\theta(\omega)} \tag{A.4}$$

where the phase response is defined as

$$\theta(\omega) = \tan^{-1} \frac{-\operatorname{Im} H(e^{j\omega T})}{\operatorname{Re} H(e^{j\omega T})} \tag{A.5}$$

From Eqs. (A.3), (A.4), and (A.5), the phase response can be expressed as

$$\theta(\omega) = -\tau\omega = \tan^{-1} \frac{-\sum_{n=0}^{N-1} h(n) \sin \omega nT}{\sum_{n=0}^{N-1} h(n) \cos \omega nT} \tag{A.6}$$

or

$$\tan\omega\tau = \frac{\sum_{n=0}^{N-1} h(n)\sin\omega nT}{\sum_{n=0}^{N-1} h(n)\cos\omega nT} \tag{A.7}$$

and the following equation is obtained,

$$\sum_{n=0}^{N-1} h(n)\sin(\omega\tau - \omega nT) = 0 \tag{A.8}$$

The solution to Eq. (A.6) is given by

$$\tau = \frac{(N-1)T}{2} \tag{A.9}$$

and

$$h(n) = h(N-1-n) \qquad \text{for } 0 < n < N-1 \tag{A.10}$$

FIR filters will have constant phase delay and group delay if the conditions of Eqs. (A.8) and (A.9) are satisfied. If only constant group delay is desired, then the impulse response is of the form

$$h(n) = -h(N-1-n) \qquad \text{for } 0 < n < N-1 \tag{A.11}$$

Appendix B

Reverse Polynomial

This section is as referred to Madsen (1999). Consider a filter polynomial of N-order:

$$H_N(z) = h_0 + h_1 z^{-1} + \ldots + h_N z^{-N} \tag{B.1}$$

or in terms of its roots:

$$H_N(z) = \Gamma z^{-N} \prod_{n=1}^{N} (z - z_n) \tag{B.2}$$

where z_n are the zeros of the polynomial . The reverse polynomial $H_N^R(z)$ is obtained when the zeros are reflected about the unit circle, $z_n \to 1/z_n^*$. Hence the reverse polynomial transfer function can be expressed in terms of its roots as:

$$H_N^R(z) = \Gamma z^{-N} \prod_{n=1}^{N} (z - 1/z_n^*) \tag{B.3}$$

The relation of $H_N^R(z)$ and $H_N(z)$ is given by

$$H_N^R(z) = z^{-N} H_N^*(z^{*-1}) \tag{B.4}$$

The product of $H_N(z)$ and $H_N^R(z)$ evaluated on the unit circle gives

$$H_N(\omega) H_N^R(\omega) = H_N(\omega) e^{-j\omega N} H_N^*(\omega) = \left| H_N(\omega) \right|^2 e^{-j\omega N} \tag{B.5}$$

The product shows the magnitude squared response times a linear delay.

Appendix C

Power Conservation

Consider transfer matrices for lossless filter. Let **S** denotes scattering matrix that relates the inputs X to the outputs Y so that Y=**S**X. Using this definition, the transfer and scattering matrices of feed-forward structures such as the MZI are identical. A lossless passive MZI will have its power conserved. The sum of the input powers must equal the sum of the output powers. It is equivalent to requiring that the scattering matrix is unitary. A matrix is unitary if $\mathbf{S}^{\dagger}\mathbf{S} = \mathbf{I}$ where **I** is the identity matrix and $\mathbf{S}^{\dagger}$ is Hermitian transpose, $(\mathbf{S}^{T})^{*}$. The determinant of a unitary matrix has a magnitude of one, |det(**S**)|=1. Given the scattering matrix

$$\mathbf{S} = \begin{pmatrix} s_{11} & s_{12} \\ s_{21} & s_{22} \end{pmatrix} \tag{C.1}$$

Let the determinant be designated by $\det(\mathbf{S}) = e^{j\theta_d}$. The unitary condition requires that $\mathbf{S}^{-1} = \mathbf{S}^{\dagger}$, or

$$e^{-j\theta_d} \begin{pmatrix} s_{22} & -s_{12} \\ -s_{21} & s_{11} \end{pmatrix} = \begin{pmatrix} s_{11}^{*} & s_{21}^{*} \\ s_{12}^{*} & s_{22}^{*} \end{pmatrix} \tag{C.2}$$

The following relations emerge:

$$\begin{aligned} &|s_{11}| = |s_{22}| \\ &|s_{12}| = |s_{21}| \\ &|s_{11}|^2 + |s_{12}|^2 = 1 \\ &|s_{21}|^2 + |s_{22}|^2 = 1 \\ &s_{11}s_{12}^{*} + s_{21}s_{22}^{*} = 0 \end{aligned} \tag{C.3}$$

For a unitary matrix, the sum of the square magnitudes of elements along any row is equal to one, which reflects the power conservation. In addition, the inner product of any column with the complex conjugate of any other column is zero.

Appendix D

Optical Filter Parameters

	Power coupling constant				Phase		
	κ_0	κ_1	κ_2	κ_3	φ_1	φ_2	φ_3
A_1B_1	0.93	0	0.72	0.5	0	0	π
A_1B_2	0.5	0.72	0	0.93	π	0	0
A_2B_1	0.5	0.73	0	0.07	0	π	0
A_2B_2	0.07	0	0.73	0.5	0	π	0

Table D.1 Optical parameters of the three-stage optical filter

	Power coupling constant					Phase			
	κ_0	κ_1	κ_2	κ_3	κ_4	φ_1	φ_2	φ_3	φ_4
$A(z)B(z)$	0.04	0.17	0.83	0.14	0.04	π	0	0	-π
$A^R(z)B(z)$	0.83	0.03	0.84	0.81	0.96	-π	π	0	-π

Table D.2 Optical parameters of the four-stage optical filter

	Power coupling constant						Phase				
	κ_0	κ_1	κ_2	κ_3	κ_4	κ_5	φ_1	φ_2	φ_3	φ_4	φ_5
A_1B_1	0.02	0	0.22	0.01	0.82	0.44	π	0	-π	0	0
A_1B_2	0.56	0.78	0.01	0.18	0	0.01	0	π	0	-π	0
A_1B_3	0.15	0.36	0.52	0.48	0.36	0.10	0.57	1.22	-0.12	-1.21	-0.47
A_1B_4	0.15	0.36	0.52	0.48	0.36	0.10	-0.57	-1.22	0.12	1.21	0.47
A_2B_1	0.56	0.82	0.01	0.22	0	0.98	π	0	-π	0	0
A_2B_2	0.99	0	0.18	0.01	0.78	0.44	π	-π	0	π	-π
A_2B_3	0.90	0.36	0.48	0.52	0.36	0.85	2.68	-1.21	-0.12	1.22	-2.57
A_2B_4	0.90	0.36	0.48	0.52	0.36	0.85	-2.68	1.21	0.12	-1.22	2.57
A_3B_1	0.14	0.38	0.54	0.46	0.35	0.87	2.61	-4.36	π	-1.83	0.36
A_3B_2	0.88	0.36	0.54	0.46	0.34	0.12	0.56	-1.94	π	-4.43	2.79
A_3B_3	0.55	0.56	0.01	0.89	0.01	0.49	1.56	-π	π	-0.01	-1.56
A_3B_4	0.50	0.01	0.91	0.01	0.51	0.49	1.66	-3.25	-0.02	0.02	1.57
A_4B_1	0.14	0.42	0.47	0.50	0.43	0.86	-2.69	4.32	-π	1.99	-0.50
A_4B_2	0.90	0.29	0.50	0.53	0.30	0.10	-0.53	1.85	-π	4.39	-2.56
A_4B_3	0.58	0.02	0.90	0.02	0.56	0.42	-π	4.63	1.43	-1.52	-1.44
A_4B_4	0.58	0.56	0.02	0.89	0.02	0.42	-1.70	1.59	-1.50	1.56	0.05

Table D.3 Optical parameters of the five-stage optical filter

	Power coupling constant							
	κ_0	κ_1	κ_2	κ_3	κ_4	κ_5	κ_6	κ_7
$A(z)B(z)$	0.99	0.02	0.02	0.74	0.68	0.04	0.02	0.99
$A^R(z)B(z)$	0.06	0.04	0.05	0.77	0.49	0.20	0.20	0.01
	Phase							
	φ_1	φ_2	φ_3	φ_4	φ_5	φ_6	φ_7	
$A(z)B(z)$	0	0	π	0	-π	0	0	
$A^R(z)B(z)$	0	0	0	0	π	0	-2π	

Table D.4 Optical parameters of the seven-stage optical filter

Appendix E

Coefficient Terms of the Seventh Order Filter

$\breve{c}_0$	1
$\breve{c}_1$	$-(z_1+z_2+z_3+z_4+z_5+z_6+z_7)$
$\breve{c}_2$	$z_2z_7+z_5z_7+z_1z_2+z_6z_7+z_2z_5+z_3z_7+z_4z_5+z_1z_4+z_3z_5+z_2z_6+z_3z_4+z_5z_6$ $+z_1z_6+z_2z_4+z_1z_3+z_4z_7+z_1z_7+z_4z_6+z_2z_3+z_3z_6+z_1z_5$
$\breve{c}_3$	$-(z_2z_3z_7+z_2z_6z_7+z_3z_4z_5+z_1z_2z_4+z_1z_3z_4+z_2z_3z_4+z_1z_2z_3+z_2z_4z_5$ $+z_2z_3z_5+z_1z_4z_5+z_1z_3z_5+z_1z_2z_5+z_1z_5z_6+z_2z_3z_6+z_1z_3z_6+z_2z_4z_6+z_3z_4z_6$ $+z_3z_5z_6+z_1z_4z_6+z_4z_5z_6+z_2z_5z_6+z_1z_2z_6+z_1z_5z_7+z_3z_6z_7+z_4z_6z_7+z_1z_3z_7$ $+z_2z_4z_7+z_1z_6z_7+z_5z_6z_7+z_3z_4z_7+z_3z_5z_7+z_1z_4z_7+z_4z_5z_7+z_2z_5z_7+z_1z_2z_7)$
$\breve{c}_4$	$z_2z_3z_4z_5+z_3z_4z_5z_7+z_1z_3z_4z_6+z_1z_2z_3z_6+z_1z_2z_3z_5+z_1z_2z_3z_4+z_2z_3z_5z_6+z_1z_2z_5z_6$ $+z_2z_3z_4z_6+z_1z_3z_4z_5+z_1z_2z_4z_5+z_1z_2z_4z_6+z_3z_4z_5z_6+z_2z_4z_5z_6+z_1z_4z_5z_6+z_1z_3z_5z_6$ $+z_1z_2z_3z_7+z_2z_3z_4z_7+z_1z_3z_4z_7+z_1z_2z_4z_7+z_2z_4z_5z_7+z_2z_3z_5z_7+z_1z_4z_5z_7+z_1z_3z_5z_7$ $+z_1z_2z_5z_7+z_1z_5z_6z_7+z_1z_4z_6z_7+z_4z_5z_6z_7+z_2z_5z_6z_7+z_1z_2z_6z_7+z_2z_3z_6z_7+z_1z_3z_6z_7$ $+z_2z_4z_6z_7+z_3z_4z_6z_7+z_3z_5z_6z_7$
$\breve{c}_5$	$-(z_1z_2z_4z_6z_7+z_1z_2z_3z_6z_7+z_2z_3z_4z_5z_6+z_1z_2z_3z_4z_5+z_1z_2z_3z_4z_6+z_1z_3z_4z_5z_6$ $+z_1z_2z_4z_5z_6+z_1z_2z_3z_5z_6+z_2z_3z_4z_6z_7+z_2z_3z_4z_5z_7+z_1z_2z_3z_4z_7+z_1z_3z_4z_5z_7+z_1z_2z_4z_5z_7$ $+z_1z_2z_3z_5z_7+z_1z_3z_4z_6z_7+z_3z_4z_5z_6z_7+z_2z_4z_5z_6z_7+z_2z_3z_5z_6z_7+z_1z_4z_5z_6z_7+z_1z_3z_5z_6z_7$ $+z_1z_2z_5z_6z_7)$
$\breve{c}_6$	$z_1z_2z_3z_4z_5z_6+z_1z_2z_3z_4z_6z_7+z_1z_3z_4z_5z_6z_7+z_2z_3z_4z_5z_6z_7+z_1z_2z_3z_4z_5z_7$ $+z_1z_2z_4z_5z_6z_7+z_1z_2z_3z_5z_6z_7$
$\breve{c}_7$	$-z_1z_2z_3z_4z_5z_6z_7$

Table E.1 Coefficient terms of the seventh order cross transfer function

Appendix F

Responses of the Simulated Filter Model

F-1

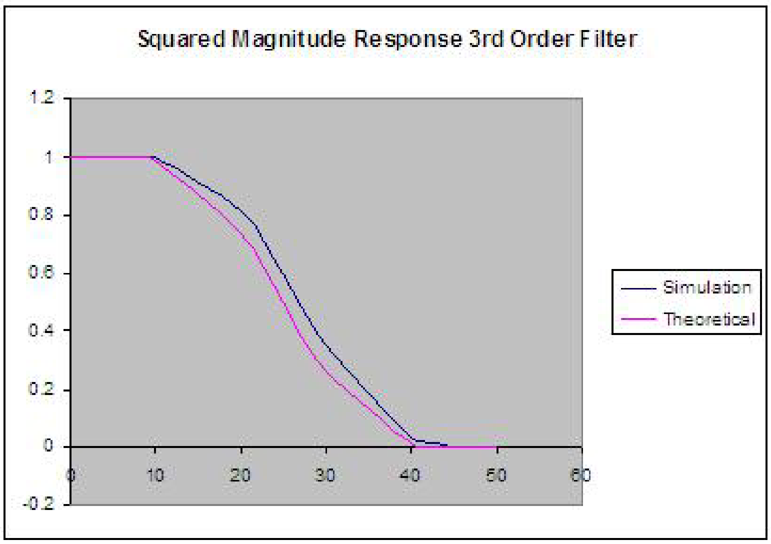

F-2

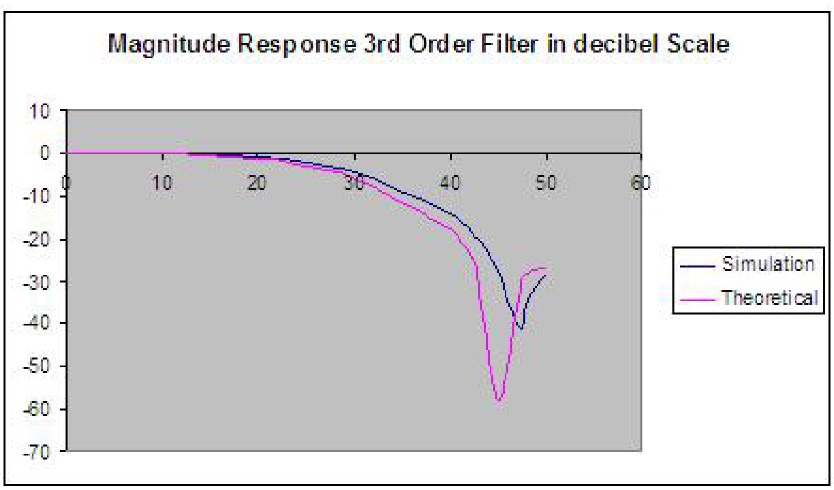

F-3

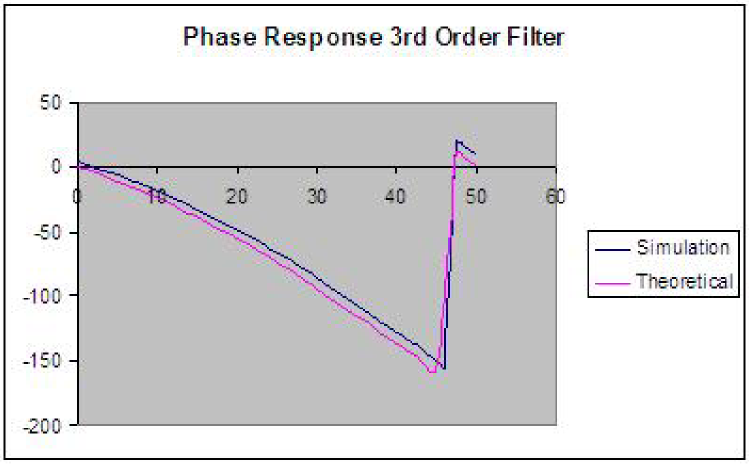
Phase Response 3rd Order Filter
50
0
-50
-100
-150
-200
0
10
20
30
40
50
60
Simulation
Theoretical

F-4

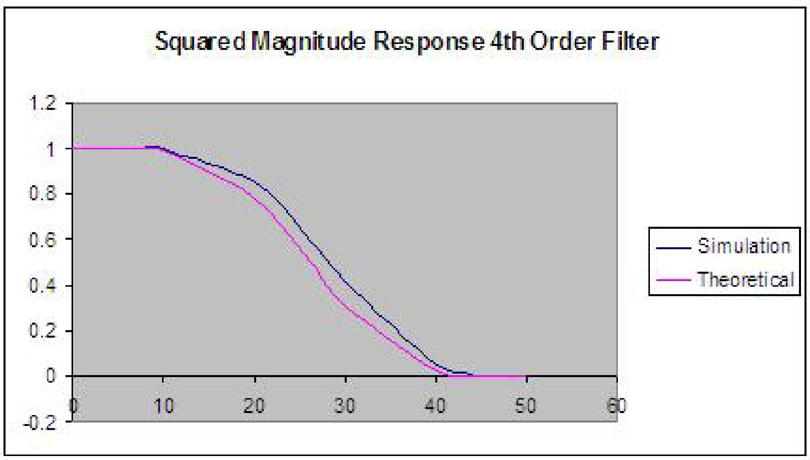
Squared Magnitude Response 4th Order Filter
1.2
1
0.8
0.6
0.4
0.2
0
-0.2
0
10
20
30
40
50
60
Simulation
Theoretical

F-5

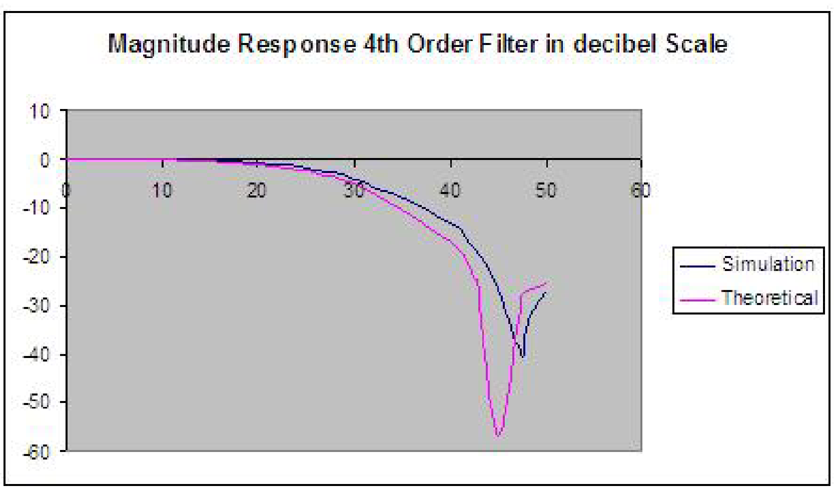
Magnitude Response 4th Order Filter in decibel Scale
10
0
-10
-20
-30
-40
-50
-60
0
10
20
30
40
50
60
Simulation
Theoretical

F-6

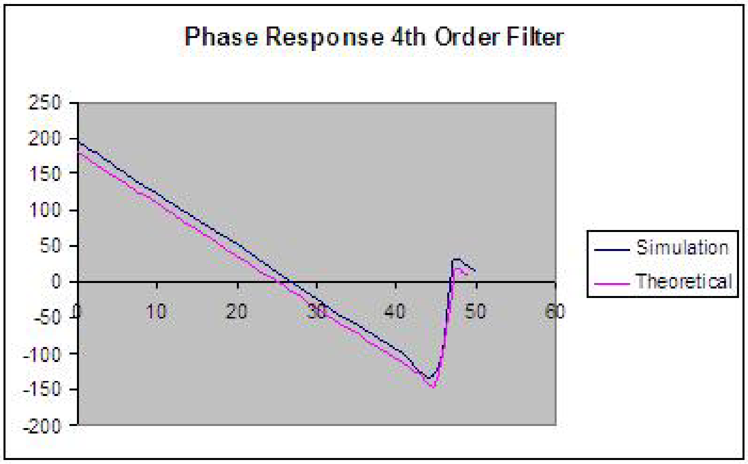
Phase Response 4th Order Filter
250
200
150
100
50
0
-50
-100
-150
-200
0
10
20
30
40
50
60
Simulation
Theoretical